NASA CR-132709

A THREE-DIMENSIONAL SOLUTION OF FLOWS OVER WINGS WITH LEADING-EDGE VORTEX SEPARATION

PART I

Engineering Document

Guenter W. Brune, James A. Weber, Forrester T. Johnson, Paul Lu, and Paul E. Rubbert

September 1975

Prepared under contracts NAS1-12185 and NAS1-13833 by

Boeing Commercial Airplane Company

Seattle, Washington 98124

for

Langley Research Center

NATIONAL AERONAUTICS AND SPACE ADMINISTRATION

1. Report No.	2. Government Accession No.	3. Recipient's Catalog No.
NASA CR-132709		

4. Title and Subtitle	5. Report Date
A THREE-DIMENSIONAL SOLUTION OF FLOWS OVER WINGS WITH LEADING-EDGE VORTEX SEPARATION Part I—Engineering Document	September 1975
	6. Performing Organization Code
7. Author(s)	8. Performing Organization Report No.
G. W. Brune, J. A. Weber, F. T. Johnson, P. Lu, and P. E. Rubbert	D6-41789
	10. Work Unit No.
9. Performing Organization Name and Address	11. Contract or Grant No.
Boeing Commercial Airplane Company P.O. Box 3707 Seattle, Washington 98124	NAS1-12185, NAS1-13833
	13. Type of Report and Period Covered
12. Sponsoring Agency Name and Address	Contractor Report May 1973—June 1975
National Aeronautics and Space Administration Washington, D.C. 20546	14. Sponsoring Agency Code

15. Supplementary Notes

16. Abstract

A method of predicting forces, moments, and detailed surface pressures on thin, sharp-edged wings with leading-edge vortex separation in incompressible flow is presented. The method employs an inviscid flow model in which the wing and the rolled-up vortex sheets are represented by piecewise, continuous quadratic doublet sheet distributions. The Kutta condition is imposed on all wing edges.

Computed results are compared with experimental data and with the predictions of the leading-edge suction analogy for a selected number of wing planforms over a wide range of angle of attack. These comparisons show the method to be very promising, capable of producing not only force predictions, but also accurate predictions of detailed surface pressure distributions, loads, and moments. Experience with the present computer program, however, is limited, and operational limitations related to doublet panel spacing and panel density requirements, behavior at large planform breaks, convergence characteristics, etc., have yet to be extensively explored.

17. Key Words (Suggested by Author(s))		18. Distribution Statement
Doublet singularity	Nonlinear	Unclassified—unlimited
Incompressible	Panel method	
Iteration	Potential flow	
Leading edge	Three-dimensional	
Separation		

19. Security Classif. (of this report)	20. Security Classif. (of this page)	21. No. of Pages	22. Price*
Unclassified	Unclassified	98	

*For sale by the National Technical Information Service, Springfield, Virginia 22151

CONTENTS

FIGURES

TABLES

A THREE-DIMENSIONAL SOLUTION OF FLOWS OVER WINGS WITH LEADING-EDGE VORTEX SEPARATION
Part I—Engineering Document

Guenter W. Brune, James A. Weber, Forrester T. Johnson,
Paul Lu, and Paul E. Rubbert

Boeing Commercial Airplane Company

SUMMARY

The application of a new, general, potential flow computational technique to the solution of the subsonic, three-dimensional flow over wings with leading-edge vortex separation is presented. The method is capable of predicting forces, moments, and detailed surface pressures on thin, sharp-edged wings of rather arbitrary planform. (It should be noted that operational limitations related to doublet panel spacing and density requirements, behavior at large planform breaks, convergence characteristics, etc., have yet to be extensively explored.) The wing geometry is arbitrary in the sense that leading and trailing edges may be curved or kinked, and the wing may have arbitrary camber and twist. The method employs an inviscid flow model in which the wing and the rolled-up vortex sheets are represented by piecewise continuous, quadratic doublet sheet distributions. The Kutta condition is imposed along all wing edges. Strengths of the doublet distributions, as well as shape and position of the free vortex sheet spirals, are computed in iterative fashion, starting with an assumed initial sheet geometry.

The numerical method has been written in FORTRAN 2.3 language for the CDC 6400/6600 digital computers. To demonstrate the validity of the method, selected planar wing geometries have been analyzed in incompressible flow over a wide range of angle of attack. These geometries include: (1) delta wings of differing aspect ratios, (2) an arrow wing, and (3) a gothic wing with swept trailing edge. Wing normal force coefficients, load distributions, and detailed surface pressure distribution are presented and compared, whenever possible, with theoretical results of the leading-edge suction analogy and with experimental data. Good agreement with the available theoretical and experimental data is demonstrated.

During the contract period only a limited number of check cases were executed. It has since been found that more general wing geometries, particularly ones with kinked leading edges, might experience convergence problems. Problems of this type can be caused by inadequate panel density, a poor initial guess for the fed sheet geometry, and inappropriate modeling at planform breaks where a second free vortex is sometimes present. Ongoing work is aimed at improving and clarifying the operational limits of the program.

INTRODUCTION

The flow at the leading and tip edges of a swept wing with sharp edges separates at moderate to high angles of attack, producing vortex sheets that roll up into strong vortices above the upper surface of the wing. The formation of these vortices is responsible for the well-known nonlinear aerodynamic characteristics exhibited over the angle-of-attack range (fig. 1).

A description of the physical aspects of the flow phenomenon is provided in references 1 and 2. A line of attachment (point A in fig. 2) is found inboard of the leading and tip edges on the lower, or windward, side of the wing. The crossflow velocity components inboard of this line are small, so the flow is swept rapidly downstream in this region. The flow velocity outboard of this line of attachment is of the order of the freestream speed, and streams outward from the leading edge. A similar outward flow occurs on the upper surface of the wing with about the same velocity but with a different direction. A shear layer is convected from the leading and tip edges to a position above the wing under the influence of its own vorticity, where it rolls up to form the principal vortex. The air outboard of the shear layer flows first upward, then inboard and around the principal vortex, and finally downward toward the wing, forming a line of reattachment on the upper surface (point B in fig. 2). The crossflow velocity inboard of this line of attachment is small, and hence the air in this region flows rapidly downstream.

Just outboard of the upper surface attachment, the flow is directed toward the leading and tip edges. It accelerates before passing under the principal vortex, and then slows as it approaches the edge. The boundary layer sometimes separates because of the adverse pressure gradient. The flow immediately reattaches, forming a secondary vortex in the opposite sense to the principal vortex, and the flow then continues outward to form the shear layer off the leading edge. A weaker tertiary vortex has also been observed in the boundary layer near the edge. The secondary and tertiary vortices, for simplicity, are not shown in figure 2. Experimental studies of the principal shear layer indicate that its form is relatively independent of Reynolds number.

The rolled-up part of the vortex sheet consists of three regions: (1) an outer region in which the distance between turns is large compared to the diffusion distance $\sqrt{\nu t}$, where ν is the kinematic viscosity and t is the time in which the fluid element in the sheet has traveled from the wing leading edge; (2) an inner region where the distance d between turns is of the same order of magnitude as the diffusion distance; and (3) an inner viscous core that is very small and represents only about 5% of the diameter of the vortex sheet. In the outer region, where $d > \sqrt{\nu t}$, convection is the dominating influence. In the second region where d is of the order of $\sqrt{\nu t}$, the vortex layers are less defined but convection is still important, while diffusion dominates the central viscous core.

The leading-edge suction analogy described in references, 3, 4, and 5 provides a method suitable for calculating the magnitude of the nonlinear vortex lift on a rather broad class of wing planforms. Polhamus (ref. 3) reasoned that the normal force needed for the

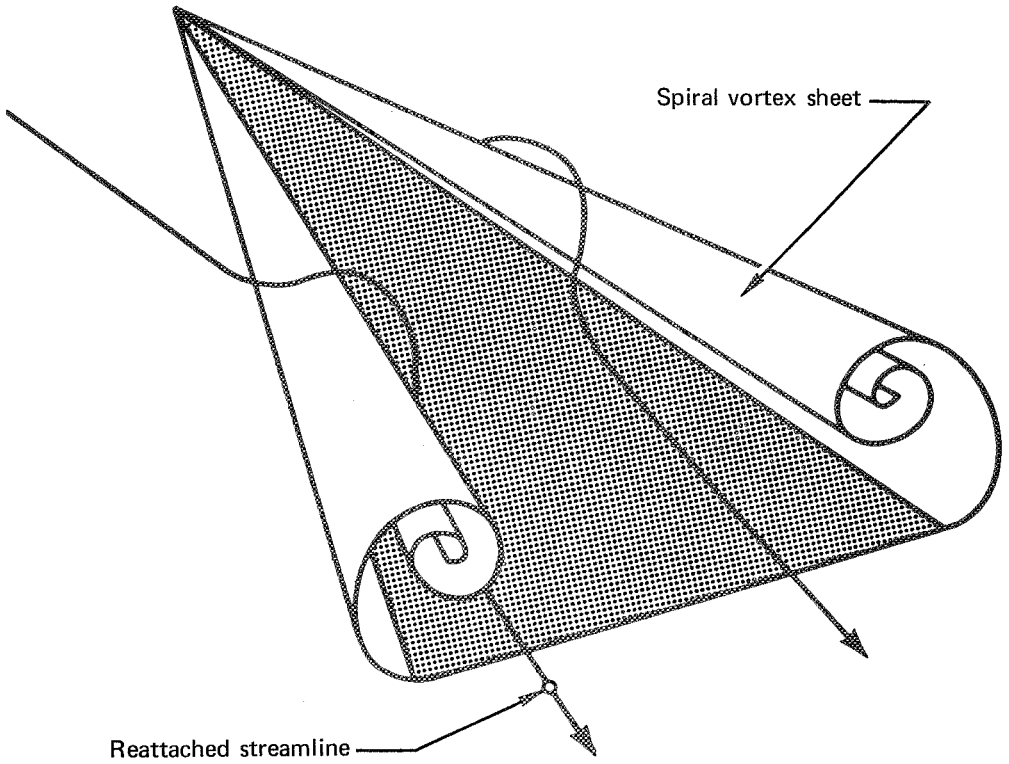

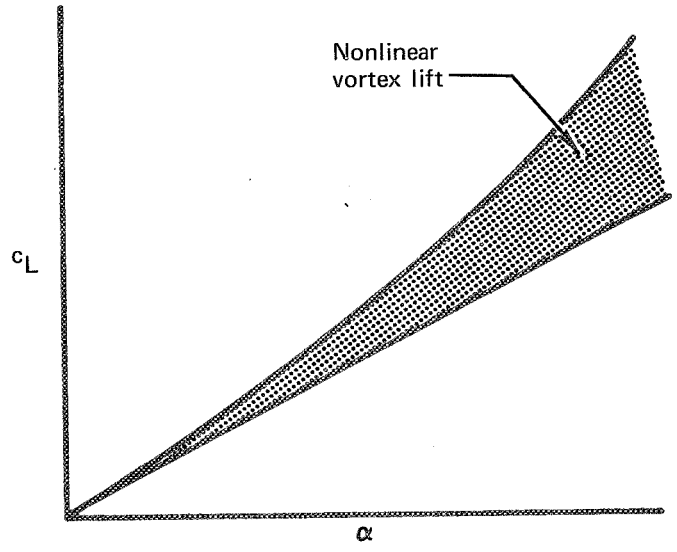

Figure 1.—Leading-Edge Vortex Flow

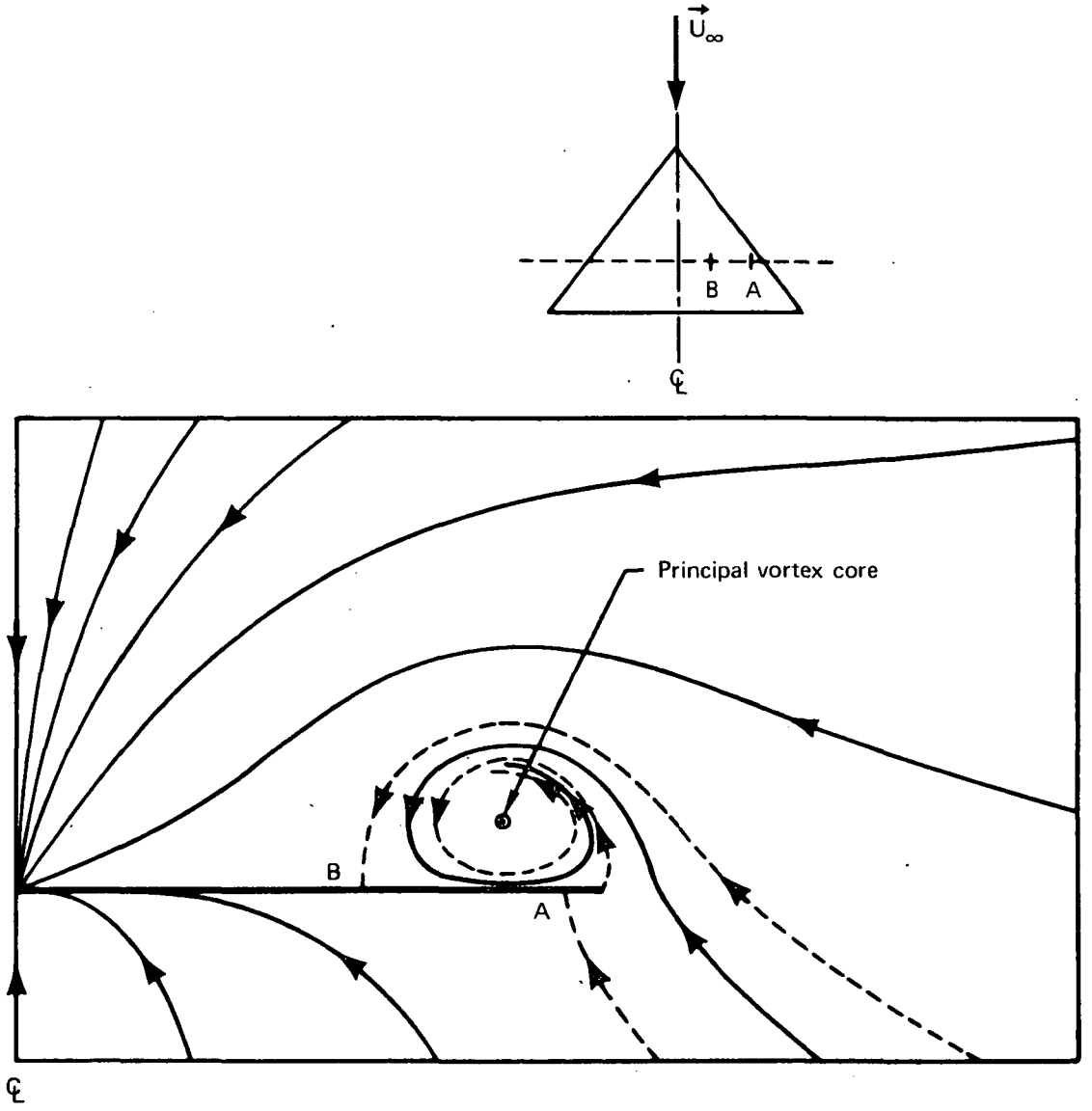

Figure 2.—Cross Section of Flow Over Delta Wing With Leading-Edge Vortex (Crossflow Model)

flow around a leading edge to reattach to the wing is equivalent to the leading-edge suction force necessary to force the flow to be attached to the leading edge in an unseparated condition. The unseparated leading-edge suction force is calculated, and then rotated normal to the wing to obtain the lift contribution of the leading-edge vortex. The total wing lift computed by this method agrees well with experimental data, but the leading-edge suction analogy does not give flow-field details or detailed surface pressure distributions.

Several attempts have been made in the past to theoretically predict detailed pressure distributions and flow fields about swept wings with leading-edge vortex separation. Most of these past methods were limited to slender configurations in which considerable simplification occurred because the problem could be reduced to a solution of Laplace's equation in the crossflow plane, for which conformal mapping became a powerful tool. Smith (ref. 6) developed the best known method of this type by improving the work done earlier in collaboration with Mangler (ref. 7). Assuming conical flow, which is approximately valid near the apex of the wing, he was able to predict qualitatively the type of pressure distributions that had been observed experimentally. Those pressure distributions (fig. 3) exhibited a vortex-induced pressure peak at about 70% local semispan of the wing. Toward the trailing edge, Smith's method overpredicted the experimental load distribution by a considerable amount, the reason being that his conical theory did not satisfy the Kutta condition at the trailing edge. Figure 3 shows qualitatively such a comparison of Smith's theory with experiments and also, for illustrative purposes, spanwise pressure distributions from linear lifting surface theory (ref. 8) and from R. T. Jones' slender wing theory (ref. 9) at two chordwise stations of a delta wing. This figure (supplied by Mr. Blair Gloss of NASA Langley), shows clearly that none of these theories can even approximately predict aerodynamic load distributions of wings with leading-edge vortex separation, and demonstrates the need for an accurate prediction method for this type of flow phenomenon.

Several authors have published prediction methods based on the vortex lattice technique, among them Rehbach (ref. 10), Mook and Maddox (ref. 11), and Kandil, Mook, and Nayfeh (refs. 12 and 13). Sufficient data on pressure distributions have not been available from these references for a thorough comparison with the method of this document.

The method described in this report models the flow over wings with leading-edge vortex separation as an inviscid and irrotational problem. The method is completely three-dimensional and capable of predicting detailed pressure distributions as well as overall wing-load coefficients. The wing, wake, and primary vortex sheet are modeled as thin surfaces. No attempt is made to model secondary flow separation or multiple primary vortex sheets. Special attention is paid to the modeling of the viscous core of the rolled-up vortex spiral within the framework of inviscid flow theory. This viscous core model is termed the "fed sheet model" in this report. A very simple treatment of the core region is adopted, justified mainly because the diameter of the viscous core region is small compared to its distance from the wing. The fed sheet model described in this report, although adequate for most wing geometries and flight conditions, can be improved and must, therefore, be viewed as an interim solution.

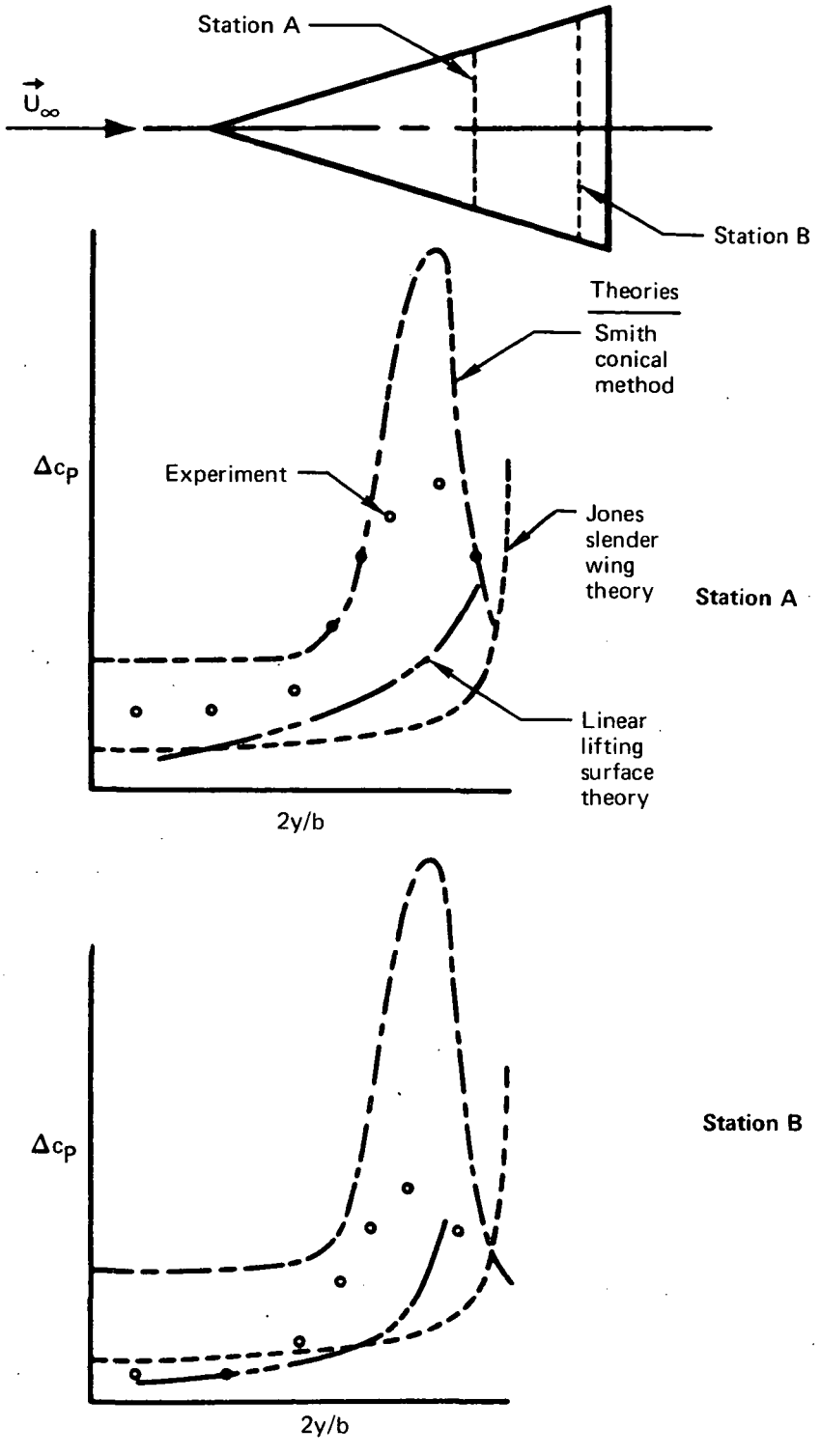

Figure 3.—Load Distribution on Delta Wing Given by Earlier Theories

An advanced aerodynamic panel method (ref. 14) is used to solve the mathematical model problem describing the leading-edge vortex flow. This new method uses source and doublet panel networks as basic building blocks from which a great variety of boundary value problem representations can be composed. In the present work, only the doublet networks are used to simulate the thin surfaces under consideration, but the computational algorithms (e.g., source networks) are available for extending the method to handle wing thickness and fuselage simulation in the presence of free vortex flows.

A short summary of the method described in this document has previously been published (ref. 15).

SYMBOLS

$[A]$	matrix of aerodynamic influence coefficients
$\vec{A}_{ij}$	vector in the near plane of a panel surface
A_{kj}	aerodynamic influence coefficient
AR	aspect ratio
a	parameter of Smith's conical solution
$[B]$	matrix, defined by equation (42)
$\vec{B}_{ij}$	vector in the near plane of a panel surface
b	wing span
$[C]$	matrix, defined by equation (23)
$[C_0]$	matrix, defined by equation (41)
C_{00}, $C_{0\xi}$, $C_{0\eta}$, $C_{0\xi\xi}$, $C_{0\xi\eta}$, $C_{0\eta\eta}$	coefficients, defined by equation (60)
c_L	lift coefficient
c_m	pitching moment coefficient
c_N	normal force coefficient
c_P	pressure coefficient
Δc_P	jump in pressure coefficient
c_r	root chord
c_{ref}	reference length
$D^{(i)}$	correction term of Jacobian
$[D]$	matrix, defined by equation (19)
$[DK]$	matrix, defined by equation (40)
E	function, see equation (46)
$\vec{e}_\xi$, $\vec{e}_\eta$, $\vec{e}_\zeta$	unit vectors of local panel coordinate system

F	function, see equation (46)
$\vec{F}$	force
$f^{(i)}$	vector, defined by equation (52)
G	function, see equation (46)
J	Jacobian
$[K]$	matrix, defined by equation (37)
$K(P,Q)$	potential of an elementary doublet
$l_{i,m}$	chord length of panel segment in transverse geometry cut
M	number of panels on one-half of configuration
M_P	pitching moment
M_∞	freestream Mach number
N	number of doublet parameters in neighborhood of panel
N_D	number of doublet parameters on one-half of the configuration
N_F	normal force
N_{FS}	number of free-sheet panels on one-half of the configuration
N_W	one-half of the number of wing panels
$\vec{n}$	panel normal vector
P_{ij}	panel corner point
$\vec{P}_{ij}$	vector defining panel corner-point location
$P_{0_{ij}}$	panel center
$P(\xi,\eta,\zeta)$	position of field point
$Q(\xi,\eta)$	position of elementary doublet
R	residual
$\vec{r}_{PQ}$	vector from elementary doublet to field point

S	panel area
S_W	wing area
s	local wing semispan
t	time
U_k	component of freestream velocity
$\vec{U}_\infty$	freestream velocity
$\vec{V}$	velocity
V_n	normal velocity component
$\vec{V}^S$	average sheet velocity
$\vec{v}$	velocity induced by a panel doublet distribution
W_k	weights
x,y,z	wing fixed Cartesian coordinate system
x_0, y_0, z_0	coordinates of panel center
x_P	pitch axis
Δx	distance between transverse geometry cuts in x-direction
α	angle of attack
Γ	strength of line vortex along terminated edge
γ	semiapex angle of delta wing
$\overline{\gamma}$	constant in Quasi-Newton method
$\vec{\gamma}$	vorticity
Δ	jump or perturbation of variable
$\delta^{(i)}$	scaling parameter
δ_{ij}	Kronecker delta
θ	panel inclination in transverse cut

Λ	sweep angle
$\mu(\xi,\eta)$	strength of panel doublet distribution
μ_e	doublet parameters along edges of networks
μ_j	doublet parameters on one-half of configuration
μ_k	doublet parameters in neighborhood of panel
μ_r	doublet parameters not located along edges of networks
μ_0, μ_ξ, μ_η, $\mu_{\xi\xi}$, $\mu_{\xi\eta}$, $\mu_{\eta\eta}$	coefficients of panel doublet distribution
ν	kinematic viscosity
Φ	velocity potential
ξ, η, ζ	local panel coordinates

Subscripts

LE	leading edge
L	left side of configuration
l	lower side of sheet
R	right side of configuration
TE	trailing edge
u	upper side of sheet
x,y,z	components in wing fixed Cartesian coordinates
ξ,η,ζ	components in local panel coordinates
∞	freestream value

Superscripts

D	difference of values across the sheet
(i)	iteration number
S	average values of both sides of the sheet
T	transpose of a vector

THEORETICAL METHOD

BOUNDARY VALUE PROBLEM

The flow over wings with leading-edge vortex separation is modeled on the following assumptions:

- The wing is a thin surface (camber surface) in steady, symmetric flight.
- The flight Mach number is low subsonic; i.e., the flow can be regarded as incompressible.
- Vortex lift is produced by a symmetric pair of primary vortex sheets separating from the leading edges of the wing.
- Secondary flow separation and boundary layer displacement effects are neglected.
- Multiple primary vortex sheets do not form.
- The flow surrounding wing and vortex sheets can be regarded as inviscid and irrotational, i.e., as potential flow.
- Vortex breakdown does not take place.
- The diameter of the viscous core of the rolled-up primary vortex sheet is small by comparison with its distance from the wing surface and by comparison with a characteristic lateral dimension of the wing.

The essential elements of this inviscid, irrotational, and incompressible flow model are the wing, wake, primary vortex sheet (termed free sheet), and the so-called fed sheet representing the core of the rolled-up vortex sheet (fig. 4).

The flow is governed by Laplace's equation for the velocity potential, Φ

$$\nabla^2\Phi = 0 \tag{1}$$

The velocity, $\vec{V}$, in turn is obtained from

$$\vec{V} = \nabla\Phi \tag{2}$$

The boundary conditions imposed on the flow model are:

- The flow must be everywhere parallel to the wing surface, i.e.,

$$\vec{n} \cdot \vec{V}^S = 0 \tag{3}$$

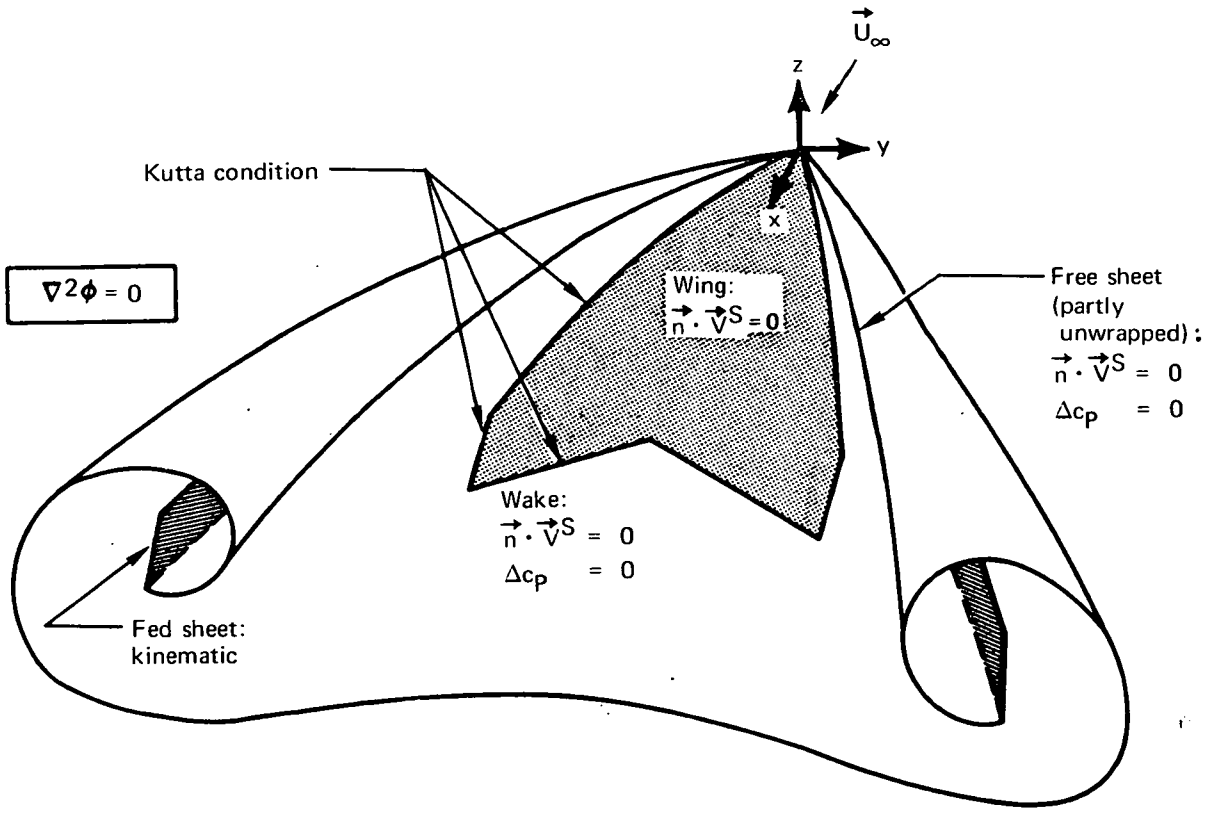

Figure 4.—Boundary Value Problem

The symbol $\vec{n}$ stands for the unit normal vector of the considered surface. The superscript S of the velocity indicates an average sheet velocity, defined by

$$\vec{V}^S = \tfrac{1}{2}(\vec{V}_u + \vec{V}_l) \tag{4}$$

where $\vec{V}_u$, $\vec{V}_l$ are the velocities on the upper and lower sides of the sheet surface, respectively.

- The free sheet and the wake cannot support a pressure differential. This statement expressed in terms of the jump in pressure coefficient across the sheet reads

$$\Delta c_p = 0 \tag{5}$$

In addition, free sheet and wake are stream surfaces; i.e., they must satisfy

$$\vec{n} \cdot \vec{V}^S = 0 \tag{6}$$

- Kutta conditions are imposed along the leading, side, and trailing edges of the wing in the presence of free sheets and wake emanating from these edges.

The Kutta condition need not be treated as a separate boundary condition. Satisfaction of the stream-surface boundary conditions (3) and (6) of wing, free sheet, and wake will result in a smooth flow off the wing edges. The additional requirement of zero pressure jump across the free sheet and wake in the immediate vicinity of the wing edges is already stated by equation (5).

- The freestream is undisturbed at infinity.

- The fed sheet (fig. 4) is an entirely kinematic extension of the free sheet. Its dimensions are taken from a conical flow solution used as the "initial guess" in the present iterative solution procedure applied to the fed sheet. This is a simplified model of the true physical vortex core region, which is viscosity dominated. The tacit assumption in this model is that the boundary conditions applied to the free sheet are sufficient to adequately position the fed sheet. Appendix A explains why this model is used instead of one in which the fed sheet is required to be force-free.

GEOMETRY DEFINITION

GENERAL DESCRIPTION

The geometry of the configuration (fig. 5) consists of four elements: wing, free sheet, wake, and fed sheet.

The wing is represented by the mean geometric surface (camber surface) with an arbitrary distribution of camber and twist. The wing must have a pointed upstream apex. Leading and trailing edges of the wing may be curved or straight, and the latter may be swept forward or backward. The panel scheme described replaces curved wing edges with straight-line segments.

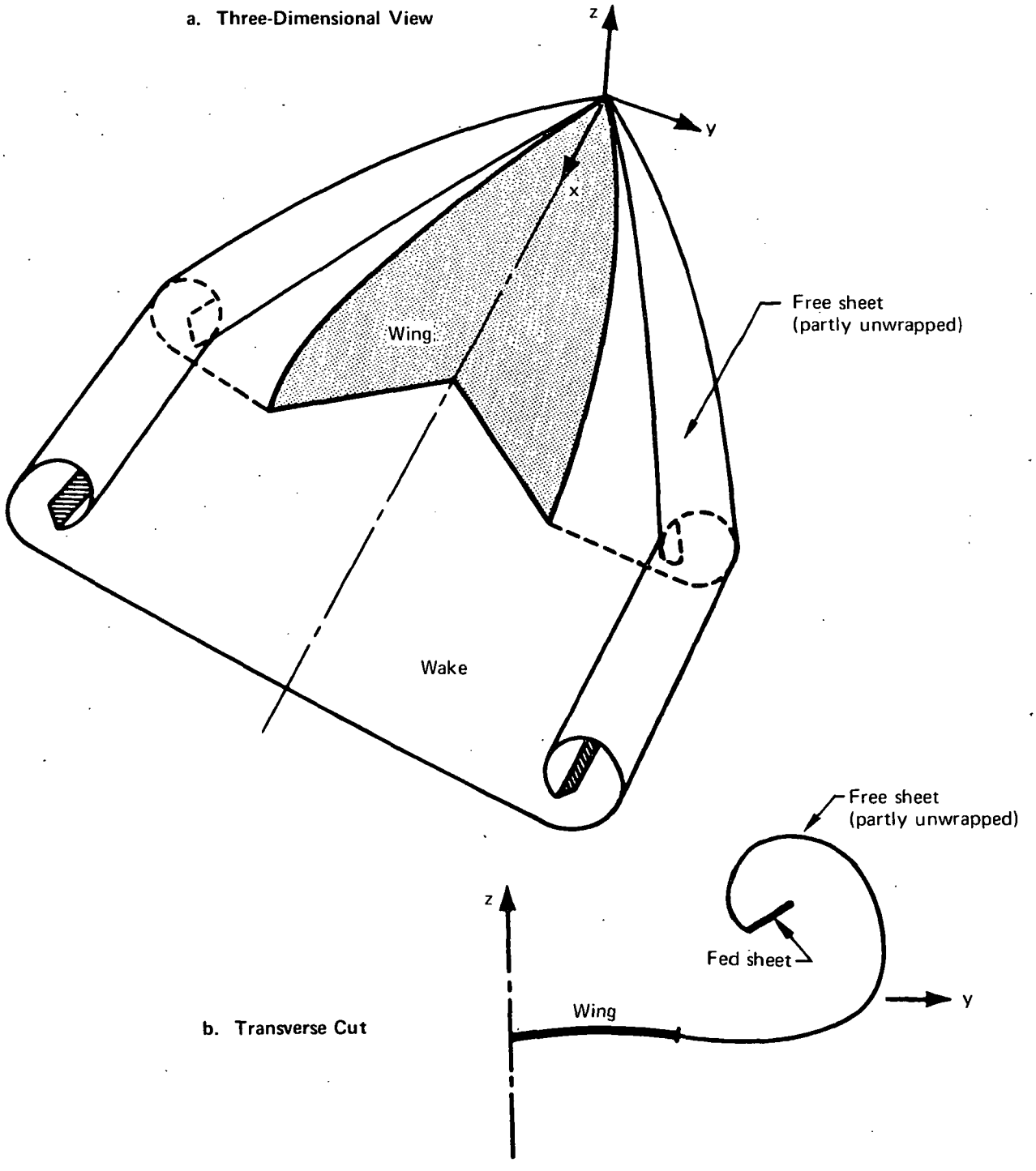

Figure 5.—Elements of Configuration

The free sheet, a thin surface attached to the leading edge of the wing, extends in the streamwise direction from the apex of the wing to the point of maximum local wing span. The shape of the free sheet in a transverse cut through the configuration approximates a spiral. Approximately one-half of the first turn of the spiral provides a sufficient model in most cases.

The wake is a thin surface attached to the trailing edge of the wing downstream of the point of maximum span and includes the extension of the free sheet in the downstream direction (fig. 5). The wake geometry is generated by straight lines parallel to the x-axis of the wing-fixed Cartesian coordinate system.

The trace of the fed sheet surface in a transverse cut (y,z-plane) through the configuration is a straight line connected to the last point of the free sheet and is approximately perpendicular to the free sheet.

The geometry of the configuration is symmetric with respect to the x,z-plane.

PANEL SCHEME

The geometry of the configuration is defined by panel corner points. A wing-fixed Cartesian coordinate system is employed to specify corner-point positions. The origin of this x,y,z-coordinate system (fig. 5) coincides with the apex of the wing. The x-axis (positive in downstream direction) is parallel to the wing root chord.

The geometry of the configuration is paneled as follows. The x-coordinates of transverse planes cutting the configuration (fig. 6) are specified. The distance Δx between cuts need not be equal. These transverse cuts define the x-coordinates of all panel corner points. The wake region is not cut, but is bounded by a transverse cut far downstream of the wing. The computer code places this last cut at 50 wing root chords downstream of the wing.

Corner points of the panels are then defined along the geometry contours of each transverse cut. This must be done such that the number of wing panels is the same in each spanwise row of panels. The same rule must be observed when paneling the free sheet. Figure 7 shows the panel corner points in a typical transverse cut through wing and free sheet. The fed sheet is represented by a single panel in the y,z-plane.

The paneling of the wake is completely determined by that of the wing, free sheet, and fed sheet. A single wake panel is used in the downstream direction. The wake panels are generated by straight lines parallel to the x-axis.

Examples of the wing panel scheme are shown in figure 8. Because of symmetry, only one-half of the configuration needs to be paneled. Curved wing planforms are approximated by straight-line segments. (The algorithms extending the numerical representation to encompass curved panels are now available, ref. 14, but were not implemented in the present work.) Figure 9 displays a spanwise row of quadrilateral free-sheet panels between two adjacent transverse cuts. An example of the wake paneling is given in figure 10 in which the wake panels downstream of the free sheet

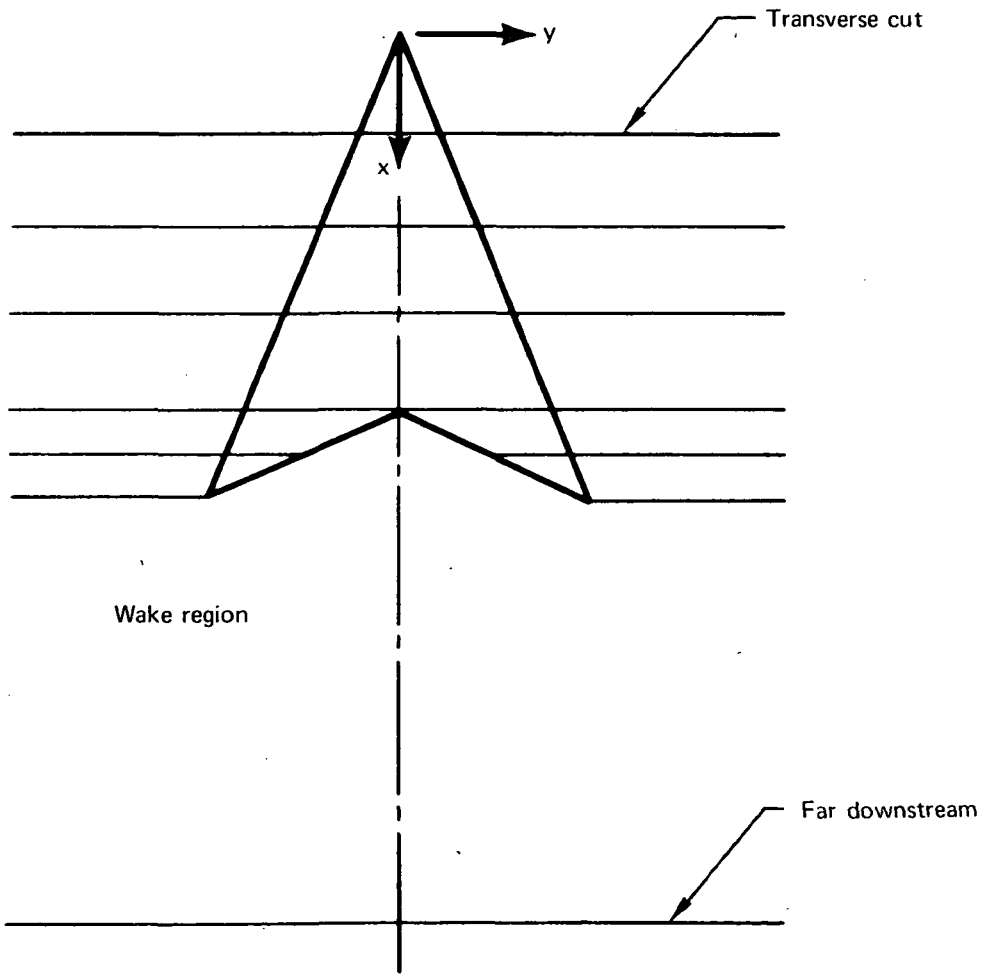

Figure 6.—Transverse Cutting Planes of Configuration

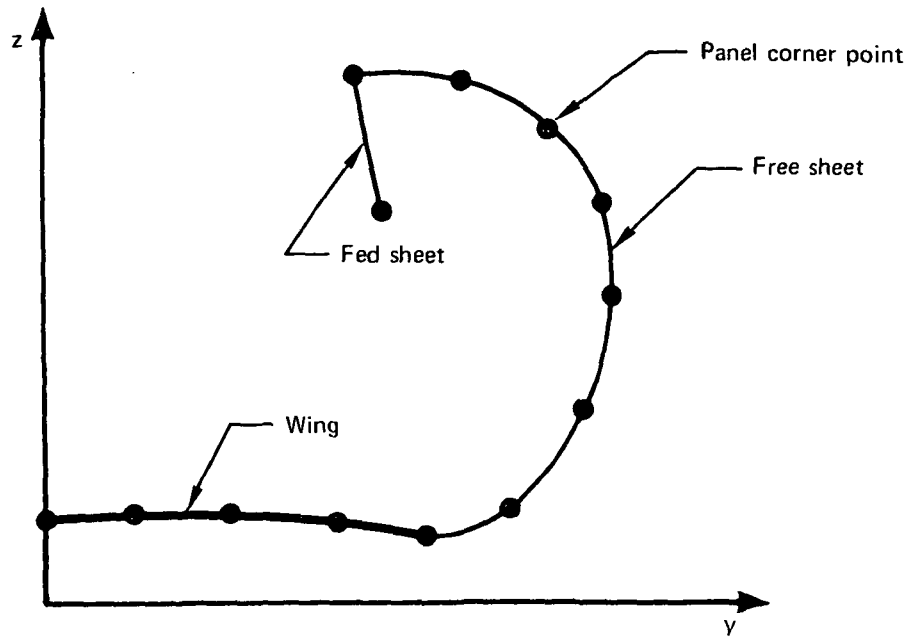

Figure 7.—Panel Corner Points in Transverse Cut of Configuration

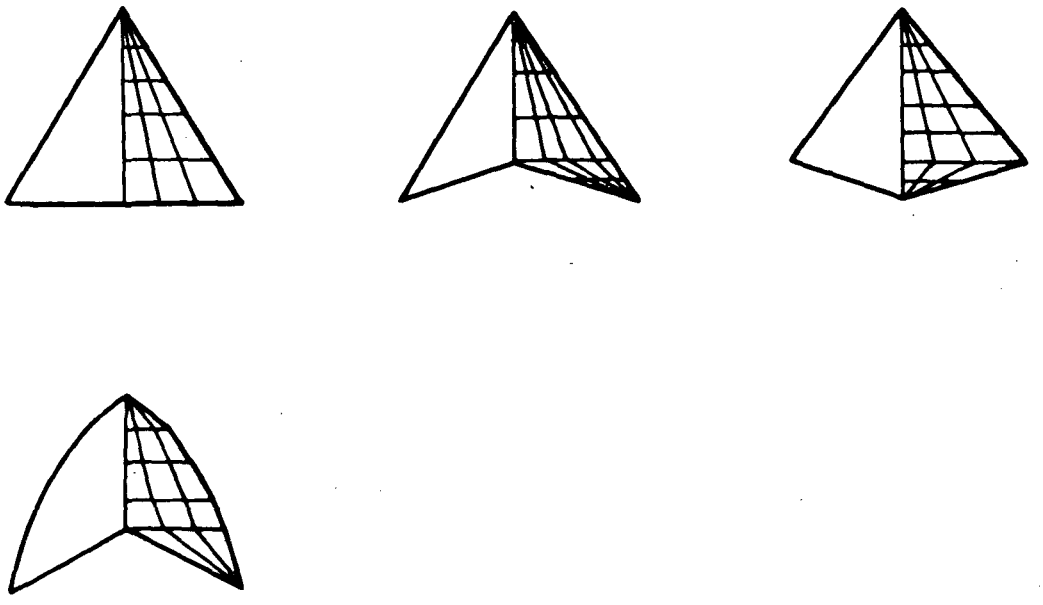

Figure 8.—Examples of Wing Paneling

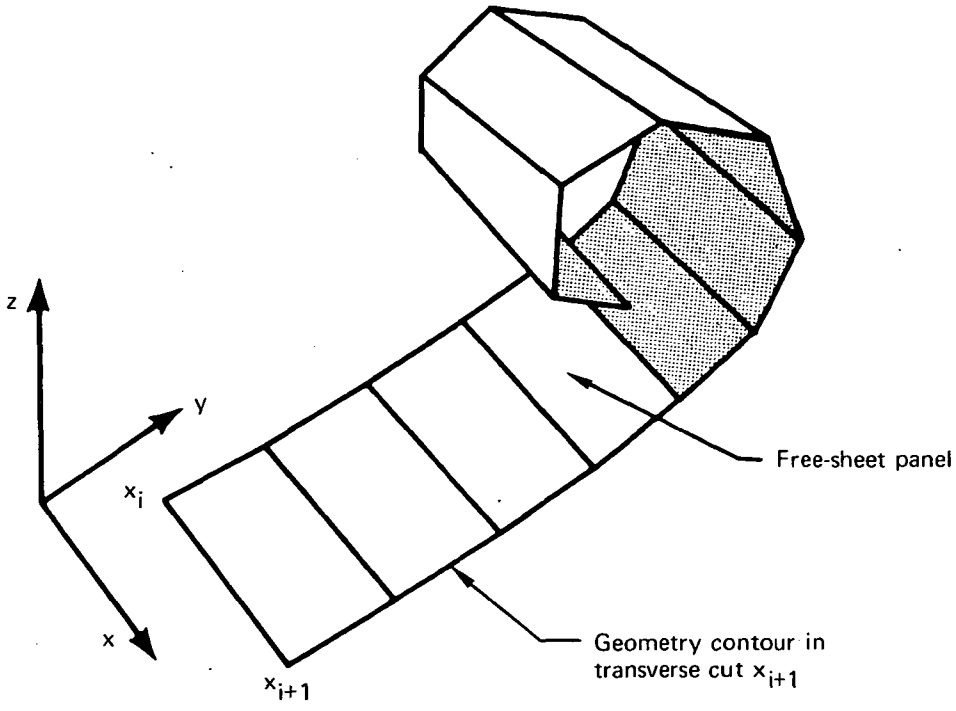

Figure 9.—Spanwise Row of Free-Sheet Panels

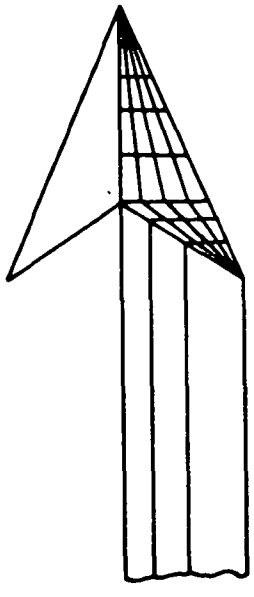

Figure 10.—Example of Wake Paneling (Not Complete)

are not visible. It can be noted in figure 10 that in the spanwise direction the number of wake panels is not always the same as the spanwise number of wing panels.

PANEL GEOMETRY

Consider the single panel shown in figure 11 located between two transverse cuts, x_i and x_{i+1}. The same type of panel geometry is used for the paneling of the wing, free sheet, fed sheet, and wake. Triangular panels such as those at the apex of the wing are special cases of the shown quadrilateral panel shape in which two corners coalesce.

The four corner points of a panel, P_{ij}; $P_{i,j+1}$; $P_{i+1,j}$; $P_{i+1,j+1}$, are used to define a planar panel surface that approximates the nonplanar geometry surface. This planar surface is the so-called near plane defined by and containing the vectors $\vec{A}_{ij}$ and $\vec{B}_{ij}$ (see fig. 11). The latter are written in terms of vectors that define the panel corner point locations as

$$\vec{A}_{ij} = \vec{P}_{ij} + \vec{P}_{i,j+1} - \vec{P}_{i+1,j} - \vec{P}_{i+1,j+1} \tag{7}$$

$$\vec{B}_{ij} = \vec{P}_{ij} + \vec{P}_{i+1,j} - \vec{P}_{i,j+1} - \vec{P}_{i+1,j+1}$$

The panel normal vector $\vec{n}$ at the center $P_{0_{ij}}$ of the (ij)th panel is then

$$\vec{n} = \frac{\vec{A}_{ij} \times \vec{B}_{ij}}{|\vec{A}_{ij} \times \vec{B}_{ij}|} \qquad \vec{n} = (n_x, n_y, n_z) \tag{8}$$

Projecting the four corner points onto the near plane and connecting the new points by straight lines defines the panel geometry. All original corner points turn out to be equidistant from their projections onto the near plane.

In addition to the global Cartesian x,y,z-coordinate system, a local panel coordinate system (fig. 11) is introduced whose ξ,η,ζ-coordinates are defined as follows. The ζ-coordinate points in the direction of the panel normal; the η-axis is perpendicular to ζ and to the x-coordinate of the global coordinate system. The ξ-axis (positive in downstream direction) forms, with η and ζ, a right-handed Cartesian coordinate system. The ξ- and x-axes are in general not parallel. The unit vectors of the local panel coordinate system are denoted by $\vec{e}_\xi$, $\vec{e}_\eta$, $\vec{e}_\zeta$.

The transformation from x,y,z- to ξ,η,ζ-coordinates is performed by

$$\begin{Bmatrix} \xi \\ \eta \\ \zeta \end{Bmatrix} = \begin{bmatrix} n_y^2 + n_z^2 & -\dfrac{n_x n_y}{\sqrt{n_y^2 + n_z^2}} & -\dfrac{n_x n_z}{\sqrt{n_y^2 + n_z^2}} \\ 0 & \dfrac{n_z}{\sqrt{n_y^2 + n_z^2}} & -\dfrac{n_y}{\sqrt{n_y^2 + n_z^2}} \\ n_x & n_y & n_z \end{bmatrix} \begin{Bmatrix} x - x_0 \\ y - y_0 \\ z - z_0 \end{Bmatrix} \tag{9}$$

where the coordinates of the panel center $P_{0_{ij}} = (x_0,y_0,z_0)_{ij}$ are the average values of the original panel corner-point coordinates.

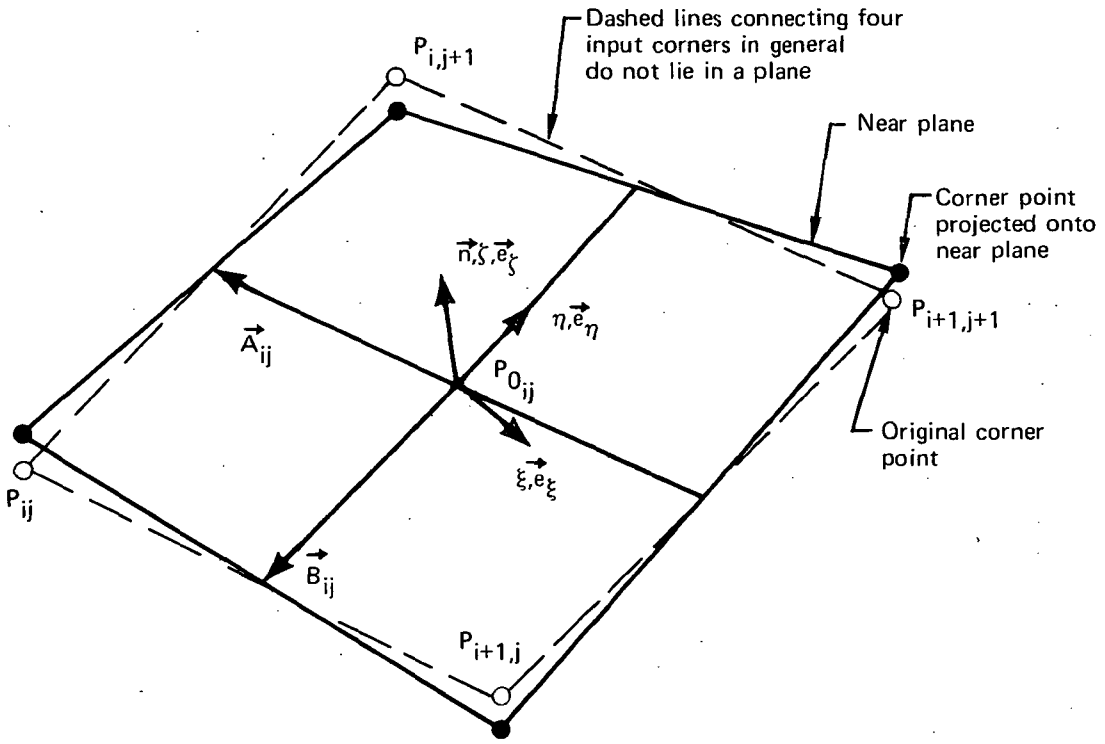

Note: All original corner points turn out to be equidistant from their projections onto the near plane

Figure 11.—Single-Panel Geometry

NUMERICAL METHOD

INTRODUCTORY REMARKS

The numerical solution of the boundary value problem is accomplished by a panel-type influence coefficient method. The numerical method formulated in this section is entirely based on an advanced panel method for the solution of Laplace's equation subject to Neumann, Dirichlet, or mixed boundary conditions (ref. 14). Only certain features of this new method that center about the use of doublet distributions to represent the various elements of the adopted aerodynamic model are employed.

The surface of the configuration is divided into panels, as explained in the section on "Geometry Definition." Doublet distributions dependent on a finite number of unknown doublet parameters are defined for each panel. A finite number of control points on the surface are selected at which the boundary conditions are satisfied. This discretization of the problem leads to an aerodynamic influence coefficient formulation wherein the solution is achieved by assembling logically independent networks of doublet panels. In this context, a network is defined as a portion of the boundary surface on which a certain distribution of doublet strength is specified, together with properly posed analysis (Neumann) or design (Dirichlet) boundary conditions. It is always composed of a rectangular array of panels that may be input independently of all other networks. A network is logically consistent in that it contributes as many equations to the overall problem as it contributes unknowns.

The essential features of the numerical method are:

- Discrete values of doublet strength are assigned to certain standard points on each network. A local distribution of surface singularity strength is obtained by fitting a quadratic doublet form to these discrete values in an immediate neighborhood by the method of least squares.

- Certain standard points on each network are assigned as control points. These points include panel center points as well as edge abutment downwash points. The latter serve to automatically impose standard aerodynamic edge conditions, e.g., the Kutta condition, zero potential jump at thin edges, continuity of singularity strength across abutting networks, etc., producing logical independence for each network. In all cases, the number of boundary conditions on each network coincides with the number of assigned surface singularity parameters.

- Two expansions are employed in the calculation of the aerodynamic influence coefficients: a near-field expansion and a far-field expansion. All resultant integrals are evaluated in closed form using recursion relations, which contain the fundamental logarithm and arc tangent transcendental terms that appear in constant-strength panel techniques.

DOUBLET PANEL

The distribution of doublet strength $\mu(\xi,\eta)$ on a panel is quadratic; i.e.,

$$\mu(\xi,\eta) = \mu_0 + \mu_\xi \xi + \mu_\eta \eta + \mu_{\xi\xi} \frac{1}{2}\xi^2 + \mu_{\xi\eta} \xi\eta + \mu_{\eta\eta} \frac{1}{2}\eta^2 \tag{10}$$

The six coefficients, $\mu_0, \mu_\xi, \mu_\eta, \mu_{\xi\xi}, \mu_{\xi\eta}, \mu_{\eta\eta}$ are not assumed independent; rather they are a linear combination of an independent set of doublet parameters μ_j. The parameters μ_j are the singularity strengths at a set of discrete points on the network surface. The linear relationships between the six coefficients and independent doublet parameters are later determined by the method of weighted least squares.

Consider now the velocity $\vec{v}$ induced by a distribution of elementary doublets over a single panel S at a field point P = (ξ,η,ζ).

$$\vec{v}(P) = \iint_S \mu(Q)\, \nabla_P K(P,Q)\, dS \tag{11}$$

The integration is to be carried out over the panel area S with Q = (ξ_1,η_1) denoting the position of the elementary doublet on the planar panel. Further,

$$dS = d\xi_1\, d\eta_1 \tag{12}$$

$$K(P,Q) = \frac{1}{4\pi} \frac{\vec{r}_{PQ} \cdot \vec{n}_Q}{r_{PQ}^3} \qquad |\vec{r}_{PQ}| = r_{PQ} \tag{13}$$

where K(P,Q) is the potential of an elementary doublet. The vector $\vec{r}_{PQ}$ is

$$\vec{r}_{PQ} = (\xi - \xi_1)\vec{e}_\xi + (\eta - \eta_1)\vec{e}_\eta + \zeta \vec{e}_\zeta \tag{14}$$

and points from the position Q of the elementary doublet to the field point P. The vector $\vec{n}_Q$ is the panel normal $\vec{n}_Q$ = (0,0,1) for planar panels. Applying the gradient operator

$$\nabla_P = \frac{\partial}{\partial\xi}\vec{e}_\xi + \frac{\partial}{\partial\eta}\vec{e}_\eta + \frac{\partial}{\partial\zeta}\vec{e}_\zeta \tag{15}$$

to K(P,Q) yields

$$\nabla_P K(P,Q) = \frac{1}{4\pi}\left[\frac{\vec{n}_Q}{r_{PQ}^3} - \frac{3\vec{r}_{PQ}}{r_{PQ}^5}(\vec{r}_{PQ} \cdot \vec{n}_Q)\right] \tag{16}$$

Appendix B contains details of the integration of equation (11). The analysis distinguishes between:

1. Field points P that are located in the vicinity of the panel S, in which case no approximation to the integrand for flat panels is used. Then

$$\frac{1}{r_{PQ}^K} = U^K \qquad U = \frac{1}{\sqrt{(\xi - \xi_1)^2 + (\eta - \eta_1)^2 + \zeta^2}} \qquad K = 3, 5 \tag{17}$$

2. Field points located a sufficient distance away from the panel surface to justify the following approximation to r_{PQ}^{-K}

$$\frac{1}{r_{PQ}^{K}} = U^{K} + KU^{K+2}(\xi\xi_1 + \eta\eta_1)\,;\ K = 3,5 \qquad U = \frac{1}{\sqrt{\xi^2 + \eta^2 + \zeta^2}} \tag{18}$$

This approximation is applied when U is greater than 2.5 times the maximum panel diagonal.

The result of the integration of equation (11) can be written in matrix form as

$$\begin{Bmatrix} v_\xi \\ v_\eta \\ v_\zeta \end{Bmatrix} = [D] \begin{Bmatrix} \mu_0 \\ \mu_\xi \\ \mu_\eta \\ \mu_{\xi\xi} \\ \mu_{\xi\eta} \\ \mu_{\eta\eta} \end{Bmatrix} \tag{19}$$

where v_ξ, v_η, v_ζ are the components of the perturbation velocity $\vec{v}$ in local panel coordinates of the inducing panel.

NETWORKS

The configuration is modeled aerodynamically by five networks termed:

- Analysis network (wing)
- Design network (free sheet)
- Fed-sheet network
- Wake network
- Network number 5

The analysis- and design-type networks are the two basic networks, whereas the remaining three are specializations of the analysis network. The last network is needed for that wake panel downstream of the last fed-sheet panel.

Figures 12 and 13 show schematically the arrangements of doublet parameters μ_j and the control point locations for the analysis and design networks, respectively. These choices of the locations of the doublet parameters ensure a stable computation. For each of these networks the number of control points at which the boundary conditions or edge conditions are satisfied equals the number of unknown doublet parameters. The edge control points serve in the matching of the various networks across their common boundaries. These points are slightly removed from the edges for this purpose (10^{-5} of the maximum panel diagonal).

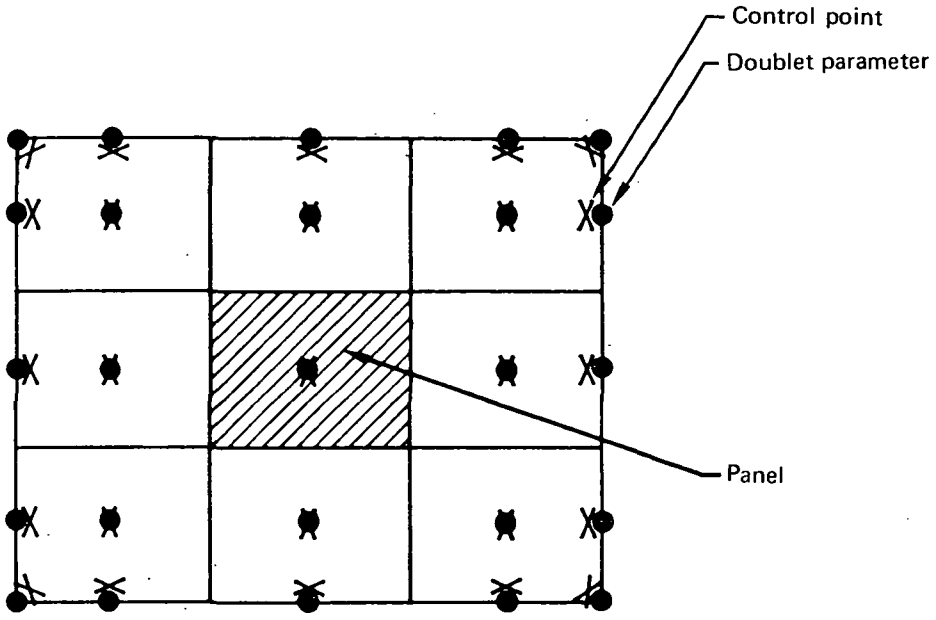

Figure 12.—Analysis Network (Wing)

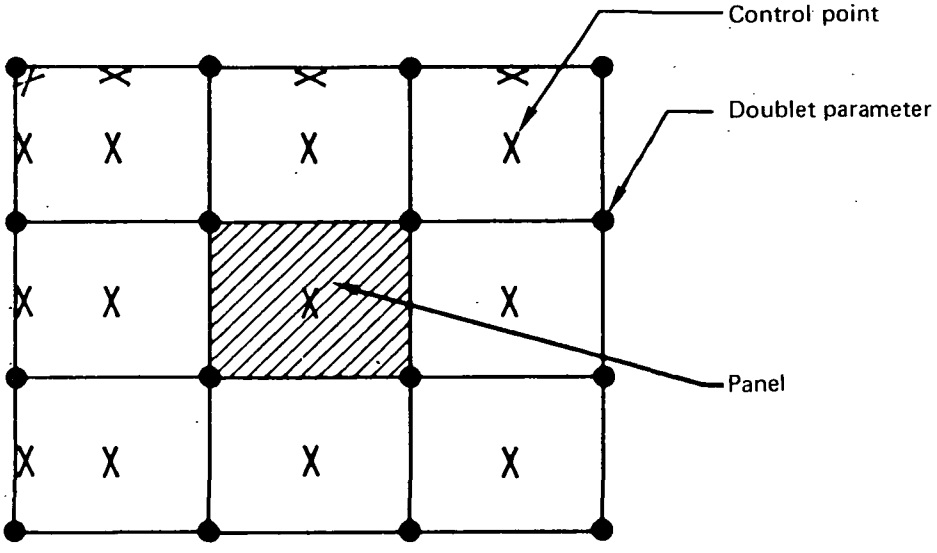

Figure 13.—Design Network (Free Sheet)

An individual panel of both the analysis and the design network is assumed to have a quadratic distribution of doublet strength, which is defined by equation (10) in terms of six coefficients. A linear relationship between these coefficients and those doublet parameters μ_k on the panel itself and on its immediate neighbors is determined by the method of least squares. For each panel S the residual R is minimized.

$$R = \frac{1}{2} \sum_{k=1}^{N} W_k \left[\mu(\xi_k, \eta_k) - \mu_k \right]^2 \tag{20}$$

The weights W_k are chosen large (10^5) when (ξ_k,η_k) actually lies on the panel S, and are unity if not. The number N of the doublet parameters μ_k depends on the position of the panel within a network. In the case of a panel of an analysis network, N equals 9 unless the quadrilateral panel and its neighbors are triangular. For most panels that are part of a design network, the summation is carried out over 16 doublet points. Only panels located along the edges of a design network have fewer neighboring doublet points, in which cases N reduces to 9 or 12.

With $\mu(\xi_k,\eta_k)$ given by equation (10), the residual R reads

$$R = \frac{1}{2} \sum_{k=1}^{N} W_k \left(\mu_0 + \mu_\xi \xi_k + \mu_\eta \eta_k + \frac{1}{2} \mu_{\xi\xi} \xi_k^2 + \mu_{\xi\eta} \xi_k \eta_k + \frac{1}{2} \mu_{\eta\eta} \eta_k^2 - \mu_k \right)^2, \tag{21}$$

which is minimized by

$$\frac{\partial R}{\partial \mu_0} = 0 \quad \frac{\partial R}{\partial \mu_\xi} = 0 \quad \frac{\partial R}{\partial \mu_\eta} = 0 \quad \frac{\partial R}{\partial \mu_{\xi\xi}} = 0 \quad \frac{\partial R}{\partial \mu_{\xi\eta}} = 0 \quad \frac{\partial R}{\partial \mu_{\eta\eta}} = 0$$

This procedure gives the following intermediate result

$$\underset{(6 \times 6)}{[C_1]} \begin{Bmatrix} \mu_0 \\ \mu_\xi \\ \mu_\eta \\ \mu_{\xi\xi} \\ \mu_{\xi\eta} \\ \mu_{\eta\eta} \end{Bmatrix} = \underset{(6 \times N)}{[C_2]} \{\mu_k\} \tag{22}$$

with

$$[C_1] = \begin{bmatrix} \sum W_k & \sum W_k\xi_k & \sum W_k\eta_k & \sum W_k \frac{1}{2}\xi_k^2 & \sum W_k\xi_k\eta_k & \sum W_k \frac{1}{2}\eta_k^2 \\ \sum W_k\xi_k & \sum W_k\xi_k^2 & \sum W_k\eta_k\xi_k & \sum W_k \frac{1}{2}\xi_k^3 & \sum W_k\xi_k^2\eta_k & \sum W_k \frac{1}{2}\eta_k^2\xi_k \\ \sum W_k\eta_k & & & & & \\ \sum W_k \frac{1}{2}\xi_k^2 & & & \text{etc.} & & \\ \sum W_k\xi_k\eta_k & & & & & \\ \sum W_k \frac{1}{2}\eta_k^2 & & & & & \end{bmatrix}$$

and

$$[C_2] = \begin{bmatrix} W_k & W_k & \cdots & W_k \\ \xi_k W_k & \xi_k W_k & \cdots & \xi_k W_k \\ \eta_k W_k & \eta_k W_k & \cdots & \eta_k W_k \\ \frac{1}{2}\xi_k^2 W_k & \frac{1}{2}\xi_k^2 W_k & \cdots & \frac{1}{2}\xi_k^2 W_k \\ \xi_k\eta_k W_k & \xi_k\eta_k W_k & \cdots & \xi_k\eta_k W_k \\ \frac{1}{2}\eta_k^2 W_k & \frac{1}{2}\eta_k^2 W_k & \cdots & \frac{1}{2}\eta_k^2 W_k \end{bmatrix}$$

The desired linear relationship between the six coefficients of the quadratic doublet distribution and the N doublet parameters μ_k can then be written as

$$\begin{Bmatrix} \mu_0 \\ \mu_\xi \\ \mu_\eta \\ \mu_{\xi\xi} \\ \mu_{\xi\eta} \\ \mu_{\eta\eta} \end{Bmatrix} = [C]\{\mu_k\} \qquad (23)$$

where the coefficients of the matrix [C] depend only on the chosen weights W_k and on the geometry of the panel scheme.

Figure 14 shows the wake network unwrapped. This network is of the analysis type but is simplified assuming that the doublet distribution varies only in the lateral or η-direction.

Figure 15 illustrates the chosen positions of doublet parameters and control points for the fed-sheet network, which is like the wake network of the analysis type. The doublet strength is constant in the η-direction, and varies quadratically in the direction parallel to the terminated edge.

The number 5 network needed for the wake panel located downstream of the fed sheet has a constant distribution of doublet strength. This is a consequence of the choice for the doublet distributions of the neighboring fed sheet and wake panels.

MATCHING OF NETWORKS

The relative positions of the five networks described in the previous section are illustrated in figure 16, which also shows the location of most of the control points, particularly those along the edges of networks. The reader will notice that at some boundaries edge control points appear in opposing pairs. This is the case along the centerline of the wing and along leading and trailing edges of the wing. At other boundaries such as the one between free sheet and fed sheet and between free sheet and wake, there is only a single point controlling the edge condition.

The downwash $V_n = \vec{n} \cdot \vec{V}^S$ is specified at edge control points. In order to explain the implications of this edge condition, the downwash in the vicinity of the common edge of two smoothly adjoining networks is expanded as

$$V_n(s) = \frac{\Delta\mu_e}{s} + \Delta\left(\frac{\partial\mu}{\partial s}\right)_e \ln s + \text{regular terms} \tag{24}$$

Here, s is a coordinate tangential to the network surface and perpendicular to the edge, $\Delta\mu_e$ is the jump in doublet strength across the edge, and $\Delta(\partial\mu/\partial s)_e$ is the jump in the derivative of doublet strength across the edge. A control point placed near the edge (e.g., at s = 0+) requiring that downwash be finite will tend to make $\Delta\mu_e$ vanish, i.e. μ_e continuous across the edge. This can easily be shown by taking the limit

$$\lim_{s\to 0+} \Delta\mu_e(s) = \lim_{s\to 0+} \left\{ sV_n(s) - \Delta\left(\frac{\partial\mu}{\partial s}\right)_e s \ln s - s(\ldots) \right\} = 0 \tag{25}$$

Placing a second control point on the opposing panel of an adjoining network will, in addition, force $\Delta(\partial\mu/\partial s)_e$ to vanish, thereby establishing continuity of $(\partial\mu/\partial s)_e$.

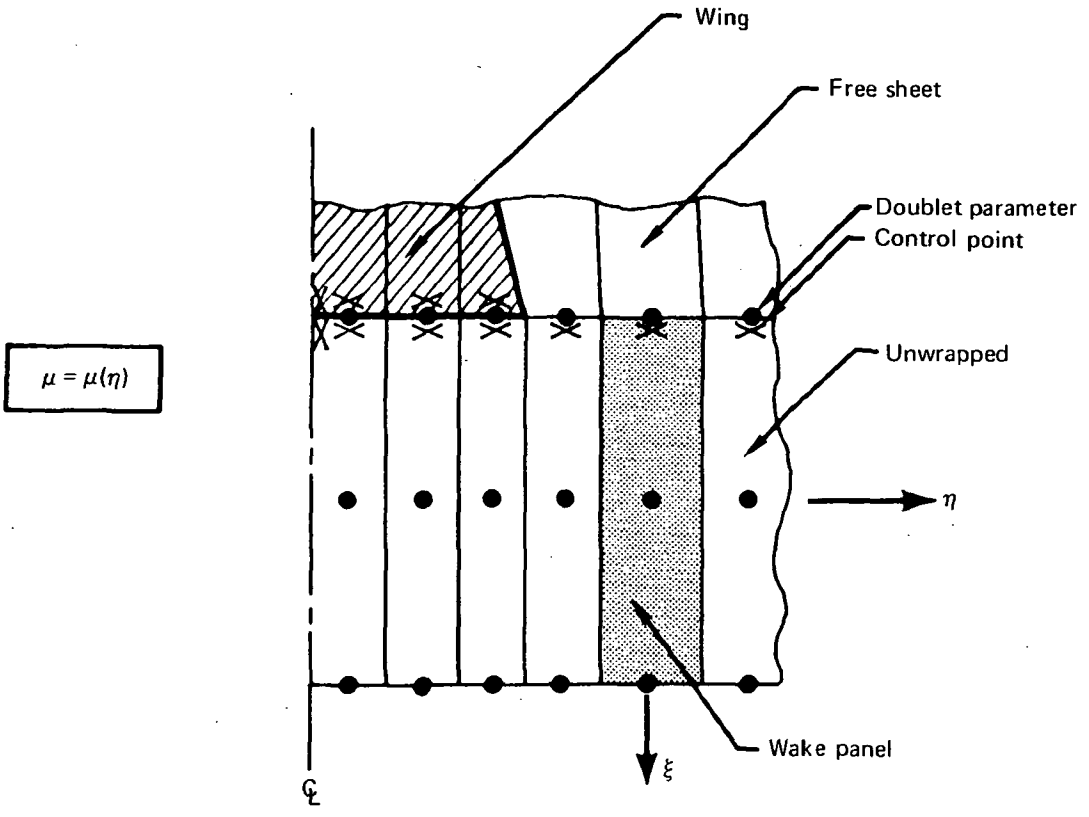

Figure 14.—Wake Network (Simplified Analysis Network)

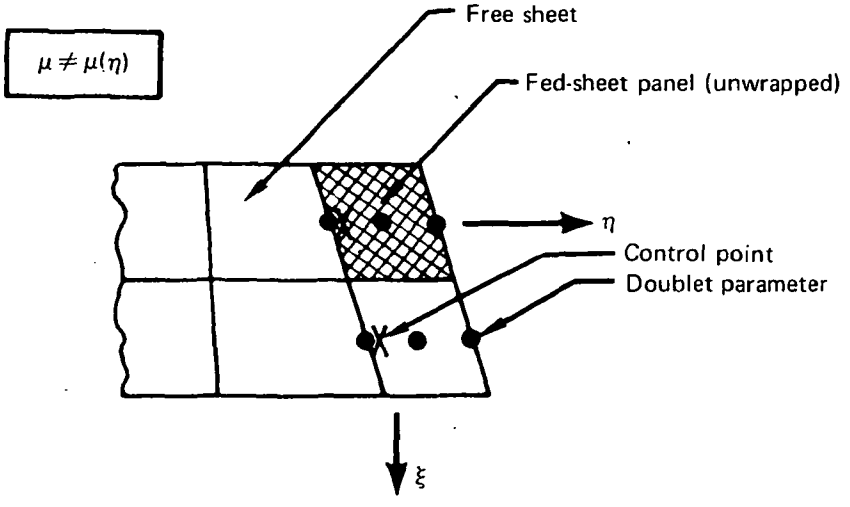

Figure 15.—Fed Sheet Network (Simplified Analysis Network)

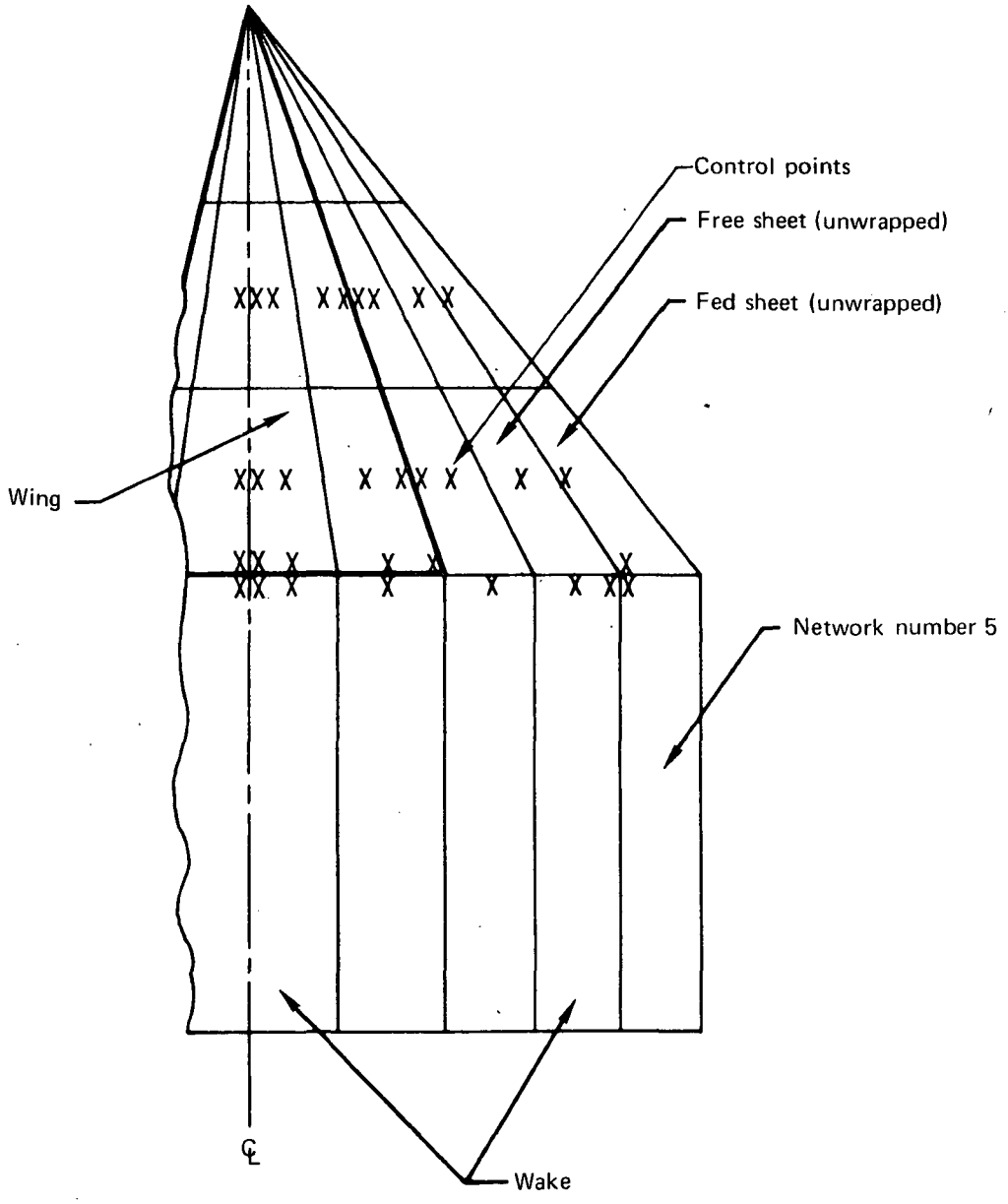

Figure 16.—Matching of Networks

Hence, across the centerline of the wing and across leading and trailing edges, μ as well as $\partial\mu/\partial s$ are continuous, since control points are grouped in pairs along these edges. In addition, the derivative of μ must vanish along the centerline to produce a symmetric distribution of μ. As a consequence of the particular construction of the wake network, the derivative of μ in the freestream direction vanishes along the trailing edge.

Doublet strength, but not its derivative, is continuous across the common boundaries of free sheet and wake, free sheet and fed sheet. Thus it will be seen that the network edge downwash points are, in essence, a logical algorithm designed to produce the desired degree of continuity in doublet strength across network edges, and are functionally quite different from the downwash points appearing in the centers of panels.

AERODYNAMIC INFLUENCE COEFFICIENTS

In subscripted notation, aerodynamic influence coefficients A_{kj} are defined by

$$\vec{V}^S = (A_{kj}\,\mu_j + U_k)\,\vec{e}_k \qquad \begin{matrix} k = \xi, \eta, \zeta \\ j = 1, 2, \ldots N_D \end{matrix} \tag{26}$$

where $\vec{V}^S$ is the average velocity at a particular control point, μ_j are the doublet parameters of one-half of the configuration, N_D is the number of these doublet parameters, and U_k are the components of the freestream velocity in the direction of the local panel coordinates

$$\vec{U}_\infty = (U_\xi, U_\eta, U_\zeta) \tag{27}$$

The vectors $\vec{e}_\xi$, $\vec{e}_\eta$, $\vec{e}_\zeta$ are the unit vectors of the local coordinate system of that panel on which the control point lies. For future reference, equation (26) is rewritten in the form

$$\begin{Bmatrix} V_\xi{}^S \\ V_\eta{}^S \\ V_\zeta{}^S \end{Bmatrix} = \begin{bmatrix} A_{\xi_j} \\ \hline A_{\eta_j} \\ \hline A_{\zeta_j} \end{bmatrix} \begin{Bmatrix} \mu_j \end{Bmatrix} + \begin{Bmatrix} U_\xi \\ U_\eta \\ U_\zeta \end{Bmatrix} \tag{28}$$

for the components of $\vec{V}^S$ in local panel coordinates.

$$\vec{V}^S = \left(V_\xi{}^S, V_\eta{}^S, V_\zeta{}^S\right) \tag{29}$$

In particular, $\vec{V}_\zeta^S$ is the component of the velocity normal to the panel surface at a control point, i.e., the downwash

$$V_\zeta{}^S = V_n = \vec{n} \cdot \vec{V}^S \tag{30}$$

To derive expressions for the aerodynamic influence coefficients, the analysis proceeds by first computing average perturbation velocities at a control point due to a panel distribution of doublet strength. The latter is represented by the six coefficients of the quadratic doublet distribution (see eq. 10). So the objective is to find equations of the form

$$\begin{Bmatrix} v_\xi S \\ v_\eta S \\ v_\zeta S \end{Bmatrix} = \begin{bmatrix} \cdots \end{bmatrix} \begin{Bmatrix} \mu_0 \\ \mu_\xi \\ \mu_\eta \\ \mu_{\xi\xi} \\ \mu_{\xi\eta} \\ \mu_{\eta\eta} \end{Bmatrix} \tag{31}$$

The perturbation velocity components v_ξ, v_η, v_ζ induced by a panel doublet distribution are already known from equation (19). These are also the average perturbation velocity components of both panel sides unless the control point is located on the influencing panel itself. In this case the average perturbation velocities change to

$$\begin{Bmatrix} v_\xi S \\ v_\eta S \\ v_\zeta S \end{Bmatrix} = \begin{Bmatrix} v_\xi - \frac{1}{2}\gamma_\eta \\ v_\eta + \frac{1}{2}\gamma_\xi \\ v_\zeta \end{Bmatrix} \tag{32}$$

where γ_ξ, γ_η are the components of the sheet vorticity $\vec{\gamma}$ in local panel coordinates. Vorticity $\vec{\gamma}$ and doublet strength μ are equivalent concepts in potential flow theory related by

$$\vec{\gamma} = \vec{n} \times \nabla\mu \tag{33}$$

Recalling the definition of the panel normal vector $\vec{n} = (0,0,1)$, the components of $\vec{\gamma}$ can be written in terms of the components of $\nabla\mu$ as follows

$$\gamma_\xi = -\frac{\partial\mu}{\partial\eta} \qquad \gamma_\eta = \frac{\partial\mu}{\partial\xi} \qquad \gamma_\zeta = 0 \tag{34}$$

or upon introducing $\mu(\xi,\eta)$ from equation (10)

$$\begin{aligned} \gamma_\xi &= -\mu_\eta - \mu_{\xi\eta}\xi - \mu_{\eta\eta}\eta \\ \gamma_\eta &= \mu_\xi + \mu_{\xi\xi}\xi + \mu_{\xi\eta}\eta \\ \gamma_\zeta &= 0 \end{aligned} \tag{35}$$

Hence,

$$\begin{Bmatrix} -\frac{1}{2}\gamma_\eta \\ \frac{1}{2}\gamma_\xi \\ 0 \end{Bmatrix} = [K] \begin{Bmatrix} \mu_0 \\ \mu_\xi \\ \mu_\eta \\ \mu_{\xi\xi} \\ \mu_{\xi\eta} \\ \mu_{\eta\eta} \end{Bmatrix} \tag{36}$$

with

$$[K] = \begin{bmatrix} 0 & -\frac{1}{2} & 0 & -\frac{1}{2}\xi & -\frac{1}{2}\eta & 0 \\ 0 & 0 & -\frac{1}{2} & 0 & -\frac{1}{2}\xi & -\frac{1}{2}\eta \\ 0 & 0 & 0 & 0 & 0 & 0 \end{bmatrix} \tag{37}$$

Combining equations (19), (32), and (36), the average perturbation velocities induced by a single panel take the form

$$\begin{Bmatrix} v_\xi{}^S \\ v_\eta{}^S \\ v_\zeta{}^S \end{Bmatrix} = [[D] + [\delta_{ij}K]] \begin{Bmatrix} \mu_0 \\ \mu_\xi \\ \mu_\eta \\ \mu_{\xi\xi} \\ \mu_{\xi\eta} \\ \mu_{\eta\eta} \end{Bmatrix} \tag{38}$$

The Kronecker delta δ_{ij} indicates that the coefficients of the matrix $[\delta_{ij}K]$ are zero if the control point i does not lie on the influencing panel j($i \neq j$), and that they are given by equation (37) if i = j.

At this point of the derivation of aerodynamic influence coefficients, advantage is taken of the symmetry properties of the flow field. The assumption is made that the vortex separation is completely symmetric with respect to the x,z-plane of the wing. Consequently, the distribution of doublet strength is also symmetric; i.e., each doublet panel on the RHS (subscript R) of the configuration has an image of equal strength on the LHS (subscript L). Hence,

$$\left\{\mu_0, \mu_\xi, \mu_\eta, \mu_{\xi\xi}, \mu_{\xi\eta}, \mu_{\eta\eta}\right\}_L = \left\{\mu_0, \mu_\xi, \mu_\eta, \mu_{\xi\xi}, \mu_{\xi\eta}, \mu_{\eta\eta}\right\}_R \tag{39}$$

However, the velocity perturbation caused by a panel of the RHS at a particular control point differs from the perturbation induced at the same point by the image panel. The sum of the average perturbation velocities of a panel and its image at a control point on the RHS of the configuration takes the form

$$\begin{Bmatrix} v_\xi{}^S \\ v_\eta{}^S \\ v_\zeta{}^S \end{Bmatrix} = [DK] \begin{Bmatrix} \mu_0 \\ \mu_\xi \\ \mu_\eta \\ \mu_{\xi\xi} \\ \mu_{\xi\eta} \\ \mu_{\eta\eta} \end{Bmatrix} \tag{40}$$

with

$$[DK] = [D]_R + [\delta_{ij}K]_R + [D]_L$$

Next, the six coefficients of a panel doublet distribution must be related to the doublet parameters μ_j defined on one-half of the configuration. Recalling that equation (23) is a linear relationship of the panel coefficients and the set μ_k of doublet parameters of the immediate neighborhood of the panel, this is easily accomplished by enlarging the coefficient matrix $[C]$. Then

$$\begin{Bmatrix} \mu_0 \\ \mu_\xi \\ \mu_\eta \\ \mu_{\xi\xi} \\ \mu_{\xi\eta} \\ \mu_{\eta\eta} \end{Bmatrix} = \left[C_0\right] \left\{\mu_j\right\} \tag{41}$$

where most of the coefficients of the enlarged matrix $[C_0]$ are zero. An indexing system explained in the description of the computer code identifies the nonzero coefficients of $[C_0]$.

Introducing equation (41) to (40) yields

$$\begin{Bmatrix} v_\xi{}^S \\ v_\eta{}^S \\ v_\zeta{}^S \end{Bmatrix} = [B]\{\mu_j\} \qquad [B] = [DK]\,[C_0] \tag{42}$$

The reader is reminded that equation (42) only gives the velocities induced by a single panel and its image, even though $\{\mu_j\}$ is the vector of all unknown doublet parameters. The perturbation velocities induced by all M panels of one-half of the configuration and their images are obtained from

$$\begin{Bmatrix} \sum v_\xi{}^S \\ \sum v_\eta{}^S \\ \sum v_\zeta{}^S \end{Bmatrix} = [A]\{\mu_j\} \tag{43}$$

$$[A] = \sum_{k=1}^{M} [B]_k$$

The matrix $[A]$ is the matrix of aerodynamic influence coefficients, i.e.,

$$[A] = \begin{bmatrix} A_{\xi_j} \\ \hline A_{\eta_j} \\ \hline A_{\zeta_j} \end{bmatrix},$$

which was introduced earlier by equation (28).

SOLUTION PROCEDURE

The boundary value problem of wings with leading-edge vortex separation is nonlinear because the shape of the separated vortex sheet as well as its strength are unknown. The solution procedure must therefore be iterative. Details of the iteration procedure are discussed in this section. First, the choice of initial values for the free-sheet geometry and the doublet distribution is described. The result is termed "Starting Solution" of the iteration. Then a description of the perturbation technique follows and

is used to update free-sheet position and doublet strength during each step of the iteration, entitled "Update Scheme." Finally, an outline of modifications of the basic update scheme, introduced to ensure stability and economy of the computation and known as the "Quasi-Newton Method," concludes the description of the solution procedure.

STARTING SOLUTION

An initial guess for the free-sheet geometry is established based on conical solutions of Smith (ref. 6). Smith's results are reproduced in figure 17, which shows the shape of the free sheet and the size of the fed sheet for various values of the parameter a. The latter is defined by

$$a = \frac{\alpha}{\tan \gamma} \tag{44}$$

where α denotes the angle of attack in radians and γ is one-half of the apex angle of a delta wing. The sheet geometries of figure 17 represent transverse cuts through the configuration normal to the wing surface. The y,z-coordinates are nondimensionalized by the wing semispan s. The locations of the line vortex along the terminated edge of the fed sheet are given for several values of a ($0.2 \leq a \leq 3.0$) and are connected by a dashline. The straight line between the last point on the free sheet and the line vortex is the trace of the fed sheet. An example is shown for $a = 1.4$.

The shape of each free sheet is subdivided into seven segments of approximately equal chord length. The corner points of the segments, as well as the nondimensional coordinates of the position of the terminated edge, are contained in the computer code.

Figure 18 explains how an initial free-sheet geometry is obtained for a nonconical wing geometry based on the tabulated data of Smith. For this purpose the assumption is made that initially the shape of the free sheet at a particular chordwise station is the same as that of a certain delta wing. This delta wing is locally equivalent to the considered nonconical wing geometry and is defined as a wing that has the same apex position and the same local semispan at that chordwise station where the initial free-sheet geometry is to be computed. Thus, the parameter a can be calculated at each transverse cut for a given angle of attack and a given angle γ=arc tan (s/x). Linear interpolation of Smith's data provides the desired initial free-sheet geometry for a chosen number of free-sheet panels. All free-sheet segments of a transverse cut (y,z-plane) have approximately the same chord length.

The described procedure also provides the size of the fed sheet at all geometry defining transverse cuts. The lateral length of the fed sheet and its relative position (i.e., local angle with the end of the free sheet) to the neighboring free-sheet panel is fixed throughout the subsequent iteration procedure; however, it changes absolute position in response to movement of the free sheet during the iteration.

It should be emphasized that Smith's conical data provide only the initial free-sheet geometry. This is a convenient choice and a good guess for wing geometries that are not

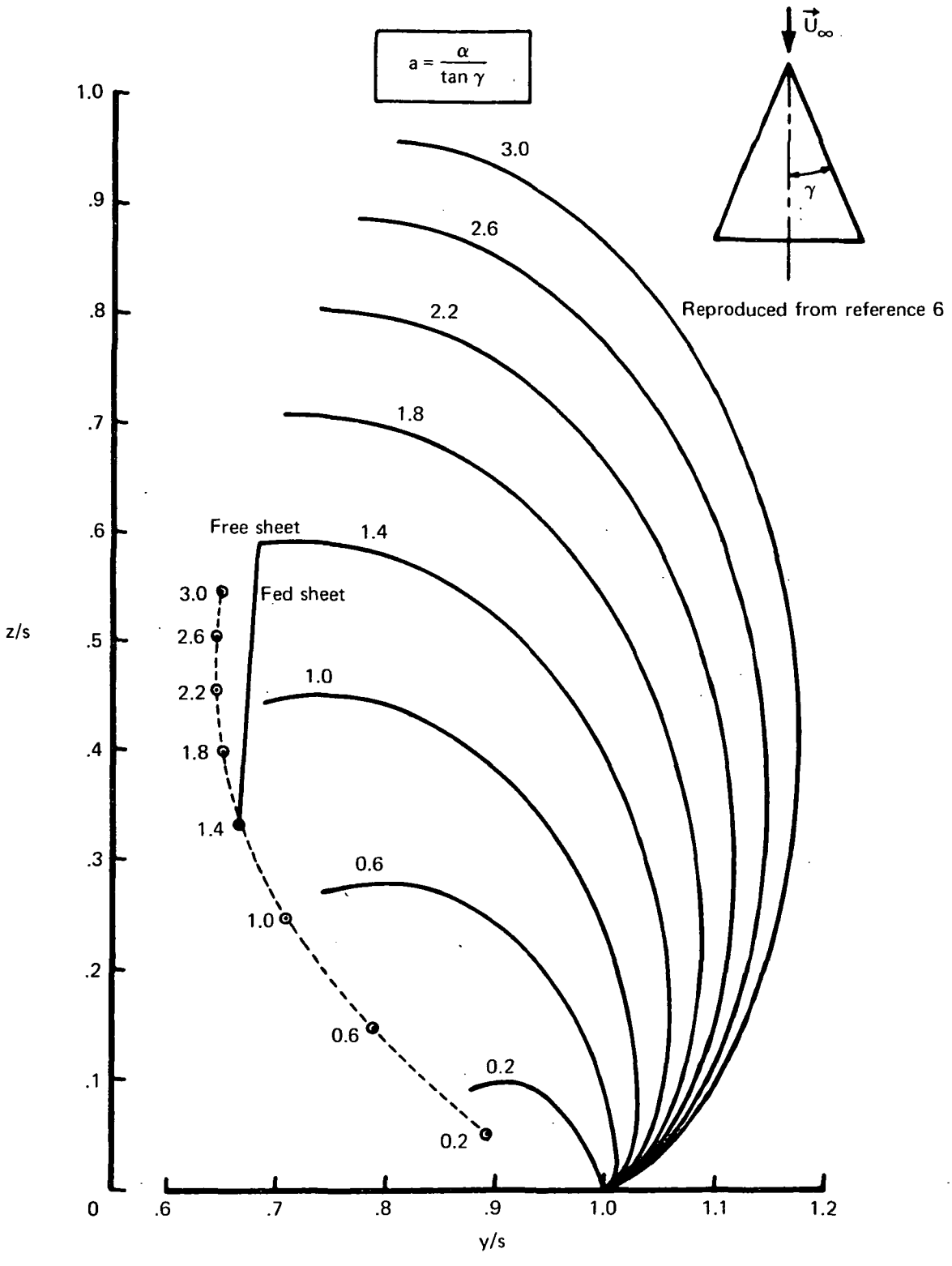

Figure 17.—Initial Free-Sheet Geometry and Size of Fed Sheet for Various a

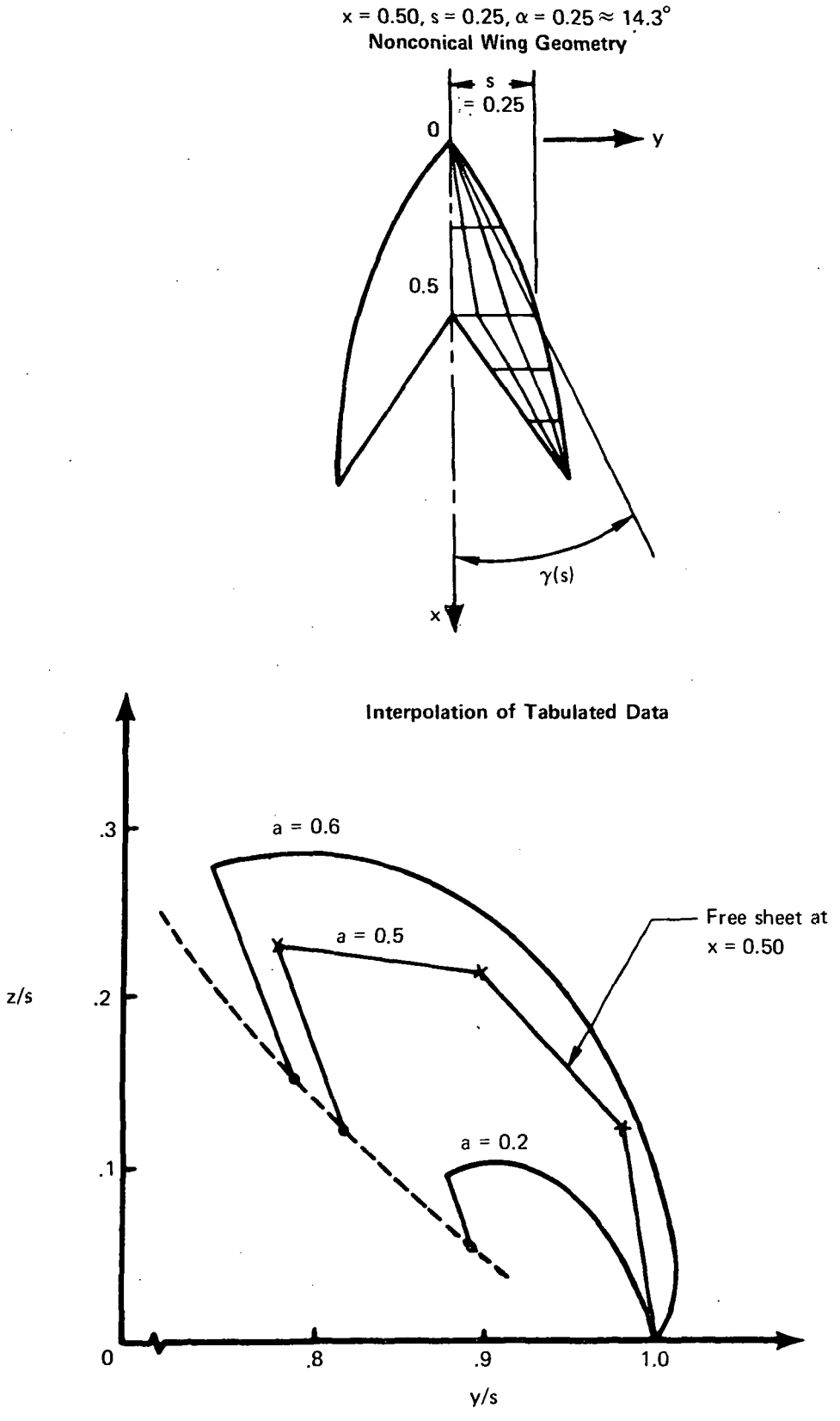

Figure 18.—Selection of Initial Geometry

too different from delta wings. The computed doublet distributions and the sheet geometries computed in subsequent cycles of the iteration procedure are, in general, not conical.

An initial guess for the doublet distribution of wing, free sheet/wake, and fed sheet is computed by satisfying identically the stream-surface boundary condition

$$\vec{n} \cdot \vec{V}^S = 0$$

at all boundary points. This equation is rewritten in terms of aerodynamic influence coefficients and doublet parameters as defined in equation (26)

$$A_{\zeta_{ij}} \mu_j + U_{\zeta_j} = 0$$

where the subscript ζ denotes components in the direction of the local panel normal at a particular control point i. Introducing matrix notation allows the computation of the initial guess of the unknown doublet distribution $\{\mu_j^{(1)}\}$ from

$$\left[A_{\zeta_{ij}}\right]\left\{\mu_j^{(1)}\right\} = -\left\{U_{\zeta_i}\right\} \tag{45}$$

UPDATE SCHEME

Beginning with an initial guess for the sheet geometry and the doublet parameters, the sheet position and doublet strength must be updated so as to satisfy more closely the pertinent boundary condition of the leading-edge vortex problem. For this purpose the governing nonlinear boundary condition equations are perturbed, and with the assumption of small perturbations, a linear set of equations is derived for the perturbation variables. The perturbation technique shall now be discussed in detail.

The boundary value problem can be written symbolically in terms of the following three equations:

$$\begin{aligned} E(\mu_e, \mu_r, \theta) &= 0 \\ F(\mu_e, \mu_r, \theta) &= 0 \\ G(\mu_e, \mu_r, \theta) &= 0 \end{aligned} \tag{46}$$

In this notation, the μ_e are those doublet strength parameters defined at the edge points of networks across which the Kutta condition has to be satisfied. The μ_r are all remaining unknown doublet parameters. The angle θ stands for the unknown free-sheet position and denotes the panel inclination in a transverse cut or y,z-plane. The above

equations state the boundary conditions of the problem and in particular have the following meaning:

$E = 0$ expresses the stream-surface boundary condition, $\vec{n} \cdot \vec{V}^S = 0$, at edge points of networks where the Kutta condition is to be satisfied.

$F = 0$ symbolizes the boundary conditions $\Delta c_P = 0$ of free sheet/wake and $\vec{n} \cdot \vec{V}^S = 0$ of the wing.

$G = 0$ stands for the stream-surface boundary condition, $\vec{n} \cdot \vec{V}^S = 0$, of free sheet and wake.

The above equations are expanded in a Taylor series in which all second-order terms of the perturbation variables $\Delta\mu_e$, $\Delta\mu_r$, $\Delta\theta$ are neglected.

$$\begin{aligned} E^{(i+1)} &= E^{(i)} + \frac{\partial E}{\partial \mu_e}\Delta\mu_e + \frac{\partial E}{\partial \mu_r}\Delta\mu_r + \frac{\partial E}{\partial \theta}\Delta\theta \\ F^{(i+1)} &= F^{(i)} + \frac{\partial F}{\partial \mu_e}\Delta\mu_e + \frac{\partial F}{\partial \mu_r}\Delta\mu_r + \frac{\partial F}{\partial \theta}\Delta\theta \\ G^{(i+1)} &= G^{(i)} + \frac{\partial G}{\partial \mu_e}\Delta\mu_e + \frac{\partial G}{\partial \mu_r}\Delta\mu_r + \frac{\partial G}{\partial \theta}\Delta\theta \end{aligned} \tag{47}$$

The superscripts (i) and (i+1) indicate the (i)th and (i+1)th cycle of the iteration, respectively. All partial derivatives are known functions of the known values $\mu_e^{(i)}, \mu_r^{(i)}, \theta^{(i)}$ of the (i)th iteration cycle. Moreover, the following abbreviations are used

$$\begin{aligned} E^{(i+1)} &= E\left(\mu_e^{(i+1)}, \mu_r^{(i+1)}, \theta^{(i+1)}\right) \\ F^{(i+1)} &= F\left(\mu_e^{(i+1)}, \mu_r^{(i+1)}, \theta^{(i+1)}\right) \\ G^{(i)} &= G\left(\mu_e^{(i)}, \mu_r^{(i)}, \theta^{(i)}\right) \end{aligned}$$

Equations (47) can be written in matrix form as a set of linear equations governing the perturbation variables. The assumption is made that all boundary conditions are satisfied at the end of each iteration cycle, i.e.,

$$\begin{aligned} E^{(i+1)} &= 0 \\ F^{(i+1)} &= 0 \\ G^{(i+1)} &= 0 \end{aligned}$$

In addition, it is assumed that as a necessary requirement for satisfying the Kutta condition along wing edges, the stream-surface boundary condition is always satisfied at edge boundary points; i.e., $E^{(i)} = E^{(i+1)} = 0$. This condition is not sufficient for the Kutta condition to be satisfied, but by nature of the free-sheet boundary condition, a second condition, $\Delta c_P = 0$ just slightly outboard of wing edges, will be satisfied when the solution is achieved. Hence, the equations governing the perturbation variables read

$$\begin{bmatrix} \frac{\partial E}{\partial \mu_e} & \frac{\partial E}{\partial \mu_r} & \frac{\partial E}{\partial \theta} \\ \frac{\partial F}{\partial \mu_e} & \frac{\partial F}{\partial \mu_r} & \frac{\partial F}{\partial \theta} \\ \frac{\partial G}{\partial \mu_e} & \frac{\partial G}{\partial \mu_r} & \frac{\partial G}{\partial \theta} \end{bmatrix} \begin{Bmatrix} \Delta\mu_e \\ \Delta\mu_r \\ \Delta\theta \end{Bmatrix} = \begin{Bmatrix} 0 \\ -F^{(i)} \\ -G^{(i)} \end{Bmatrix} \tag{48}$$

According to the terminology used in Newton-type iteration schemes, the coefficient matrix is called the Jacobian. The coefficients of the Jacobian are calculated with the following assumptions:

- Changes of the aerodynamic influence coefficients due to changes of the panel inclination θ are neglected during each cycle of the iteration.
- The vector normal to the free sheet at control points in the vicinity of wing edges is not affected by changes of θ.
- The length of panel segments in transverse geometry cuts, x = constant, does not change during the iteration. (This is a fixed constraint throughout the iteration that serves to fix the transverse length of the free sheet.)
- The free-sheet geometry is updated such that panel corner points remain in their initial transverse cuts.

Details of the derivation of the Jacobian are contained in appendices C and D. The listed assumptions imply, in particular, that the coefficient

$$\frac{\partial E}{\partial \theta} = 0$$

The number of equations in (48) can be reduced by eliminating $\Delta\mu_e$ as follows:

$$\left\{\Delta\mu_e\right\} = -\left[\frac{\partial E}{\partial \mu_e}\right]^{-1}\left[\frac{\partial E}{\partial \mu_r}\right]\left\{\Delta\mu_r\right\} \tag{49}$$

Upon introducing this expression to (48) one obtains

$$\begin{bmatrix} \frac{\partial F}{\partial \mu_r} - \frac{\partial F}{\partial \mu_e}\left(\frac{\partial E}{\partial \mu_e}\right)^{-1}\frac{\partial E}{\partial \mu_r} & \frac{\partial F}{\partial \theta} \\ \frac{\partial G}{\partial \mu_r} - \frac{\partial G}{\partial \mu_e}\left(\frac{\partial E}{\partial \mu_e}\right)^{-1}\frac{\partial E}{\partial \mu_r} & \frac{\partial G}{\partial \theta} \end{bmatrix} \begin{Bmatrix} \Delta\mu_r \\ \Delta\theta \end{Bmatrix} = \begin{Bmatrix} -F^{(i)} \\ -G^{(i)} \end{Bmatrix} \tag{50}$$

QUASI-NEWTON METHOD

This scheme (ref. 16) is used to solve for doublet strength and free-sheet position.

Represent the quantities of equation (50) symbolically as $\Delta x = (\Delta\mu_r, \Delta\theta)$, the coefficient matrix (Jacobian) as J, and the right-hand side as (-f). Equation (50) becomes,

$$J\Delta x = -f \tag{51}$$

These equations are solved iteratively. Represent the ith iteration by superscript (i). The scheme proceeds to find the corrections $\Delta x^{(i)}$ from the equation

$$J^{(i)}\,\Delta x^{(i)} = -f^{(i)} \tag{52}$$

and forms the new approximate solution (next iterate)

$$x^{(i+1)} = x^{(i)} + \delta^{(i)}\,\Delta x^{(i)} \tag{53}$$

where $J^{(i)} = J(x^{(i)})$, $f^{(i)} = f(x^{(i)})$ and $\delta^{(i)}$ is a scaling parameter to limit the step size of the correction vector. The Jacobian at $x^{(i+1)}$ is obtained by using the following update formula

$$J^{(i+1)} = J^{(i)} + D^{(i)} \tag{54}$$

where

$$D^{(i)} = \frac{\{f^{(i+1)} - f^{(i)} - J^{(i)}\,\Delta x^{(i)}\}\,\Delta x^{(i)^T}}{\Delta x^{(i)^T}\,\Delta x^{(i)}}$$

In this way, there is no need to reevaluate the n^2 partial derivatives for the Jacobian at every iteration. The superscript T denotes the transpose of a vector.

Since the aerodynamic influence coefficients form an essential part of the method, a procedure of generating new aerodynamic influence coefficients only after every five iterations is included in the iterative scheme. This approach can help to reduce the overall computing costs.

The scaling parameter $\delta^{(i)}$ is introduced to alleviate the problem of overshoot in the classical Newton scheme. For each iteration cycle, the following criteria are used to determine $\delta^{(i)}$

$$0 < \delta^{(i)} \leqslant 1$$

and

$$\delta^{(i)} \, ||\Delta x^{(i)}|| \leqslant \bar{\gamma} \, ||x^{(i)}||$$

where $\bar{\gamma}$ is a predetermined quantity ($\bar{\gamma} = 0.1$ is presently used in the computer code), and $||\ ||$ is the Euclidean norm representing the length of a vector. In addition, a halving process of the scaling parameter $\delta^{(i)}$ is applied to ensure the inequality

$$||f^{(i+1)}|| < ||f^{(i)}||$$

The quality of the solution is monitored by examination of the residual defined by

$$R = \sum_{k} \left[\left\{ \Delta \left(\Delta c_{P_{sheet}} \right) \right\}^2 + \left\{ \Delta \left(\vec{n} \cdot \vec{V}^S_{wing} \right) \right\}^2 \right] \tag{55}$$

where k ranges over all appropriate boundary condition points.

The edge doublets μ_e are updated at the end of each iteration cycle.

WING LOAD AND SURFACE PRESSURES

Once a converged solution has been calculated the pressure jump across the wing and the pressures on upper and lower wing surfaces are obtained from the following equations, which are derived in appendix E.

$$\Delta c_P = \frac{2}{U_\infty{}^2} \vec{V}^S \cdot \nabla \mu \tag{56}$$

$$c_{P_u} = 1 - \frac{1}{U_\infty{}^2} \left(\vec{V}^S \cdot \vec{V}^S + \vec{V}^S \cdot \nabla \mu + \frac{1}{4} \nabla \mu \cdot \nabla \mu \right) \tag{57}$$

$$c_{P_l} = 1 - \frac{1}{U_\infty{}^2} \left(\vec{V}^S \cdot \vec{V}^S - \vec{V}^S \cdot \nabla \mu + \frac{1}{4} \nabla \mu \cdot \nabla \mu \right) \tag{58}$$

The average velocity $\vec{V}^S = (\vec{V}^S_\xi, \vec{V}^S_\eta, \vec{V}^S_\zeta)$ is calculated from equation (28) with the final converged distribution of the doublet parameters μ_j. The gradient of μ can be determined from

$$\nabla \mu = \left(\mu_\xi + \mu_{\xi\xi} \xi + \mu_{\xi\eta} \eta \right) \vec{e}_\xi + \left(\mu_\eta + \mu_{\xi\eta} \xi + \mu_{\eta\eta} \eta \right) \vec{e}_\eta \tag{59}$$

which is derived by applying the operator

$$\nabla = \frac{\partial}{\partial \xi}\vec{e}_\xi + \frac{\partial}{\partial \eta}\vec{e}_\eta + \frac{\partial}{\partial \zeta}\vec{e}_\zeta$$

to the quadratic distribution of doublet strength $\mu(\xi,\eta)$ of the panel (see eq. 10). The coefficients μ_ξ, μ_η, etc., of the doublet distribution, in turn are linearly related to the distribution of doublet parameters by equation (41). This equation can be written as

$$\begin{Bmatrix} \mu_0 \\ \mu_\xi \\ \mu_\eta \\ \mu_{\xi\xi} \\ \mu_{\xi\eta} \\ \mu_{\eta\eta} \end{Bmatrix} = \begin{bmatrix} C_{00} \\ C_{0\xi} \\ C_{0\eta} \\ C_{0\xi\xi} \\ C_{0\xi\eta} \\ C_{0\eta\eta} \end{bmatrix} \left\{\mu_j\right\} \tag{60}$$

where C_{00}, $C_{0\xi}$, $C_{0\eta}$ etc., denote the rows of the coefficient matrix $[C_0]$. With this notation $\nabla\mu$ becomes

$$\nabla\mu = \left[C_{0\xi} + \xi C_{0\xi\xi} + \eta C_{0\xi\eta}\right]\left\{\mu_j\right\}\vec{e}_\xi + \left[C_{0\eta} + \xi C_{0\xi\eta} + \eta C_{0\eta\eta}\right]\left\{\mu_j\right\}\vec{e}_\eta \tag{61}$$

Having calculated Δc_P from equation (56), the normal force coefficient of the wing c_N defined by

$$c_N = \frac{N_F}{\frac{\rho}{2} U_\infty{}^2 S_W} \tag{62}$$

becomes

$$c_N = \frac{2}{S_W}\sum_{j=1}^{N_W} \Delta c_{P_j}(n_z S)_j \tag{63}$$

The various symbols have the following meaning

N_F normal force

S_W total wing area

S panel area

n_z component of normal vector in z-direction

N_W number of wing panels on one-half of the configuration

The pitching moment coefficient c_m, defined by

$$c_m = \frac{M_P}{\frac{\rho}{2} U_\infty{}^2 c_{ref} S_W} \tag{64}$$

takes the form

$$c_m = \frac{2}{c_{ref} S_W} \sum_{j=1}^{N_W} \Delta c_{P_j} \left[n_z (x_0 - x_P) S \right]_j \tag{65}$$

where

M_P pitching moment

x_0 x-coordinate of panel center

x_P pitch axis

c_{ref} reference length

COMPUTER PROGRAM USE

PRACTICAL INSTRUCTIONS

Some practical hints are given in this section to assist the user in preparing a computer run. The code is written in FORTRAN 2.3 for the CDC 6600 digital computer and is also operational on the CDC 6400 system. The program occupies 120 000 octal locations of central memory in an overlay structure, and uses eight disk files. Many cases have been executed to check out the code and to gain confidence in the solution procedure. Most computations were highly successful, but there were a few that did not converge to a solution within the allotted computer time. These were mostly wing geometries with kinked leading edges. The user must be warned that he might occasionally encounter a case which, in spite of careful preparation of the input data, does not converge as rapidly as desired. If this occurs, numerical experimentation with different paneling and/or different choices for the initial geometry might hasten convergence.

Number of Unknowns: The code is presently limited to 130 unknown doublet parameters μ_j and panel inclinations θ (in sum total). The doublet parameters μ_e located along the centerline and the edges of the wing are not counted in the sum. There are as many unknown doublet parameters μ_r on wing and free sheet as there are panels, and the number of unknown angles of the free sheet also equals the number of free-sheet panels. Hence, the total number of unknowns is equal to the number of wing panels N_W plus twice the number of free sheet panels N_{FS}, and must satisfy

$$N_W + 2N_{FS} \leqslant 130 \tag{66}$$

An example of a panel layout is given in figure 19. Table 1 provides additional information for this particular case.

Number of Wing Panels: At least 25 wing panels should be used. Cases with sparser wing paneling probably converge to a low-quality solution. The user should also recall that the number of panels in all spanwise rows of wing panels must be the same.

Relative Panel Size: The numerical scheme is not sensitive to strong variations in panel size. Convergence difficulties, however, might be encountered when using a small free-sheet panel next to a large wing panel along the leading edge.

Number of Iterations and Updates of Aerodynamic Influence Coefficients: Sixteen iteration steps should be sufficient to obtain a converged solution in most cases. The program automatically updates the AIC's after every five iteration steps, so that during 15 cycles the aerodynamic influence coefficients are calculated four times.

Monitoring of Convergence: The residual defined by equation (55) is a measure of how closely the boundary conditions are satisfied. The residual must decrease rapidly in an iteration with good convergence characteristics. In addition, the behavior of the wing normal force coefficient c_N as well as the pressure jump Δc_P across the free sheet should be monitored to judge the quality of the solution procedure.

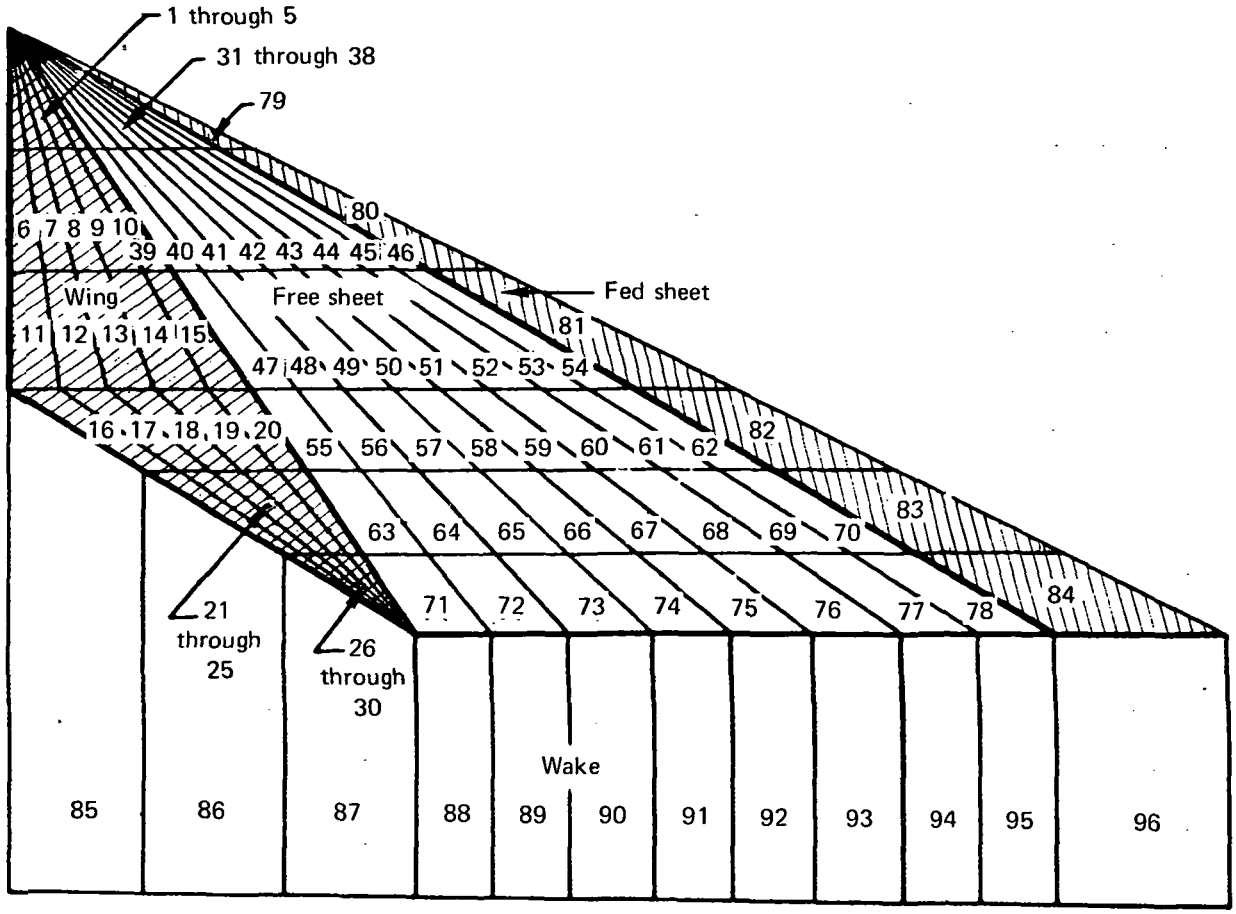

Figure 19.—Panel Layout for Arrow Wing

Table 1.—Arrow-Wing Data

Network	Panels	Control points at panel center, doublets μ_r	Edge control points	θ
Wing	30	30	14	0
Free sheet	48	48	7	48
Fed sheet	6	0	8	0
Wake	11	0	13	0
Network number 5	1	0	1	0
Sum	96	78	43	48

Total number of unknowns = 78 + 48 = 126

Computer Time: The code uses most of the execution time for the computation of the aerodynamic influence coefficients. In order to obtain a first estimate of the total solution time, the following procedure is suggested. First, a trial run with one iteration cycle and one AIC update should be made. Multiplying the computation time of this trial run by the total number of AIC updates and adding approximately 25% to it gives an estimate of the total execution time.

INPUT DATA PREPARATION

The keywords with the $ sign are important for identifying the corresponding input data values. Only the first three characters of the keywords following the $ sign will be needed in the program. All data cards with numerical values use format 6E10.0. Table 2 shows an example for the printed card image of the input data.

Card Number	Card Column	Variable Name (Default Value)	Description/Comment
1	1-5		$CASE
2	1-70		Title information
3	1-70		User identification
4	1-16		$ALPHA (DEGREES)
5	1-10	ALPHAD	Angle of attack in degrees
6	1-13		$ASPECT RATIO
7	1-10	AR	Wing aspect ratio (defined as 4s/x); this value will be used for delta and arrow-wing preprocessors
8	1-16		$TRANSVERSE CUTS
9	1-10	TRAN	Number of transverse cuts of the wing network ($\leq$ 10)
10	1-60	X (I)	x-coordinates of transverse cuts for the wing network
11	1-14		$SPANWISE CUTS
12	1-10	SPAN	Number of spanwise cuts of the wing network ($\leq$ 10)
13	1-60	YSP (I) (0.0)	Percent values for spanwise cuts (100% = 1); this card is intended for use with preprocessor
14	1-15		$CENTERLINE
15	1-10	CTRA	Number of transverse cuts along centerline

Table 2.—Card Image of Input Data

A COMPUTER PROGRAM
FOR
A THREE DIMENSIONAL SOLUTION OF FLOWS OVER WINGS
WITH LEADING EDGE VORTEX SEPARATION

- LIST OF INPUT DATA CARDS -

NO.	CARD IMAGES
1	$CASE
2	IDCASE - PREDICTING WING AERODYNAMIC LOADS FOR A DELTA WING
3	IDUSER - SAMPLE CASE FOR USING DELTA WING PREPROCESSOR
4	$ALPHA (DEGREES)
5	20.0
6	$ASPECT RATIO
7	1.
8	$TRANSVERSE CUTS
9	6.
10	0. 1. 2. 3. 4. 5.
11	$SPANWISE CUTS
12	6.
13	.0 .2 .4 .6 .8 1.
14	$CENTERLINE
15	6.
16	$DELTA WING PREPROCESSOR
17	0.
18	$FREE VORTEX
19	9.
20	$PITCH AXIS
21	0.25
22	$ITERATION
23	15.
24	$PRINT
25	5.
26	$END OF CASE

Beginning with card 16, the input format distinguishes between preprocessors for planar delta wing, arrow wing, or gothic wing, and a general cambered wing geometry.

Card Number	Card Column	Variable Name (Default Value)	Description/Comment
16	1-25		$DELTA WING PREPROCESSOR
		or	$ARROW WING PREPROCESSOR
		or	$GOTHIC WING PREPROCESSOR
17	1-60	YLE(I) (0.0)	y-coordinates of wing leading edge for each transverse cut; this card is intended for use with gothic-wing preprocessor
18	1-12		$FREE VORTEX
19	1-10	SFS	Number of spanwise cuts for the free-sheet network
20	1-11		$PITCH AXIS
21	1-10	XPITCH	x-value of pitch axis
22	1-10		$ITERATION
23	1-10	TMX	Maximum number of iterations allowed for the iteration procedure; the given number should be a multiple of 5 since the AIC's are updated at every 5th iteration
24	1-6		$PRINT
25	1-10	PRINT (5.0)	Printing output occurs at every PRINT iteration; the given number is recomended to be a multiple of 5 (see reason given in card 23)
26	1-12		$END OF CASE

The input format of a general cambered wing geometry is:

Card Number	Card Column	Variable Name (Default Value)	Description/Comment
16	1-19		$INPUT WING NETWORK
17	1-10	FNZ	Number of corner points; this number should be equal to the product of number of transverse cuts and number of spanwise cuts

Card Number	Card Column	Variable Name (Default Value)	Description/Comment
18	1-60	ZM(2,I) ZM(3,I)	y,z-coordinates of corner points input by each transverse cut
19	1-10	FNLE	Number of wing leading-edge corner points
20	1-60	YLE(I)	Indices of wing network corner points for leading edge from nose to tail
21	1-10	FNTE	Number of wing trailing-edge corner points
22	1-60	YTE(I)	Indices of wing network corner points for trailing edge (from centerline to leading edge)
23	1-12		$FREE VORTEX
24	1-10	SFS	Number of spanwise cuts for free-sheet network
25	1-11		$PITCH AXIS
26	1-10	XPITCH	x-value of pitch axis
27	1-10		$ITERATION
28	1-10	TMX (5.0)	Maximum number of iterations allowed for the iterative procedure; the given number should be a multiple of 5 since AIC's are updated at every 5th iteration
29	1-6		$PRINT
30	1-10	PRINT (5.0)	Printing output occurs at every PRINT iteration. The given number is recommended to be a multiple of 5 (see reason given in card 28)
31	1-12		$END OF CASE

PRINTED OUTPUT DATA

An example of the printed output format is given in table 3, which shows the results for a delta wing of aspect ratio 1 at 20° angle of attack computed in the 15th cycle of the iteration procedure. The input data of this case are contained in table 2. The output format is self-explanatory, but a few symbols and words must be defined:

STEP SIZE is the length of the vector $\Delta x^{(i)}$ obtained from equation (52).

CIRCULATION ALONG TERMINATED EDGE OF FED SHEET is the strength Γ of the line vortex along the terminated edge computed at the midpoint of the side edge of the fed-sheet panel.

Table 3.—Example of Printed Output Data

ITERATION NO. 15 SUM OF SQUARES OF RESIDUALS = 4.851045814 8E-03

STEP SIZE (LENGTH OF CORRECTION VECTOR) = 3.568957E+00

WING PANEL NUMBER	1 TO 25
FREE SHEET PANEL NUMBER	26 TO 65
FED SHEET PANEL NUMBER	66 TO 70
WAKE PANEL NUMBER	71 TO 84

CIRCULATION ALONG TERMINATED EDGE OF FED SHEET

X	Y	Z	PANEL	CIRCULATION
.5000	.0812	.0397	66	.2005
1.5000	.2405	.1189	67	.5675
2.5000	.3947	.1984	68	.8914
3.5000	.5700	.2806	69	1.1929
4.5000	.7687	.3728	70	1.4725

CIRCULATION ALONG WING TRAILING EDGE

X	Y	Z	PANEL	CIRCULATION
5.0000	.1250	.0000	71	1.3456
5.0000	.3750	.0000	72	1.3990
5.0000	.6250	.0000	73	1.5324
5.0000	.8750	.0000	74	1.7389
5.0000	1.1250	.0000	75	1.9542

PANEL	XCV	YCV	ZCV	VUX	VUY	VUZ	VLX	VLY	VLZ	DCP	CPU	CPL	AREA
1	.5000	.0125	.0000	1.2316	.1144	-.0065	.9196	.0865	-.0065	.7916	-.4570	.3246	.0250
2	.5000	.0375	.0000	1.1730	.5408	-.0064	.8184	.0819	-.0064	1.0361	-.6827	.3234	.0250
3	.5000	.0625	.0000	1.1103	1.1263	.0010	.8075	.1907	.0010	1.0309	-1.5192	.3116	.0250
4	.5000	.0875	.0000	1.0961	1.3111	.0155	.7772	.3676	.0155	2.1813	-1.9207	.2606	.0250
5	.5000	.1125	.0000	1.2742	.4653	.0179	.6698	.8485	.0179	.6715	-.8402	-.1687	.0250
6	1.5000	.0375	.0000	1.1677	.1363	-.0067	.8307	.0330	-.0067	.6909	-.3821	.3088	.0750
7	1.5000	.1125	.0000	1.1460	.5169	-.0070	.8291	.0848	-.0070	.8859	-.5805	.3054	.0750
8	1.5000	.1875	.0000	1.0997	1.0487	.0004	.8164	.2072	.0004	1.5777	-1.2872	.2905	.0750
9	1.5000	.2625	.0000	1.0770	1.1878	.0162	.7950	.3642	.0162	1.8093	-1.5584	.2508	.0750
10	1.5000	.3375	.0000	1.1946	.5441	.0091	.7124	.6556	.0091	.7953	-.7327	.1627	.0750
11	2.5000	.0625	.0000	1.1772	.1376	-.0049	.8435	.0279	-.0049	.5307	-.3030	.2877	.1250
12	2.5000	.1875	.0000	1.1178	.4335	-.0053	.8426	.1658	-.0053	.7567	-.4836	.2826	.1250
13	2.5000	.3125	.0000	1.0568	.9984	.0016	.8299	.2109	.0016	1.3905	-1.1136	.2669	.1250
14	2.5000	.4375	.0000	1.0493	1.1041	.0157	.7999	.3439	.0157	1.5535	-1.3119	.2415	.1250
15	2.5000	.5625	.0000	1.1634	.5147	.0093	.7345	.5990	.0093	.7201	-.6185	.1415	.1250
16	3.5000	.0875	.0000	1.1804	.1262	.0005	.9639	.0222	.0005	.4364	-.1833	.2532	.1750

Table 3.—Example of Printed Output Data (Continued)

17	3.5000	.2625	.0000	1.0546	.4546	-.0007	.8616	.0698	-.0007	.5715	-.3188	.2527	.1750
18	3.5000	.4375	.0000	.9974	.9199	-.0037	.8479	.1763	-.0037	1.0726	-.8226	.2510	.1750
19	3.5000	.6125	.0000	.9756	1.0551	-.0019	.9131	.7242	-.0019	1.2986	-1.0651	.2337	.1750
20	3.5000	.7875	.0000	1.1038	.5462	.0019	.7790	.5460	.0019	.6116	-.5167	.0958	.1750
21	4.5000	.1125	.0000	1.0064	.1104	.0049	.9208	.0114	.0049	.1770	-.0250	.1520	.2250
22	4.5000	.3375	.0000	.9861	.4084	.0035	.9123	.0419	.0035	.3050	-.1391	.1659	.2250
23	4.5000	.5625	.0000	.9375	.8233	-.0059	.8681	.1300	-.0059	.7463	-.5519	.1944	.2250
24	4.5000	.7875	.0000	.9016	.9923	-.0205	.8490	.3043	-.0205	.9940	-.7979	.1861	.2250
25	4.5000	1.0125	.0000	.9754	.5433	-.0108	.8135	.5112	-.0108	.3234	-.2468	.0767	.2250
26	.5000	.1276	.0056	1.2960	.4125	.2229	.7298	.6165	.9797	.0012			
27	.5000	.1306	.0176	1.2972	.3552	.3845	.8128	.2849	1.1014	.0021			
28	.5000	.1301	.0301	1.3150	.2586	.5393	.8739	.0404	1.1475	.0051			
29	.5000	.1267	.0423	1.3432	.1137	.6627	.9348	-.2011	1.1553	.0072			
30	.5000	.1207	.0534	1.3846	-.0768	.7220	1.0047	-.4648	1.1008	.0071			
31	.5000	.1122	.0625	1.4388	-.2914	.6856	1.0857	-.7375	.9470	.0058			
32	.5010	.1015	.0689	1.5025	-.4925	.5295	1.1755	-.9801	.6573	.0159			
33	.5000	.0893	.0714	1.5688	-.6228	.2376	1.2677	-1.1212	.1948	.0033			
34	1.5000	.3819	.0172	1.2270	.3783	.2081	.7505	.5419	.9141	-.0005			
35	1.5000	.3896	.0534	1.2502	.3243	.3609	.8346	.2468	1.0207	-.0009			
36	1.5000	.3871	.0911	1.2694	.2353	.5090	.8866	.0359	1.0646	.0026			
37	1.5000	.3766	.1275	1.2917	.0990	.6288	.9359	-.1824	1.0765	.0056			
38	1.5000	.3586	.1607	1.3267	-.0803	.6877	.9940	-.4257	1.0313	.0166			
39	1.5000	.3333	.1882	1.3744	-.2831	.6562	1.0636	-.6806	.8935	.0069			
40	1.5000	.3013	.2076	1.4308	-.4739	.5121	1.1415	-.9093	.6302	.0069			
41	1.5000	.2647	.2150	1.4925	-.6612	.2321	1.2258	-1.1479	.1943	.0043			
42	2.5000	.6352	.0292	1.1993	.3559	.1887	.7649	.4905	.8813	-.0019			
43	2.5000	.6464	.0900	1.2092	.3103	.3385	.8313	.2314	.9643	-.0016			
44	2.5000	.6412	.1527	1.2186	.2221	.4833	.8746	.0310	1.0011	-.0010			
45	2.5000	.6228	.2132	1.2446	.0925	.5964	.9257	-.1721	1.0116	.0033			
46	2.5000	.5921	.2681	1.2809	-.0780	.6531	.9842	-.3978	.9703	.0051			
47	2.5000	.5496	.3137	1.3262	-.2706	.6244	1.0503	-.6351	.8430	.0049			
48	2.5000	.4961	.3459	1.3813	-.4528	.4882	1.1256	-.8499	.5979	.0046			
49	2.5000	.4351	.3583	1.4358	-.5748	.2236	1.2001	-.9804	.1935	.0032			
50	3.5000	.8929	.0393	1.1452	.3731	.1644	.7677	.5493	.7634	.0037			
51	3.5000	.8178	.1226	1.1059	.3289	.3474	.7774	.2741	.8823	-.0061			
52	3.5000	.9098	.2106	1.1324	.2500	.4860	.8251	.0866	.9498	-.0094			
53	3.5000	.8865	.2958	1.1592	.1216	.6012	.8761	-.1174	.9777	-.0091			
54	3.5000	.8449	.3733	1.2036	-.0484	.6599	.9331	-.3443	.9497	-.0048			
55	3.5000	.7861	.4378	1.2652	-.2420	.6332	1.0122	-.5829	.8345	-.0036			
56	3.5000	.7117	.4835	1.3360	-.4233	.4974	1.1009	-.7975	.6007	.0025			
57	3.5000	.6264	.5039	1.3889	-.5425	.2361	1.1711	-.9255	.2193	-.0030			
58	4.5000	1.1408	.0499	1.0618	.3766	.2061	.8266	.5162	.8024	-.0009			
59	4.5000	1.1827	.1559	1.0904	.3409	.3691	.8724	.3400	.7492	.0036			
60	4.5000	1.1859	.2690	1.0602	.2553	.5201	.8491	.1704	.8406	.0032			
61	4.5000	1.1677	.3804	1.0698	.1282	.6290	.8596	-.0236	.9051	-.0010			
62	4.5000	1.1162	.4929	1.0975	-.0443	.6791	.8957	-.2555	.9231	-.0165			
63	4.5000	1.0442	.5687	1.1482	-.2384	.6463	.9475	-.5002	.8077	-.0075			
64	4.5000	.9503	.6301	1.2131	-.4167	.5095	1.0198	-.7177	.5940	-.0041			
65	4.5000	.8412	.6574	1.2878	-.5337	.2536	1.1022	-.8563	.2427	.0017			

NORMAL FORCE COEFFICIENT = .7965
PITCHING MOMENT COEFFICIENT = .4278
PITCH AXIS = .2500
ROOT CHORD = 5.0000
WING AREA = 6.2500

Table 3.—Example of Printed Output Data (Concluded)

X Y Z COORDINATES OF CORNER POINTS

FREE SHEET NETWORK

.000	.000	.000	.000	.000	.000	.000	.000	.000	.000	.000	.000	.000	.000	.000
.000	.000	.000	.000	.000	.000	.000	.000	.000	.000	.000	.000	1.000	.250	.000
1.000	.260	.123	1.000	.262	.048	1.000	.258	.173	1.000	.240	.096	1.000	.234	.117
1.000	.215	.133	1.000	.191	.147	1.000	.166	.143	2.000	.500	.000	2.000	.517	.046
2.000	.519	.197	2.000	.509	.147	2.000	.490	.194	2.000	.461	.239	2.000	.423	.268
2.000	.376	.287	2.000	.325	.287	3.000	.750	.000	3.000	.774	.070	3.000	.776	.146
3.000	.761	.221	3.000	.731	.291	3.000	.686	.352	3.000	.628	.401	3.000	.558	.429
3.000	.491	.439	4.000	1.000	.000	4.000	1.048	.087	4.000	1.058	.187	4.000	1.045	.288
4.000	1.010	.383	4.000	.953	.467	4.000	.877	.532	4.000	.784	.573	4.000	.683	.580
5.000	1.250	.000	5.000	1.301	.113	5.000	1.324	.237	5.000	1.317	.364	5.000	1.283	.486
5.000	1.219	.595	5.000	1.127	.681	5.000	1.012	.734	5.000	.885	.742			

FED SHEET NETWORK

.000	.000	.000	.000	.000	.000	1.000	.166	.143	1.000	.162	.079	2.000	.325	.287
2.000	.318	.159	3.000	.491	.439	3.000	.471	.238	4.000	.683	.580	4.000	.669	.324
5.000	.985	.742	5.000	.868	.422									

CIRCULATION ALONG WING TRAILING EDGE is computed at the midpoints of the panel trailing edges.

ZCX	$= x_0$	coordinates of panel center
ZCY	$= y_0$	
ZCZ	$= z_0$	
VUX	$= (V_u)_x$	components of $\vec{V}_u$ on upper side of the sheet surface in x,y,z-coordinates
VUY	$= (V_u)_y$	
VUZ	$= (V_u)_z$	
VLX	$= (V_l)_x$	components of $\vec{V}_l$ on lower side of the sheet surface in x,y,z-coordinates
VLY	$= (V_l)_y$	
VLZ	$= (V_l)_z$	
DCP	$= \Delta c_P$	jump in pressure coefficient across the sheet
CPU	$= c_{P_u}$	pressure coefficient on upper wing surface
CPL	$= c_{P_l}$	pressure coefficient on lower wing surface
AREA	$= S_j$	wing panel area

VERIFICATION OF THE METHOD

RESULTS

Numerous example cases have been executed to validate the method and its generality. Cases selected are compared with available theoretical and experimental data for a range of different geometric configurations including delta, gothic, and arrow wings.

The capability of the method to predict overall wing coefficients is shown in figure 20 for a delta wing of aspect ratio 1 at low subsonic speed ($M_\infty = 0$). This figure shows the well-known nonlinear variation of the normal-force coefficient c_N with angle of attack. Several values of c_N were computed for angles of attack up to 20° and agree well with the experimental data of Peckham (ref. 17) and theoretical results from the leading-edge-suction analogy of Polhamus (ref. 3). The corresponding load distribution at $\alpha = 20°$ is plotted in figure 21 and compared with Peckham's experimental results. Although only 25 wing panels were used on one-half of the configuration, the completely three-dimensional, nonconical load distribution was well predicted, including the location of the vortex-induced pressure peaks and the decrease of the load toward the trailing edge.

Figures 22, 23, and 24 show detailed surface pressure distributions for a delta wing of aspect ratio 1.4559 at $\alpha = 8.8°$, $\alpha = 14°$, and $\alpha = 19.1°$. Upper and lower surface pressures are well predicted for the higher angles of attack, as the comparison with experimental data (ref. 18) illustrates. At 8.8° the differences, although unclear, may be due to the blunt trailing edge of the experimental model or an inadequate definition for the fed-sheet geometry. The experimental results clearly show the effect of the secondary vortex separation, which takes place on the upper surface just slightly outboard of the main vortex. The present method does not model secondary vortex separation and, consequently, produces a slightly different shape for the pressure peaks.

The method can be applied to more general configurations. For example, figure 25 shows the method applied to a gothic wing having a swept trailing edge and a curved leading edge. This figure shows good agreement of the normal-force coefficient c_N with experiments (ref. 17) at the relatively high angle of attack of 14.3°.

Figure 26 shows the predicted load distribution of an arrow wing. Experimental data are not available for comparison, but the plotted loads appear to be realistic and demonstrate that the method is capable of handling other than delta-wing planforms.

CONVERGENCE CHARACTERISTICS

The progress of the solution is monitored by examining the residual errors in the zero pressure jump boundary condition on the free sheet and wake, and the stream-surface boundary condition on the wing. Figure 27 shows the convergence characteristics for a delta wing of aspect ratio 1 and a gothic wing of aspect ratio 1.60. Each configuration has 25 wing panels.

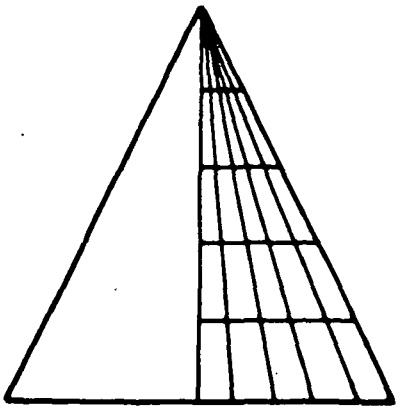

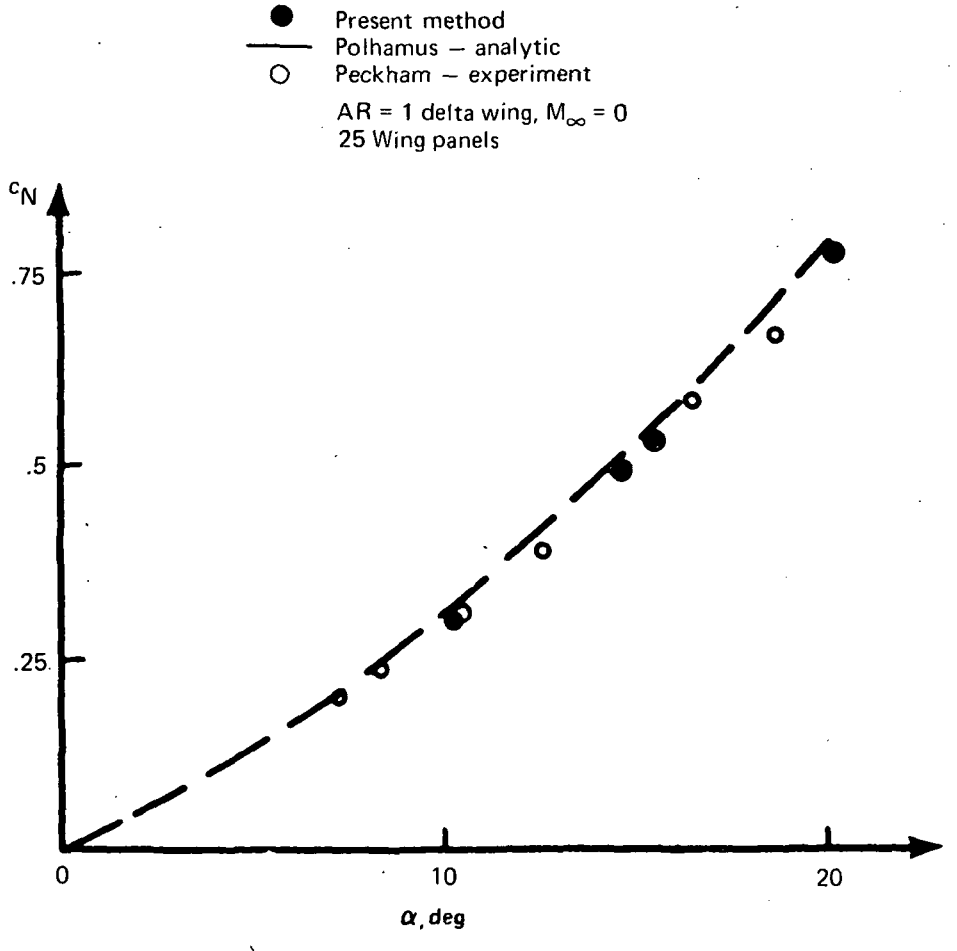

Figure 20.–Normal Force Coefficient c_N, Delta Wing

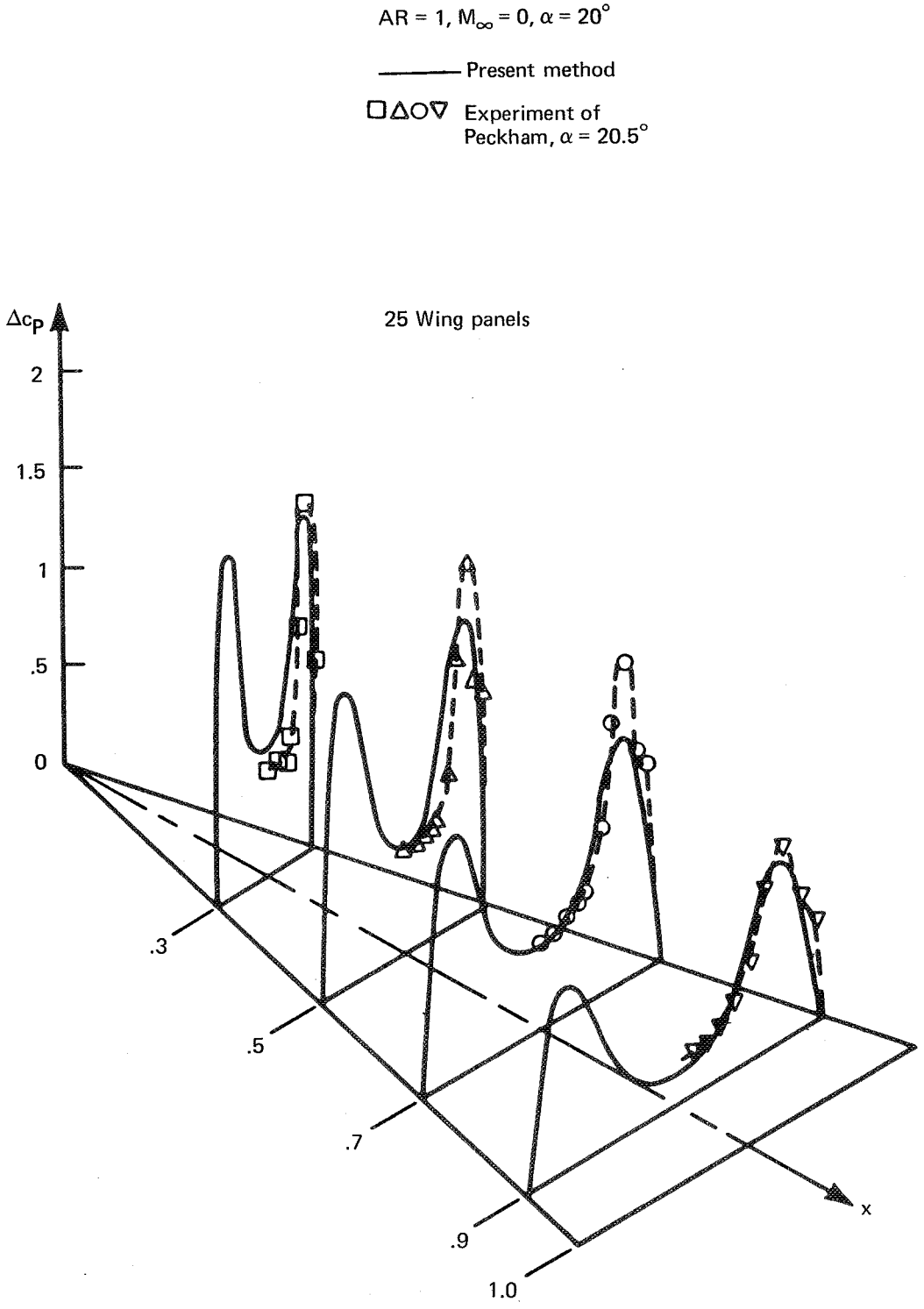

Figure 21.—Load Distribution of Delta Wing, $\alpha = 20°$

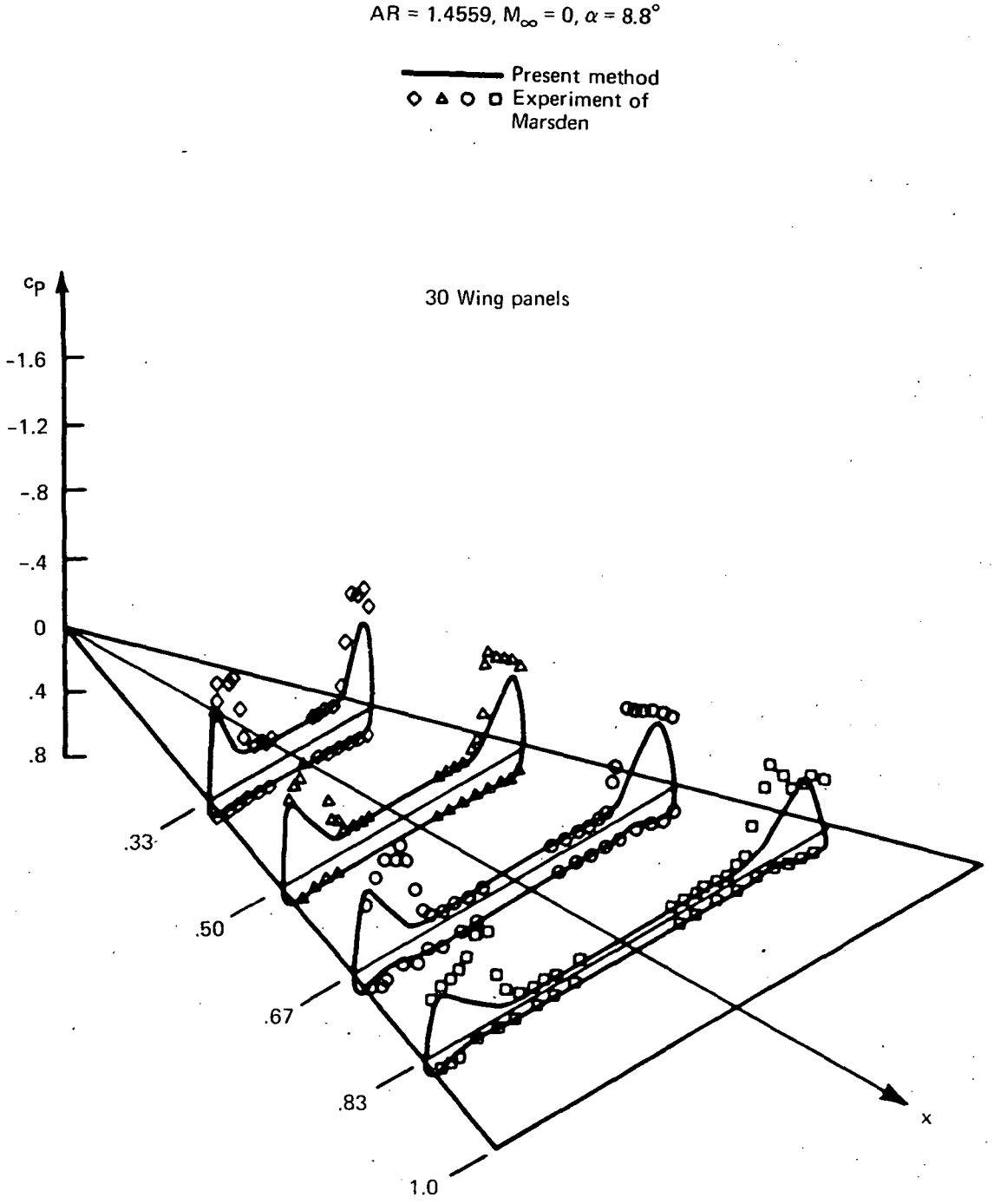

Figure 22.—Surface Pressure Distribution of Delta Wing, α = 8.8°

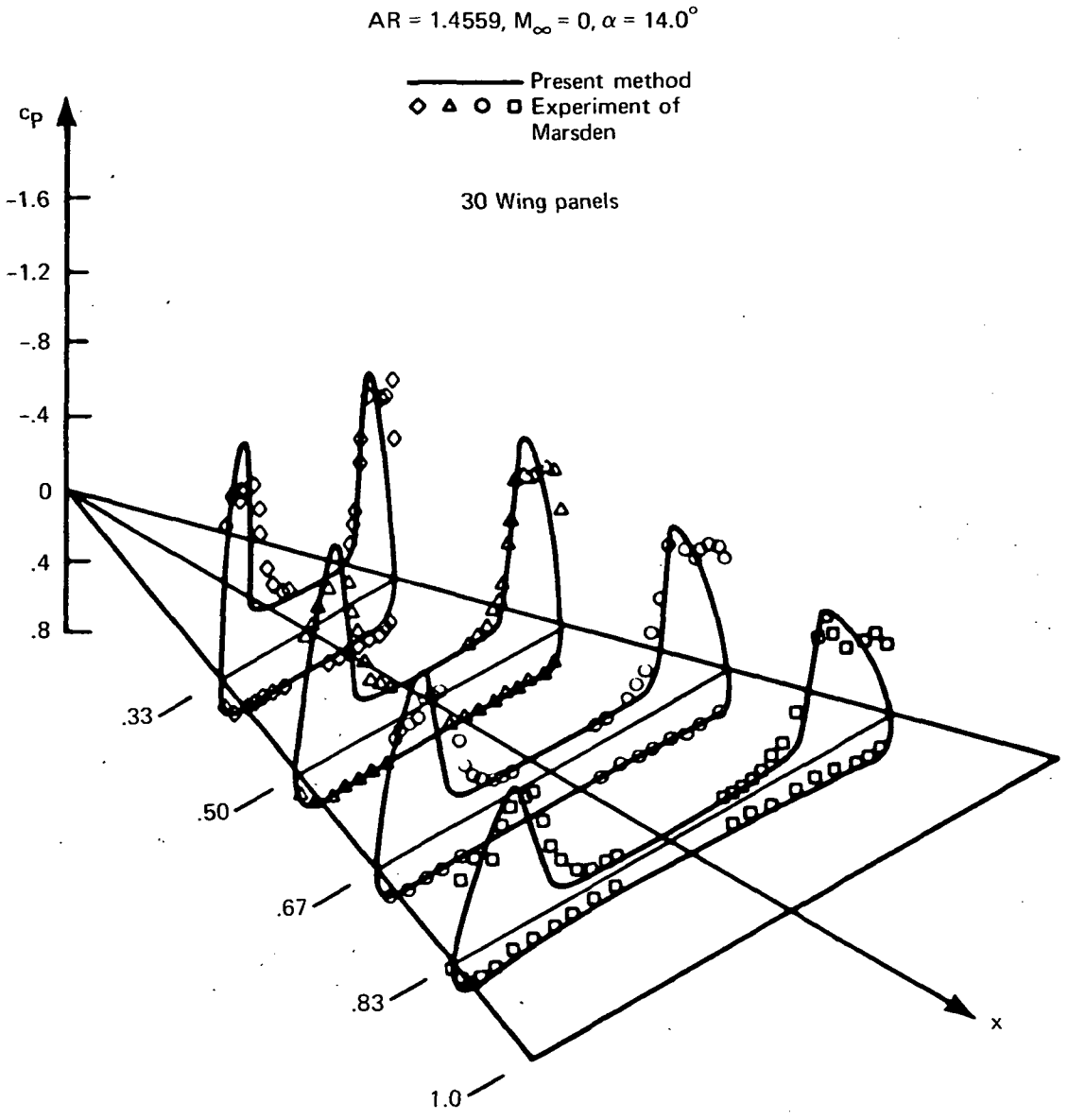

Figure 23.–Surface Pressure Distribution of Delta Wing, α = 14.0°

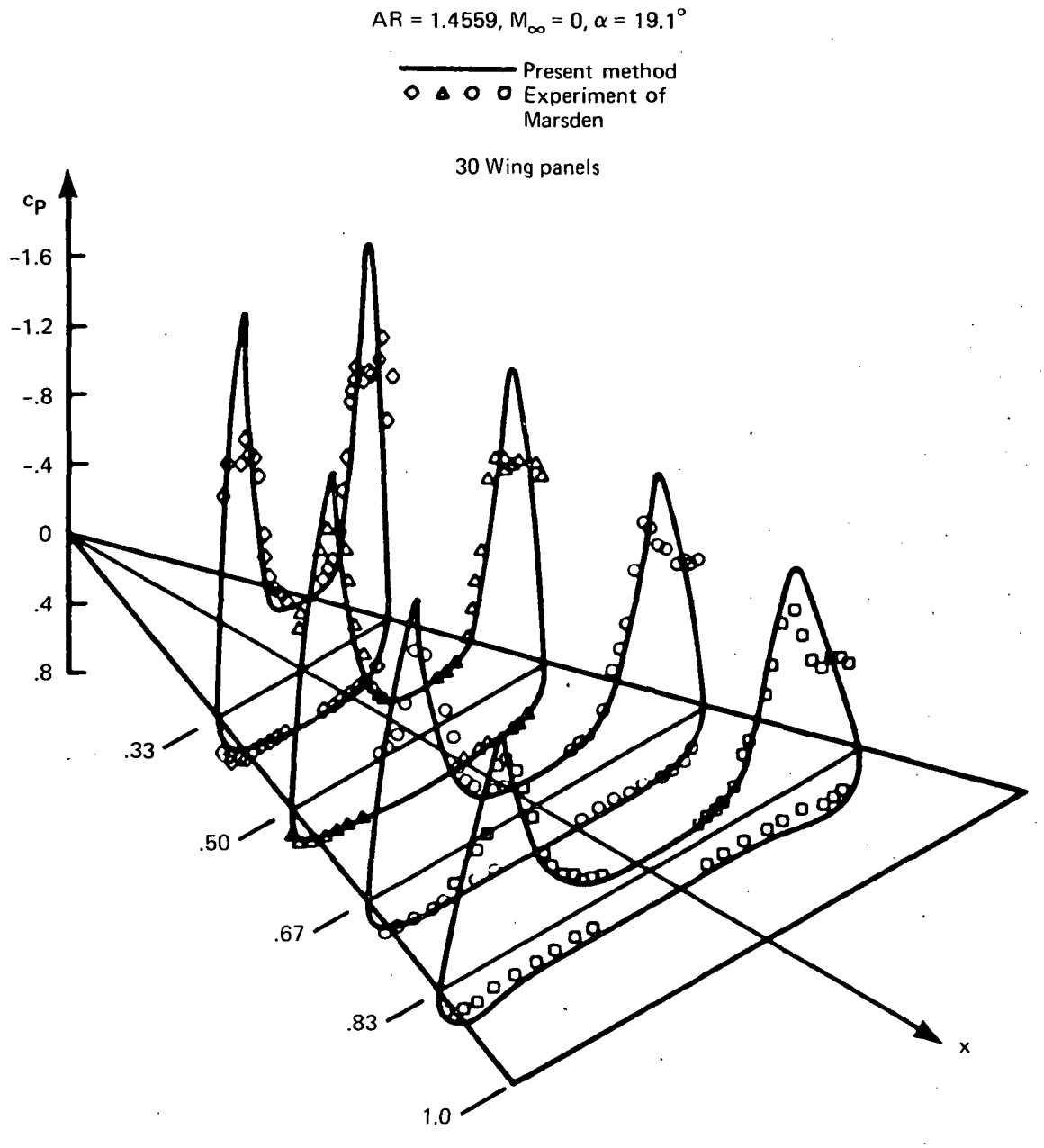

Figure 24.—Surface Pressure Distribution of Delta Wing, α = 19.1°

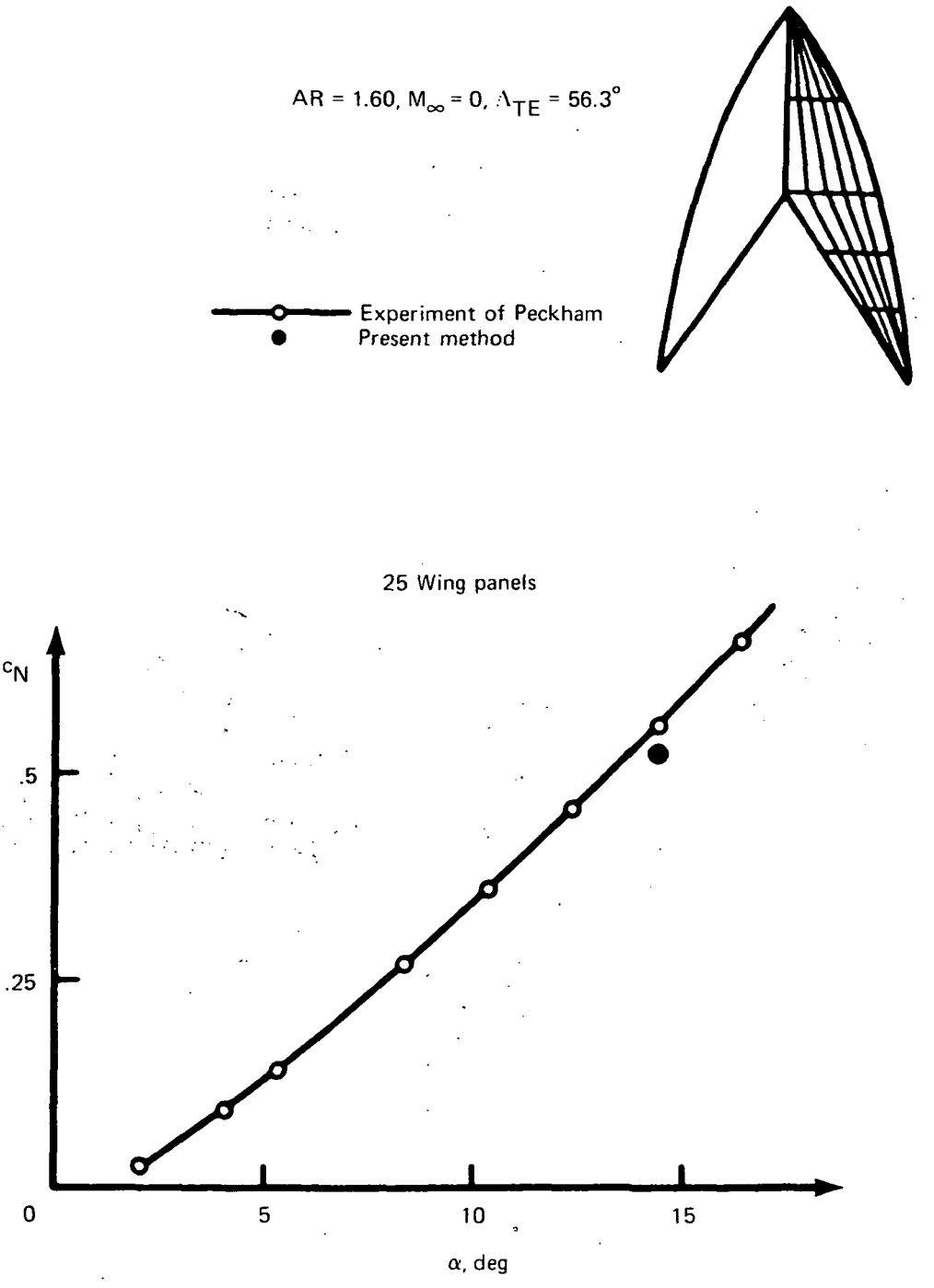

Figure 25.—Normal Force Coefficient c_N, Gothic Wing

α = 15.8°
Λ_{LE} = 71.2°

M_∞ = 0
c_r = 111.96 cm
b = 112.88 cm

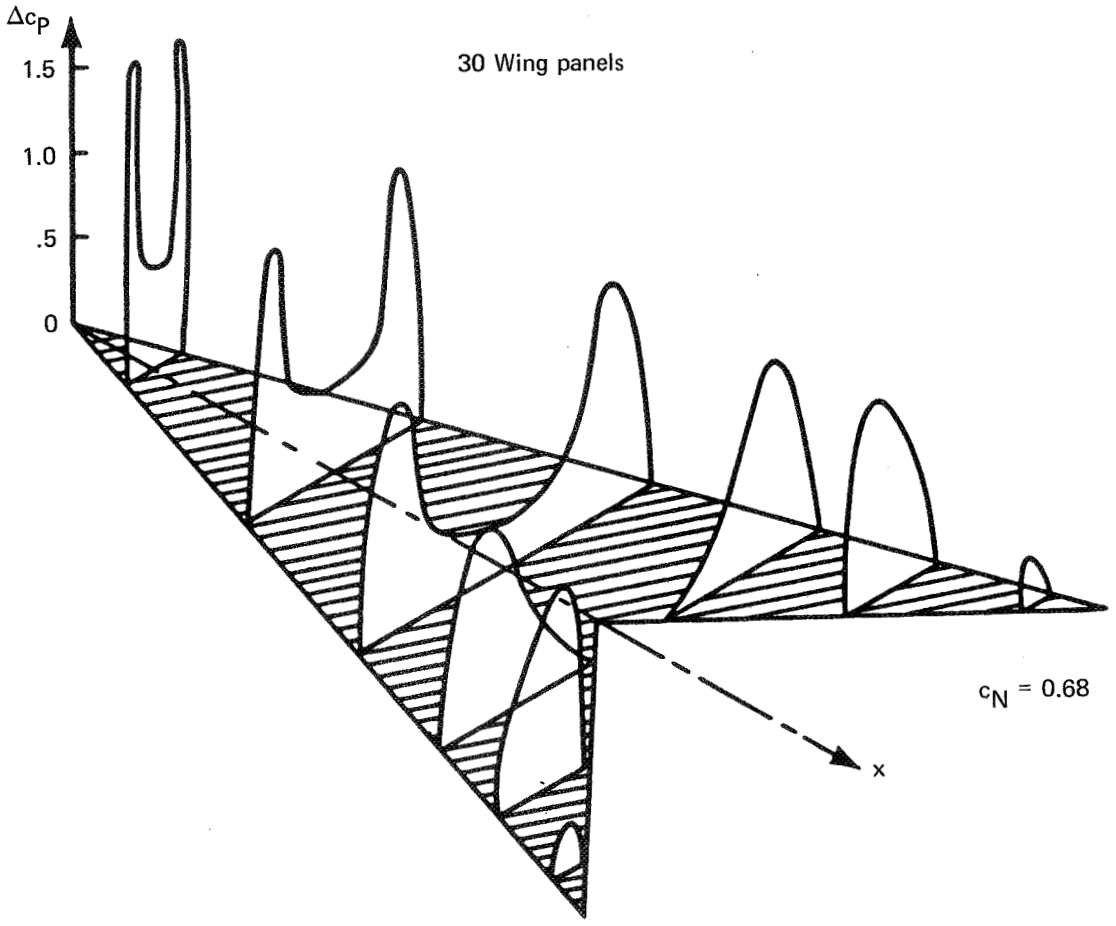

Figure 26.—Load Distribution of Arrow Wing

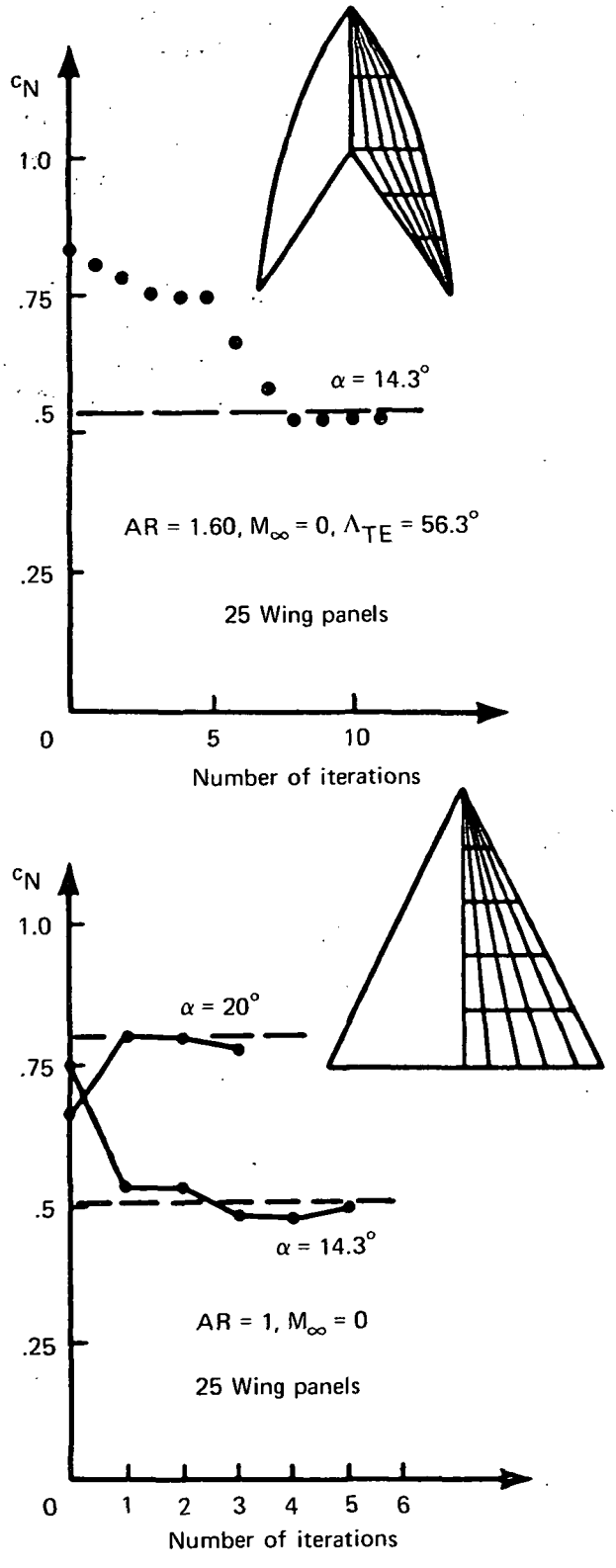

Figure 27.—Convergence Characteristics

The paneling and convergence characteristics for the delta wing are shown at the lower side of figure 27, where the normal-force coefficient c_N is shown as a function of iteration number for two different angles of attack. The dashed lines indicate the value of c_N obtained from the leading-edge-suction analogy. For this case, the aerodynamic influence coefficients were updated in each cycle of the iteration. The solution quickly seeks a level after only one or two iterations and then exhibits some oscillation, often a characteristic of Newton schemes.

The paneling and convergence characteristics for the gothic wing are shown at the upper side of figure 27. For this case, the aerodynamic influence coefficients (whose computation consumes the largest fraction of computer run time) were updated only after the fifth and tenth iterations. The difference in convergence characteristics for the two cases is apparent.

CONCLUSIONS

The work reported here demonstrates one of the applications of a new general, subsonic potential flow computational technique recently developed (reported in ref. 14). With the use of this technique, a three-dimensional method has been formulated for predicting the flow field about swept, sharp-edged wings characterized by the presence of vortex separation at the leading edge. The basic approach has been verified for selected wing planforms such as delta wings of different aspect ratios, a gothic wing, and an arrow wing. Further numerical experiments conducted after completion of the contract work uncovered convergence problems with the present computer code for more general wing geometries like double delta-wing planform, diamond wings, and cropped delta wings. The problems do not appear to be fundamental in nature and are due in part to a lack of experience concerning panel density requirements, the accuracy of the initial guess, and the appearance of a second vortex at a planform break that is not modeled in the present code. The work to date has been successful in overcoming the most difficult aspects of the problem and provides the basis for development of this initial capability into a method suitable for supersonic flow and for complete configuration analysis in subsonic and supersonic flow. In addition, it can be applied to related problems involving free vortex sheets that are encountered in the areas of powered lift, jet interactions, jet flaps, and so forth.

Boeing Commercial Airplane Company
P.O. Box 3707
Seattle, Washington 98124
September 24, 1975

APPENDIX A
COMMENTS ON CHOICE OF FED-SHEET MODEL

A simple method for treating the core of the rolled-up primary vortex sheet was used by Smith (ref. 6) in his conical approach to the leading-edge vortex problem. This model consists of a single vortex with a fed sheet (see fig. 28), which he calls "feeder sheet." The sheet size and orientation are adjusted so that the total force on the vortex and on the fed sheet is zero to provide a unique solution.

The three-dimensional method described in this document uses an even simpler representation of the viscous core region. The fed sheet is treated as an entirely kinematic extension of the free sheet, and no boundary condition is applied to the fed sheet. The tacit assumption in this simplified model is that boundary conditions applied to the free sheet are sufficient to adequately position the fed sheet, whose typical dimension is small compared with dimensions associated with the free sheet and with distance from the wing. Size and initial position of the fed sheet are taken from conical flow results of Smith.

This fed-sheet model was the outcome of a theoretical investigation of the relation of mathematical discrete line vortices to the problem of leading-edge vortex separation. In particular, it was discovered that Smith's fed-sheet model, when applied to the three-dimensional nonconical flow problem, would contain two self-induced infinite forces, with no possibility of mutual cancellation, and that for this reason the boundary condition of zero integrated force over the vorticity could not be applied (ref. 19).

The origin of these infinite forces can be explained with the aid of figure 29, in which the fed sheet carrying a surface distribution of vorticity $\vec{\gamma}$ is shown. This vorticity merges into a discrete line vortex of strength Γ along the terminated edge. The line vortex along that edge will be curved in the three-dimensional and nonconical flow problem. This curvature is responsible for one of the infinite forces, since any curved discrete line vortex induces on itself an infinite component of velocity. When a curved vortex is free to move with the surrounding fluid (as is the case with free leading-edge vortices), it will move with infinite speed and will change, in general, its shape with infinite speed (ref. 19). The curved discrete vortex forming the terminated edge is not allowed to move with infinite speed and, for that reason, will always sustain a transverse component of force that is infinite in magnitude.

The other infinite force is experienced by the fed sheet and acts in the direction parallel to the terminated edge. It is present in all cases where the fed sheet is feeding vorticity into the edge vortex, i.e., when the strength of the edge vortex changes along its length.

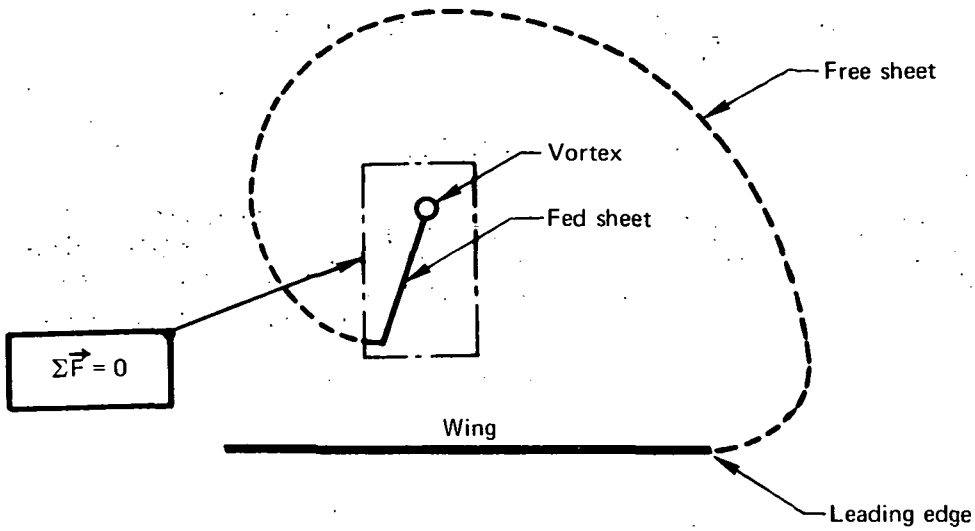

Figure 28.—Fed-Sheet Model of Smith

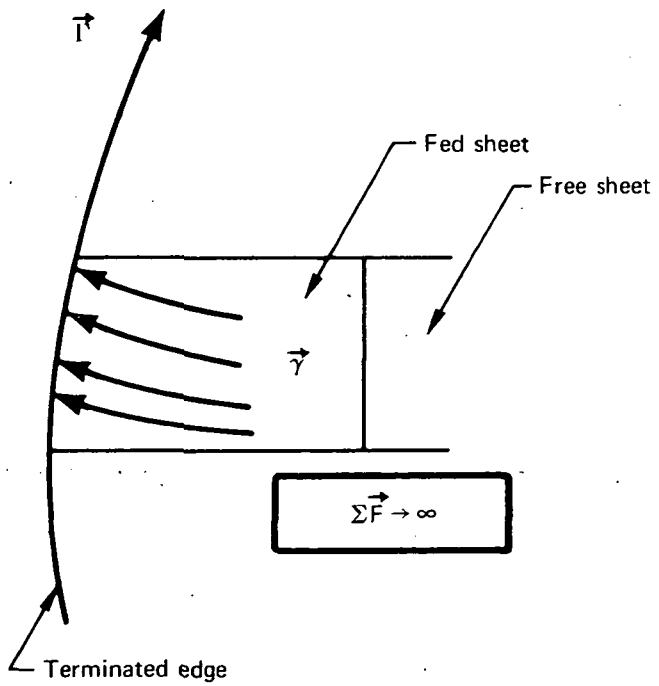

Figure 29.—Fed-Sheet Model With Infinite Forces

APPENDIX B
PANEL INFLUENCE COEFFICIENTS

B.1 INTRODUCTION

In this appendix we shall calculate the potential and velocity induced by a source or doublet distribution on a curved panel. As shown in figure 30, let S be the curved panel surface, Σ its tangent plane projection, $\vec{Q}$ a point on S, $\hat{n}$ the normal to S at $\vec{Q}$, and $\vec{P}$ a field point. The potential ϕ at $\vec{P}$ induced by a source distribution σ on S is defined by

$$\phi = \iint_S \sigma\left(\frac{-1}{4\pi R}\right) dS \tag{B-1}$$

where

$$\vec{R} = (\xi - x, \eta - y, \zeta - z) = \vec{Q} - \vec{P} \tag{B-2}$$

and

$$R = |\vec{R}| = \sqrt{(\xi - x)^2 + (\eta - y)^2 + (\zeta - z)^2}$$

The potential ϕ at $\vec{P}$ induced by a doublet distribution μ on S is defined by

$$\begin{aligned} \phi &= \iint_S \mu \vec{\nabla}_Q\left(\frac{-1}{4\pi R}\right)\cdot\hat{n}\, dS \\ &= \iint_S \mu\left(\frac{-\vec{R}\cdot\hat{n}}{4\pi R^3}\right) dS \end{aligned} \tag{B-3}$$

The velocity $\vec{V}$ induced at $\vec{P}$ by a source or doublet distribution on S is defined by

$$\vec{V} = \vec{\nabla}\phi \tag{B-4}$$

We assume that the surface S is defined by

$$\zeta = a\,\xi^2 + b\,\eta^2, \quad (\xi,\eta)\,\epsilon\,\Sigma \tag{B-5}$$

We also assume that S does not deviate significantly from Σ, more precisely that

$$\delta << 1 \tag{B-6}$$

where

$$\delta = \frac{1}{2}\underset{(\xi,\eta)\epsilon\Sigma}{\text{Max}}\left\{\sqrt{a^2\xi^2 + b^2\eta^2}\right\} \tag{B-7}$$

(Nominally we assume $\delta < 0.066$.)

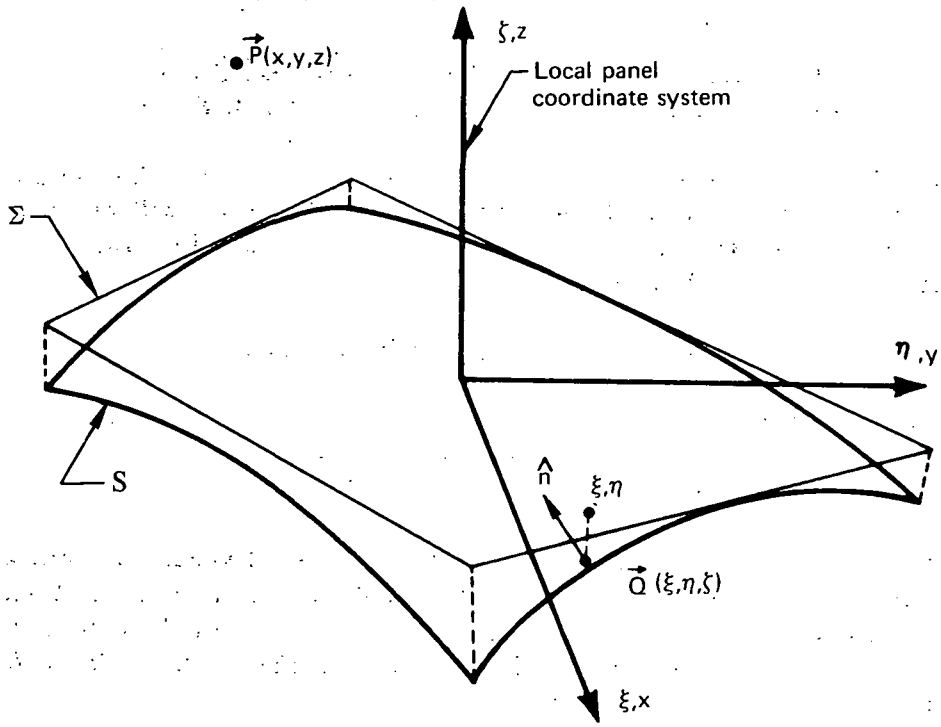

Figure 30.—Field Point/Panel Geometry

The distribution of singularity strength on S is assumed to be linear in the case of a source panel and quadratic in the case of a doublet panel. To be specific we assume

$$\sigma = \sigma_0 + \sigma_\xi \xi + \sigma_\eta \eta , \quad (\xi,\eta) \epsilon \Sigma \tag{B-8}$$

and

$$\mu = \mu_0 + \mu_\xi \xi + \mu_\eta \eta + \frac{1}{2}\mu_{\xi\xi}\xi^2 + \mu_{\xi\eta}\xi\eta + \frac{1}{2}\mu_{\eta\eta}\eta^2 , \quad (\xi,\eta) \epsilon \Sigma . \tag{B-9}$$

B.2 EVALUATION OF SOURCE AND DOUBLET INTEGRALS FOR AN ARBITRARY FIELD POINT

Let us first consider the evaluation of source potential defined by equation (B-1). Evaluation of source velocity and doublet potential and velocity will be quite similar. The first step in the evaluation procedure is to transfer the integral over S to the equivalent integral over Σ. We have

$$\phi = \iint_\Sigma \sigma\left(\frac{-1}{4\pi R}\right) \sec(\hat{\zeta},\hat{n})\, d\xi\, d\eta , \tag{B-10}$$

From equation (B-5) we obtain

$$\sec(\hat{\zeta},\hat{n}) = \sqrt{1 + 4a^2\xi^2 + 4b^2\eta^2} . \tag{B-11}$$

Substitution of equations (B-2), (B-8), and (B-11) into (B-10) yields an explicit integral for ϕ. However, the integral cannot be evaluated in closed form as it stands. By employing the hypothesis that δ^2 is negligible compared to unit (hypothesis (B-6)) the integrand can be approximated by terms that are integrable in closed form. A uniform approximation to $\sec(\hat{\zeta},\hat{n})$ can be obtained by noting that

$$4a^2\xi^2 + 4b^2\eta^2 \leqslant 16\delta^2 \tag{B-12}$$

hence

$$\sec(\hat{\zeta},\hat{n}) \approx 1 \tag{B-13}$$

A uniform approximation to 1/R is somewhat more difficult to obtain since this factor is singular. Let (x_0,y_0) be the point on Σ closest to (x,y) and set

$$z_0 = \zeta(x_0, y_0), \; h = z - z_0, \text{ and } r = \sqrt{(\xi - x)^2 + (\eta - y)^2} . \tag{B-14}$$

Then

$$\begin{aligned} R &= \sqrt{(r^2 + h^2) - 2h(\zeta - z_0) + (\zeta - z_0)^2} \\ &= \sqrt{r^2 + h^2} \cdot \sqrt{1 + \frac{-2h(\zeta - z_0) + (\zeta - z_0)^2}{r^2 + h^2}} \end{aligned} \tag{B-15}$$

Let

$$\epsilon = \underset{(\xi,\eta)\,\epsilon\,\Sigma}{\text{Max}} \left\{ \frac{|\zeta - z_0|}{r} \right\} . \tag{B-16}$$

Then

$$\left| \frac{-2h(\zeta - z_0) + (\zeta - z_0)^2}{r^2 + h^2} \right| \leqslant \frac{2\epsilon r h + \epsilon^2 r^2}{r^2 + h^2} \leqslant \epsilon + \epsilon^2 . \tag{B-17}$$

Therefore if ϵ^2 is everywhere negligible, equation (B-15) yields

$$\frac{1}{R} \approx \frac{1}{\rho} + \frac{h(\zeta - z_0)}{\rho^3} , \quad \rho = \sqrt{r^2 + h^2} . \tag{B-18}$$

But

$$\begin{aligned}
\epsilon &= \underset{(\xi,\eta)\,\epsilon\,\Sigma}{\text{Max}} \left\{ \frac{|\zeta(\xi,\eta) - \zeta(x_0, y_0)|}{r} \right\} \\
&= \underset{(\xi,\eta)\,\epsilon\,\Sigma}{\text{Max}} \left\{ \frac{|a(\xi + x_0)(\xi - x_0) + b(\eta + y_0)(\eta - y_0)|}{r} \right\} \\
&\leqslant \underset{(\xi,\eta)\,\epsilon\,\Sigma}{\text{Max}} \left\{ \sqrt{a^2(\xi + x_0)^2 + b^2(\eta + y_0)^2} \cdot \frac{\sqrt{(\xi - x_0)^2 + (\eta - y_0)^2}}{r} \right\} \\
&\leqslant \underset{(\xi,\eta)\,\epsilon\,\Sigma}{\text{Max}} \left\{ \sqrt{a^2(\xi + x_0)^2 + b^2(\eta + y_0)^2} \cdot 2 \right\} \\
&\leqslant 8\delta .
\end{aligned} \tag{B-19}$$

A much better bound on ϵ is available when (x,y) is several panel diameters away from Σ and the assumption that δ^2 is negligible becomes unnecessary. However, in this case a far-field expansion will be used to obtain an efficient approximation to the right side of equation (B-10).

Substituting equations (B-8), (B-13), and (B-18) into (B-10) and rearranging we obtain

$$\phi = \sigma(x, y)\, I(1, 1) + \sigma_x(x, y)\, I(2, 1) + \sigma_y(x, y)\, I(1, 2) \tag{B-20}$$

where

$$\begin{aligned}
\sigma(x, y) &= \sigma_0 + \sigma_\xi x + \sigma_\eta y \\
\sigma_x(x, y) &= \sigma_\xi \\
\sigma_y(x, y) &= \sigma_\eta .
\end{aligned} \tag{B-21}$$

Here

$$I(M, N) = -\frac{1}{4\pi}\Big[H(M, N, 1) + a\Big(hH(M+2, N, 3) + 2xhH(M+1, N, 3)\Big) + b\Big(hH(M, N+2, 3) + 2yhH(M, N+1, 3)\Big) + c\Big(hH(M, N, 3)\Big)\Big] \quad . \tag{B-22}$$

where

$$c = a\,x^2 + b\,y^2 - z_0 \tag{B-23}$$

and

$$H(M, N, K) = \iint_{\Sigma} \frac{(\xi - x)^{M-1}\,(\eta - y)^{N-1}}{\left(\sqrt{(\xi - x)^2 + (\eta - y)^2 + h^2}\right)^K}\,d\xi\,d\eta \quad . \tag{B-24}$$

The H integrals will be evaluated in the next section.

To find $\vec{V}$, equation (B-20) can be differentiated. For this purpose z_0 may be treated as a constant since its derivatives with respect to x and y either cancel or are negligible on account of hypothesis (B-6). The derivatives of the H integrals, then, are simple combinations of the H integrals themselves; i.e.,

$$\begin{aligned}
\frac{\partial}{\partial x} H(M, N, K) &= -(M-1)\,H(M-1, N, K) + KH(M+1, N, K+2) \\
\frac{\partial}{\partial y} H(M, N, K) &= -(N-1)\,H(M, N-1, K) + KH(M, N+1, K+2) \\
\frac{\partial}{\partial z} H(M, N, K) &= -KhH(M, N, K+2)\,.
\end{aligned} \tag{B-25}$$

Actually, it turns out to be easier to calculate $\vec{V}$ by differentiating equation (B-10) and using a generalized form of equation (B-18); that is,

$$\frac{1}{R^K} = \frac{1}{\rho^K} + \frac{Kh(\zeta - z_0)}{\rho^{K+2}}, \qquad \rho = \sqrt{r^2 + h^2}\,. \tag{B-26}$$

In either case we obtain

$$\vec{V} = \sigma(x, y)\,\vec{J}(1, 1) + \sigma_x(x, y)\,\vec{J}(2, 1) + \sigma_y(x, y)\,\vec{J}(1, 2) \tag{B-27}$$

where

$$\vec{J}(M, N) = \Big(J_x(M, N), J_y(M, N), J_z(M, N)\Big) \tag{B-28}$$

and

$$J_x(M, N) = -\frac{1}{4\pi}\Big[H(M+1, N, 3) + a\big(3hH(M+3, N, 5) + 6xhH(M+2, N, 5)\big) + b\big(3hH(M+1, N+2, 5) + 6yhH(M+1, N+1, 5)\big) + c\big(3hH(M+1, N, 5)\big)\Big]$$

$$J_y(M, N) = -\frac{1}{4\pi}\Big[H(M, N+1, 3) + a\big(3hH(M+2, N+1, 5) + 6xhH(M+1, N+1, 5)\big) + b\big(3hH(M, N+3, 5) + 6yhH(M, N+2, 5)\big) + c\big(3hH(M, N+1, 5)\big)\Big]$$

$$J_z(M, N) = -\frac{1}{4\pi}\Big[-hH(M, N, 3) + a\big(H(M+2, N, 3) - 3h^2H(M+2, N, 5) + 2xH(M+1, N, 3) - 6xh^2H(M+1, N, 5)\big) + b\big(H(M, N+2, 3) - 3h^2H(M, N+2, 5) + 2yH(M, N+1, 3) - 6yh^2H(M, N+1, 5)\big) + c\big(H(M, N, 3) - 3h^2H(M, N, 5)\big)\Big] .$$

Doublet potential and velocity can be evaluated similarly starting with equations (B-3) and using

$$\hat{n} = \frac{1}{\sqrt{1 + 4a^2\xi^2 + 4b^2\eta^2}}(-2a\xi, -2b\eta, 1) \tag{B-29}$$

along with equation (B-26) and hypothesis (B-6). We obtain

$$\phi = \mu(x, y)\, I(1, 1) + \mu_x(x, y)\, I(2, 1) + \mu_y(x, y)\, I(1, 2) + \frac{1}{2}\mu_{xx}(x, y)\, I(3, 1) + \mu_{xy}(x, y)\, I(2, 2) + \frac{1}{2}\mu_{yy}(x, y)\, I(1, 3) \tag{B-30}$$

where

$$\begin{aligned} \mu(x, y) &= \mu_0 + \mu_\xi x + \mu_\eta y + \frac{1}{2}\mu_{\xi\xi}x^2 + \mu_{\xi\eta}xy + \frac{1}{2}\mu_{\eta\eta}y^2 \\ \mu_x(x, y) &= \mu_\xi + \mu_{\xi\xi}x + \mu_{\xi\eta}y \\ \mu_y(x, y) &= \mu_\eta + \mu_{\xi\eta}x + \mu_{\eta\eta}y \\ \mu_{xx}(x, y) &= \mu_{\xi\xi} \\ \mu_{xy}(x, y) &= \mu_{\xi\eta} \\ \mu_{yy}(x, y) &= \mu_{\eta\eta} \end{aligned} \tag{B-31}$$

and

$$I(M, N) = \frac{1}{4\pi}\Big[hH(M, N, 3) + a\Big(H(M+2, N, 3) + 3h^2H(M+2, N, 5) + 6xh^2H(M+1, N, 5)\Big) + b\Big(H(M, N+2, 3) + 3h^2H(M, N+2, 5) + 6yh^2H(M, N+1, 5)\Big) + c\Big(-H(M, N, 3) + 3h^2H(M, N, 5)\Big)\Big]. \quad \text{(B-32)}$$

We also obtain

$$\vec{V} = \mu(x, y)\,\vec{J}(1, 1) + \mu_x(x, y)\,\vec{J}(2, 1) + \mu_y(x, y)\,\vec{J}(1, 2) + \frac{1}{2}\mu_{xx}(x, y)\,\vec{J}(3, 1) + \mu_{xy}(x, y)\,\vec{J}(2, 2) + \frac{1}{2}\mu_{yy}(x, y)\,\vec{J}(1, 3) \quad \text{(B-33)}$$

where

$$\vec{J}(M, N) = \Big(J_x(M, N), J_y(M, N), J_z(M, N)\Big) \quad \text{(B-34)}$$

and

$$J_x(M, N) = \frac{1}{4\pi}\Big[3hH(M+1, N, 5) + a\Big(3H(M+3, N, 5) - 2H(M+1, N, 3) + 15h^2H(M+3, N, 7) - 2xH(M, N, 3) + 30xh^2H(M+2, N, 7)\Big) + b\Big(3H(M+1, N+2, 5) + 15h^2H(M+1, N+2, 7) + 30yh^2H(M+1, N+1, 7)\Big) + c\Big(-3H(M+1, N, 5) + 15h^2H(M+1, N, 7)\Big)\Big]$$

$$J_y(M, N) = \frac{1}{4\pi}\Big[3hH(M, N+1, 5) + a\Big(3H(M+2, N+1, 5) + 15h^2H(M+2, N+1, 7) + 30xh^2H(M+1, N+1, 7)\Big) + b\Big(3H(M, N+3, 5) - 2H(M, N+1, 3) + 15h^2H(M, N+3, 7) - 2yH(M, N, 3) + 30yh^2H(M, N+2, 7)\Big) + c\Big(-3H(M, N+1, 5) + 15h^2H(M, N+1, 7)\Big)\Big]$$

$$J_z(M, N) = \frac{1}{4\pi}\Big[H(M, N, 3) - 3h^2H(M, N, 5) + a\Big(3hH(M+2, N, 5) - 15h^3H(M+2, N, 7) + 12xhH(M+1, N, 5) - 30xh^3H(M+1, N, 7)\Big) + b\Big(3hH(M, N+2, 5) - 15h^3H(M, N+2, 7) + 12yhH(M, N+1, 5) - 30yh^3H(M, N+1, 7)\Big) + c\Big(9hH(M, N, 5) - 15h^3H(M, N, 7)\Big)\Big] .$$

B.3 CALCULATION OF H INTEGRALS

In this section we shall compute in closed form the integrals

$$H(M, N, K) = \iint_{\Sigma} \frac{(\xi - x)^{M-1} (\eta - y)^{N-1}}{\rho^K} \, d\xi \, d\eta, \tag{B-35}$$

$$\rho = \sqrt{(\xi - x)^2 + (\eta - y)^2 + h^2}$$

for M = 1, MXQ; N = 1, MXQ-M + 1; K = 1, MXK,2.

Here MXQ is the maximum value of M + N-1 required and MXK is the maximum value of K required. The following values of MXQ and MXK are evident from the previous section.

Panel Type	MXQ	MXK
Source potential (flat panel)	2	1
Source velocity (flat panel)	3	3
Doublet potential (flat panel)	3	3
Doublet velocity (flat panel)	4	5
Source potential (curved panel)	4	3
Source velocity (curved panel)	5	5
Doublet potential (curved panel)	5	5
Doublet velocity (curved panel)	6	7

(B-36)

The integrals H(M,N,K) may be computed with the aid of the following algebraic recursion relations. We have the obvious identity

$$H(M + 2, N, K) + H(M, N + 2, K) + h^2 H(M, N, K) = H(M, N, K - 2) \tag{B-37}$$

Integration by parts yields

$$(K - 2) H(M, N, K) = (M - 2) H(M - 2, N, K) - \sum_{1}^{4} \nu_{\xi} F(M - 1, N, K - 2) \tag{B-38}$$

and

$$(K - 2) H(M, N, K) = (N - 2) H(M, N - 2, K - 2) - \sum_{1}^{4} \nu_{\eta} F(M, N - 1, K - 2) . \tag{B-39}$$

The summations on the right sides of equations (B-38) and (B-39) are over all four sides of Σ with the contribution of a typical side L displayed. Here $\hat{\nu}$ is the unit outer normal of the side L (see fig. 31) and F(M,N,K) is the line integral defined by

$$F(M, N, K) = \int_{L} \frac{(\xi - x)^{M-1} (\eta - y)^{N-1}}{\rho^K} \, d\ell, \quad \rho = \sqrt{(\xi - x)^2 + (\eta - y)^2 + h^2} . \tag{B-40}$$

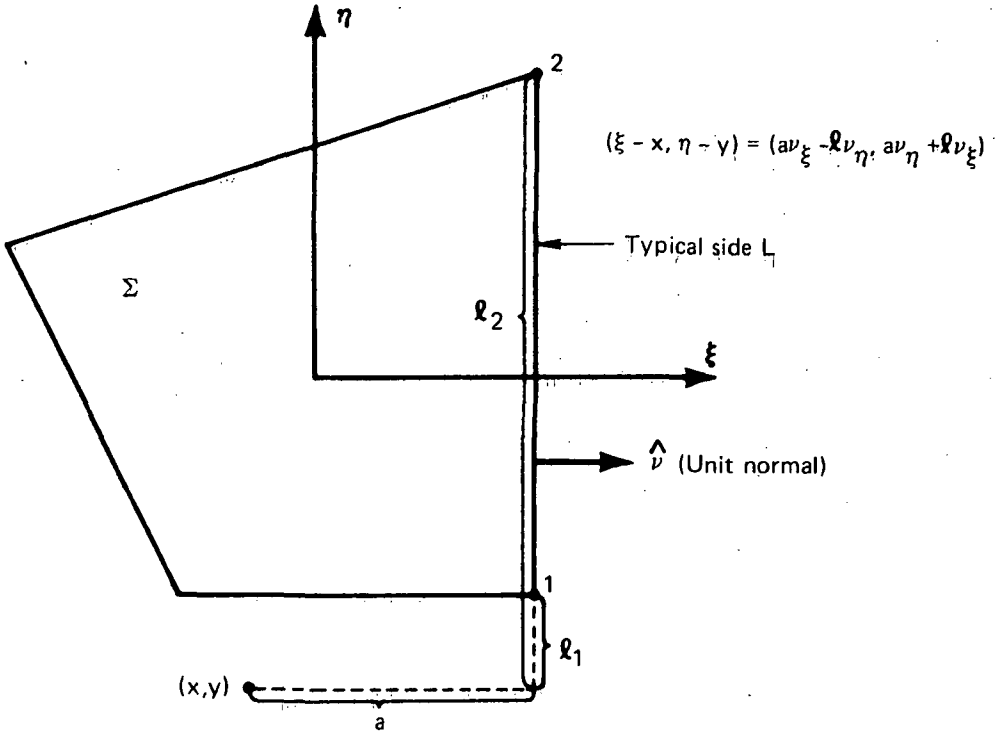

Figure 31.—Quadrilateral Geometry

The procedure for evaluating the F integrals will be described later. Assuming the F integrals are known, the recursion relations (B-37), (B-38), and (B-39) may be recombined to yield an efficient procedure for calculating the H integrals. Because some of the H integrals are singular on the edge of S, it is actually necessary to consider three slightly different procedures, depending on the relationship of the field point to the panel. Let us define d_H to be the minimum distance of the point (x,y) to the perimeter of Σ. If δ_h is some small number (nominally chosen as 0.01), we have the following three procedures.

Procedure 1: $|h| \geqslant \delta_h \, d_H$

1.

$$H(1,1,1) = -|h| \sum_1^4 \tan^{-1}\left[a(\ell_2 c_1 - \ell_1 c_2), c_1 c_2 + a^2 \ell_1 \ell_2\right] + \sum_1^4 aF(1,1,1) \quad \text{(B-41)}$$

where

$$c_1 = g^2 + |h|\sqrt{\ell_1^{\,2} + g^2}\,, \quad c_2 = g^2 + |h|\sqrt{\ell_2^{\,2} + g^2}$$

and

$$g = \sqrt{a^2 + h^2}$$

2.

$$H(1,1,K) = \frac{1}{(K-2)\,h^2}\left[(K-4)\,H(1,1,K-2) + \sum_1^4 aF(1,1,K-2)\right]; \quad \text{(B-42)}$$

$$K = 3, MXK, 2\,.$$

3.

$$H(2,N,1) = \frac{1}{(N+1)}\left[h^2 \sum_1^4 \nu_\xi F(1,N,1) + \sum_1^4 aF(2,N,1)\right]; \quad \text{(B-43)}$$

$$N = 1, MXQ - 1\,.$$

4.

$$H(1,N,1) = \frac{1}{N}\left[-h^2(N-2)\,H(1,N-2,1) + h^2 \sum_1^4 \nu_\eta F(1,N-1,1) + \sum_1^4 aF(1,N,1)\right]; \quad N = 2, MXQ\,. \quad \text{(B-44)}$$

5.

$$H(M, N, 1) = \frac{1}{(M + N - 1)}\left[-h^2(M - 2)\, H(M - 2, N, 1) + h^2 \sum_{1}^{4} \nu_\xi F(M - 1, N, 1) + \sum_{1}^{4} aF(M, N, 1)\right]; \quad M = 3, MXQ \text{ and } N = 1, MXQ - M + 1 . \tag{B-45}$$

6.

$$H(1, N, K) = \frac{1}{(K - 2)}\left[(N - 2)\, H(1, N - 2, K - 2) - \sum_{1}^{4} \nu_\eta F(1, N - 1, K - 2)\right]; \tag{B-46}$$

N = 2, MXQ and K = 3, MXK, 2.

7.

$$H(2, N, K) = \frac{1}{(K - 2)}\left[- \sum_{1}^{4} \nu_\xi F(1, N, K - 2)\right]; \tag{B-47}$$

N = 1, MXQ -1 and K = 3, MXK, 2.

$$H(M, N, K) = -H(M - 2, N + 2, K) - h^2 H(M - 2, N, K) + H(M - 2, N, K - 2); \tag{B-48}$$

M = 3, MXQ and N = 1, MXQ - M + 1 and K = 3, MXK, 2.

Procedure 2: $|h| < \delta_h d_H$ and $(x, y) \epsilon \Sigma$

1. $H(1, 1, NHK + MXK) = 0.0$ (B-49)

where NHK is a positive integer (nominally taken to be 16).

2.

$$H(1, 1, K - 2) = \frac{1}{(K - 4)}\left[h^2(K - 2)\, H(1, 1, K) - \sum_{1}^{4} aF(1, 1, K - 2)\right]; \tag{B-50}$$

K = NHK + MXK, 3, 2.

3. All remaining steps are as for Procedure 1.

Procedure 3: $|h| < \delta_h d_H$ and $(x, y) \epsilon \Sigma$

Define

$$H^*(M, N, K) = H(M, N, K) - 2\pi\lambda(M, N, K)\, |h|^{M+N-K} \tag{B-51}$$

where

$$\lambda(M, N, K) = \begin{cases} 0 \text{ if M or N is even} \\ \dfrac{[1 \cdot 1 \cdot 3 \cdot 5 \ldots (M-2)][1 \cdot 1 \cdot 3 \cdot 5 \ldots (N-2)]}{[(K-2)(K-4)(K-6) \ldots (K-M-N)]} \text{ otherwise.} \end{cases} \tag{B-52}$$

Then Procedure 2 may be used to calculate H*.

We now evaluate the integrals F(M,N,K) for the indices M,N,K required by the H evaluation procedures. It is apparent that we need only the following F integrals:

$$\begin{aligned} &F(1, 1, K) \ ; \ K = 1, MXFK, 2 \\ &F(M, N, 1) \ ; \ M = 1, MXQ \text{ and } N = 1, MXQ - M + 1 \\ &F(1, N, K) \ ; \ N = 2, MXQ \text{ and } K = 3, MXK - 2, 2 \end{aligned} \tag{B-53}$$

where

$$MXFK = \begin{cases} MXK - 2 \text{ if } |h| \geq \delta_h d_H \\ NHK + MXK - 2 \text{ if } |h| < \delta_h d_H \end{cases} \tag{B-54}$$

These integrals may be obtained with the aid of three recursion relations. We have the following obvious identities:

$$F(M + 2, N, K) + F(M, N + 2, K) + h^2 F(M, N, K) = F(M, N, K - 2) \tag{B-55}$$

and

$$\nu_\xi F(M + 1, N, K) + \nu_\eta F(M, N + 1, K) = aF(M, N, K) . \tag{B-56}$$

Integration by parts yields

$$\begin{aligned} &-(M - 1)\, \nu_\eta F(M - 1, N, K - 2) + (N - 1)\, \nu_\xi F(M, N - 1, K - 2) \\ &+(K - 2)\, \nu_\eta F(M + 1, N, K) - (K - 2)\, \nu_\xi F(M, N + 1, K) = E(M, N, K - 2) \end{aligned} \tag{B-57}$$

where

$$E(M, N, K) = \left. \frac{(\xi - x)^{M-1} (\eta - y)^{N-1}}{\rho^K} \right|_1^2 , \tag{B-58}$$

$$\rho = \sqrt{(\xi - x)^2 + (\eta - y)^2 + h^2} \quad .$$

The quantities E(M,N,K) may be evaluated directly or else recursively with the aid of the formula

$$P(I) = (x_2 + x_1)\,P(I-1) - x_1 x_2 P(I-2) \qquad \text{(B-59)}$$

where

$$P(I) = A_2 x_2^{I-1} - A_1 x_1^{I-1}$$

The recursion relations (B-55), (B-56), and (B-57) may be recombined to yield an efficient procedure for evaluating the required F integrals. Here, again, the singular behavior of some of the F integrals near the edges of S requires a special case. Let us define d_F to be the minimum distance of the point (x,y,z) to the perimeter of S. Then if δ_g is some small number (nominally chosen as 0.01), we have the following two procedures.

Procedure 4: $g \geqslant \delta_g d_F$

1.

$$F(1,1,1) = \log\left(\sqrt{\ell^2+g^2}+\ell\right)\Big|_1^2$$

$$= \begin{cases} \log\left(\dfrac{\sqrt{\ell_2^2+g^2}+\ell_2}{\sqrt{\ell_1^2+g^2}+\ell_1}\right); & \ell_1,\ell_2 \geqslant 0 \\ \log\left(\dfrac{\sqrt{\ell_1^2+g^2}-\ell_1}{\sqrt{\ell_2^2+g^2}-\ell_2}\right); & \ell_1,\ell_2 < 0 \\ \log\left(\dfrac{\left(\sqrt{\ell_1^2+g^2}-\ell_1\right)\left(\sqrt{\ell_2^2+g^2}+\ell_2\right)}{g^2}\right); & \ell_2 \geqslant 0, \ell_1 < 0 \end{cases} \qquad \text{(B-60)}$$

2.

$$F(1,1,K) = \frac{1}{g^2(K-2)}\left[(K-3)\,F(1,1,K-2) - \nu_\eta E(2,1,K-2) + \nu_\xi E(1,2,K-2)\right]; \qquad \text{(B-61)}$$

K = 3, MXFK, 2.

3. a. If $|\nu_\eta| \leqslant |\nu_\xi|$

(i) $$F(1, N, 1) = \frac{1}{(N-1)}\Big[(2N-3)\, a\nu_\eta F(1, N-1, 1) - (N-2)(a^2 + \nu_\xi{}^2 h^2)\, F(1, N-2, 1) + \nu_\xi E(1, N-1, -1)\Big]; \quad \text{(B-62)}$$

$N = 2, MXQ.$

(ii) $$F(M, N, 1) = \frac{-\nu_\eta}{\nu_\xi} F(M-1, N+1, 1) + \frac{a}{\nu_\xi} F(M-1, N, 1); \quad \text{(B-63)}$$

$M = 2, MXQ$ and $N = 1, MXQ - M + 1.$

b. If $|\nu_\xi| \leqslant |\nu_\eta|$

(i) $$F(M, 1, 1) = \frac{1}{(M-1)}\Big[(2M-3)\, a\nu_\xi F(M-1, 1, 1) - (M-2)(a^2 + \nu_\eta{}^2 h^2)\, F(M-2, 1, 1) - \nu_\eta E(M-1, 1, -1)\Big]; \quad \text{(B-64)}$$

$M = 2, MXQ.$

(ii) $$F(M, N, 1) = \frac{-\nu_\xi}{\nu_\eta} F(M+1, N-1, 1) + \frac{a}{\nu_\eta} F(M, N-1, 1); \quad \text{(B-65)}$$

$N = 2, MXQ$ and $M = 1, MXQ - N + 1.$

4. $$F(1, 2, K) = \nu_\eta a F(1, 1, K) - \left.\frac{\nu_\xi}{(K-2)(\ell^2 + g^2)^{\frac{K-2}{2}}}\right|_1^2; \quad \text{(B-66)}$$

$K = 3, MXK - 2, 2.$

5. $$F(1, N, K) = 2a\nu_\eta F(1, N-1, K) - (a^2 + \nu_\xi{}^2 h^2)\, F(1, N-2, K) + \nu_\xi{}^2 F(1, N-2, K-2); \quad \text{(B-67)}$$

$N = 3, MXQ$ and $K = 3, MXK - 2, 2.$

Procedure 5: $g < \delta_g d_F$

1. $$F(1, 1, MXFK + NFK) = 0 \quad \text{(B-68)}$$

where NFK is a positive integer (nominally taken as 16) .

2.

$$F(1,1,K-2) = \frac{1}{(K-3)}\left[g^2(K-2)\,F(1,1,K) + \nu_\eta E(2,1,K-2) - \nu_\xi E(1,2,K-2)\right];$$

$$K = MXFK + NFK,\ 5,\ 2. \tag{B-69}$$

3. F(1,1,1) as well as all other F integrals may be computed in the same manner as for Procedure 4.

This completes the calculation of the H integrals.

B.4 EVALUATION OF SOURCE AND DOUBLET INTEGRALS FOR A DISTANT FIELD POINT

If the point $\vec{P}$ is a large distance from S, the approximation (B-18) may be replaced by an approximation based on this fact. Let

$$P = |\vec{P}| \text{ and } Q = |\vec{Q}| \tag{B-70}$$

Then

$$\frac{1}{R} = \frac{1}{\sqrt{P^2 - 2(\vec{P}\cdot\vec{Q}) + Q^2}} = \frac{1}{P}\,\frac{1}{\sqrt{1 + \dfrac{-2(\vec{P}\cdot\vec{Q}) + Q^2}{P^2}}} \tag{B-71}$$

Let

$$\epsilon = \frac{1}{P}\underset{(\xi,\eta)\,\epsilon\,\Sigma}{\text{Max}}\left\{Q\right\} \tag{B-72}$$

Then

$$\left|\frac{-2(\vec{P}\cdot\vec{Q}) + Q^2}{P^2}\right| \leqslant 2\epsilon + \epsilon^2 \tag{B-73}$$

Hence, if

$$\epsilon << 1, \tag{B-74}$$

we have

$$\frac{1}{R} \approx \frac{1}{P} + \frac{(\vec{P}\cdot\vec{Q})}{P^3} - \frac{1}{2}\left(\frac{Q^2}{P^3} - \frac{3(\vec{P}\cdot\vec{Q})^2}{P^5}\right) \tag{B-75}$$

Only the first three terms of the binomial expansion are displayed (monopole, dipole, and quadrupole). In practice this expansion is used only when ϵ is less than 1/5. All three terms are used unless ϵ is less than 1/8, in which case only the first two terms are required.

Substituting (B-75) into (B-10) and using hypothesis (B-6), we obtain for the source potential

$$\phi = \sigma_0 I(1,1) + \sigma_\xi I(2,1) + \sigma_\eta I(1,2) \tag{B-76}$$

Here

$$I(M, N) = -\frac{1}{4\pi}\left[\frac{1}{P} C(M, N) + \frac{1}{P^2}(\vec{q}(M, N) \cdot \vec{p}) - \frac{1}{2}\frac{1}{P^3}(qq(M, N) - 3\vec{p} \cdot \vec{pq}(M, N))\right] \quad \text{(B-77)}$$

where

$$C(M, N) = \iint_{\Sigma} \xi^{M-1} \eta^{N-1} \, d\xi \, d\eta \,, \quad \text{(B-78)}$$

$$\vec{q}(M, N) = \left(C(M + 1, N), C(M, N + 1), aC(M + 2, N) + bC(M, N + 2)\right), \quad \text{(B-79)}$$

$$qq(M, N) = C(M + 2, N) + C(M, N + 2), \quad \text{B-80)}$$

$$\vec{pq}(M, N) = \left(\vec{p} \cdot \vec{q}(M + 1, N), \vec{p} \cdot \vec{q}(M, N + 1), a\vec{p} \cdot \vec{q}(M + 2, N) + b\vec{p} \cdot \vec{q}(M, N + 2)\right), \quad \text{(B-81)}$$

and

$$p = \frac{\vec{P}}{P}. \quad \text{(B-82)}$$

In computing the last component of $\vec{pq}$, the last component of $\vec{q}$ may be ignored on account of hypothesis (B-6). The integrals C(M,N) will be evaluated later. The induced source velocity may be obtained by differentiating equation (B-76) and is given by

$$\vec{V} = \sigma_0 \vec{J}(1, 1) + \sigma_\xi \vec{J}(2, 1) + \sigma_\eta \vec{J}(1, 2) \quad \text{(B-83)}$$

where

$$\vec{J}(M, N) = -\frac{1}{4\pi}\left[-\frac{1}{P^2} C(M, N) \vec{P} + \frac{1}{P^3}\left(\vec{q}(M, N) - 3\left(\vec{p} \cdot \vec{q}(M, N)\right)\vec{p}\right) + \frac{1}{P^4}\left(3\vec{pq}(M, N) + \frac{3}{2}\left(qq(M, N) - 5\left(\vec{p} \cdot \vec{pq}(M, N)\right)\right)\vec{p}\right)\right]. \quad \text{(B-84)}$$

A similar expansion may be obtained for the doublet-induced potential and velocity. Substituting the approximation (B-75) into equation (B-3) and using hypothesis (B-6), we obtain:

$$\phi \approx \mu_0 I(1, 1) + \mu_\xi I(2, 1) + \mu_\eta I(1, 2) + \frac{1}{2}\mu_{\xi\xi} I(3, 1) + \mu_{\xi\eta} I(2, 2) + \frac{1}{2}\mu_{\eta\eta} I(1, 3). \quad \text{(B-85)}$$

Here

$$I(M, N) = \frac{1}{4\pi}\left[\frac{1}{P^2}\left(\vec{p} \cdot \vec{n}(M, N) - \frac{1}{P^3}\left(nq(M, N) - 3\vec{p} \cdot \vec{pn}(M, N)\right)\right)\right], \quad \text{(B-86)}$$

where

$$\vec{n}(M, N) = \left(-2aC(M+1, N), -2bC(M, N+1), C(M, N)\right), \quad \text{(B-87)}$$

$$nq(M, N) = -aC(M+2, N) - bC(M, N+2), \quad \text{(B-88)}$$

and

$$\vec{pn}(M, N) = \left(\vec{p} \cdot \vec{n}(M+1, N), \vec{p} \cdot \vec{n}(M, N+1), a\vec{p} \cdot \vec{n}(M+2, N) + b\vec{p} \cdot \vec{n}(M, N+2)\right). \quad \text{(B-89)}$$

In computing the last component of $\vec{pn}$ the first two components of $\vec{n}$ may be ignored on account of hypothesis (B-6). The induced velocity may be obtained by differentiating equation (B-85) and is given by

$$\vec{V} = \mu_0 \vec{J}(1, 1) + \mu_\xi \vec{J}(2, 1) + \mu_\eta \vec{J}(1, 2) + \frac{1}{2}\mu_{\xi\xi} \vec{J}(3, 1) + \mu_{\xi\eta} \vec{J}(2, 2) + \frac{1}{2}\mu_{\eta\eta} \vec{J}(1, 3). \quad \text{(B-90)}$$

Here

$$\vec{J}(M, N) = \frac{1}{4\pi}\left[\frac{1}{p^3}\left(\vec{n}(M, N) - 3\left(\vec{p} \cdot \vec{n}(M, N)\right)\vec{p}\right) + \frac{1}{p^4}\left(\left(3nq(M, N) - 15\left(\vec{p} \cdot \vec{pn}(M, N)\right)\right)\vec{p} + 3\vec{pn}(M, N) + 3n\vec{p}(M, N)\right)\right], \quad \text{(B-91)}$$

where

$$n\vec{p}(M, N) = \left(-2a\vec{p} \cdot \vec{q}(M+1, N), -2b\vec{p} \cdot \vec{q}(M, N+1), \vec{p} \cdot \vec{q}(M, N)\right). \quad \text{(B-92)}$$

In computing the first two components of $\vec{np}$, the last component of $\vec{q}$ may be ignored on account of hypothesis (B-6). Note that the quadrupole term of expansion (B-75) is not used in the computation of doublet-induced potential and velocity.

The computation of the C(M,N) integrals of equation (B-78) is similar to the computation of the H integrals of section (B.3) but much simpler. The range for the indices M and N is the same as that for the H integrals; i.e.,

$$M = 1, MXQ; \quad N = 1, MXQ - M + 1 \quad \text{(B-93)}$$

where MXQ is given in (B-36). Using the same notation as that of figure 31, we note that integration by parts yields

$$C(M, N) = \frac{1}{(M+N)} \sum_{1}^{4} aG(M, N); \quad M = 1, MXQ \text{ and } N = 1, MXQ - M + 1 \quad \text{(B-94)}$$

where

$$G(M, N) = \int_L \xi^{M-1} \eta^{N-1} \, d\ell; \quad M = 1, MXQ \text{ and } N = 1, MXQ - M + 1 \quad \text{(B-95)}$$

The integrals G(M,N) may be obtained with the aid of two recursion relations. We have the obvious identity

$$\nu_\xi G(M+1, N) + \nu_\eta G(M, N+1) = aG(M, N) \tag{B-96}$$

Integration by parts yields

$$-(M-1)\,\nu_\eta G(M-1, N) + (N-1)\,\nu_\xi G(M, N-1) = D(M, N) \tag{B-97}$$

where

$$D(M, N) = \xi^{M-1}\,\eta^{N-1}\Big|_1^2 \tag{B-98}$$

The quantities D(M,N) may be evaluated directly or else recursively with the aid of equation (B-59). The recursion relations (B-96) and (B-97) may be recombined to yield an efficient procedure for evaluating the G integrals.

Procedure 6:

1. a. If $|\nu_\eta| \leq |\nu_\xi|$

(i) $$G(1, N) = \frac{1}{N\nu_\xi} D(1, N+1);\ N = 1, MXQ. \tag{B-99}$$

(ii) $$G(M, N) = -\frac{\nu_\eta}{\nu_\xi} G(M-1, N+1) + \frac{a}{\nu_\xi} G(M-1, N); \tag{B-100}$$

$M = 2, MXQ$ and $N = 1, MXQ - M + 1$.

b. If $|\nu_\xi| < |\nu_\eta|$

(i) $$G(M, 1) = -\frac{1}{M\nu_\eta} D(M+1, 1);\ N = 1, MXQ \tag{B-101}$$

(ii) $$G(M, N) = -\frac{\nu_\xi}{\nu_\eta} G(M+1, N-1) + \frac{a}{\nu_\eta} G(M, N-1); \tag{B-102}$$

$N = 2, MXQ$ and $M = 1, MXQ - N + 1$.

This completes the evaluation of the source and doublet potential and velocity for a distant field point.

APPENDIX C
GEOMETRY UPDATE COEFFICIENTS

The coefficients $\partial E/\partial\theta$, $\partial F/\partial\theta$, and $\partial G/\partial\theta$ of the Jacobian, equation (48), are termed geometry update coefficients. They are calculated based on the following assumptions:

a) Changes of the aerodynamic influence coefficients due to changes of the panel inclination θ are neglected.

b) The vector normal to the free sheet at control points close to wing edges is not affected by changes of θ.

c) The chord length of panel segments in transverse geometry cuts (y,z-planes) does not change during the iteration, i.e., $l_{i,m}$ = constant (see fig. 32a).

d) The free-sheet geometry is updated such that panel corner points move only in transverse cuts, i.e., $\Delta x = 0$.

Coefficient $\partial E/\partial\theta$

$E = \vec{n} \cdot \vec{V}^S$ is defined as the normal velocity at boundary points in the vicinity of wing edges. Hence,

$$\frac{\partial E}{\partial\theta} = \frac{\partial\vec{n}}{\partial\theta} \cdot \vec{V}^S + \vec{n} \cdot \frac{\partial\vec{V}^S}{\partial\theta} = 0 \qquad \text{(C-1)}$$

The coefficient is zero due to assumptions a) and b) and because $\partial\vec{n}/\partial\theta = 0$ at all boundary points on the wing.

Coefficient $\partial F/\partial\theta$

The quantity F stands for $\vec{n} \cdot \vec{V}^S$ on the wing and the pressure jump Δc_P across the free sheet. Let

$$F_1 = \vec{n} \cdot \vec{V}^S \qquad \text{(wing)} \qquad \text{(C-2)}$$

and

$$F_2 = \Delta c_P = \frac{2}{U_\infty^2} \vec{V}^S \cdot \nabla\mu \qquad \text{(free sheet)} \qquad \text{(C-3)}$$

which is given by equation (E-11). Application of assumption a) results in

$$\frac{\partial F_1}{\partial\theta} = \vec{n} \cdot \frac{\partial\vec{V}^S}{\partial\theta} = 0 \qquad \text{(C-4)}$$

a. Transverse Cut Through Free Sheet

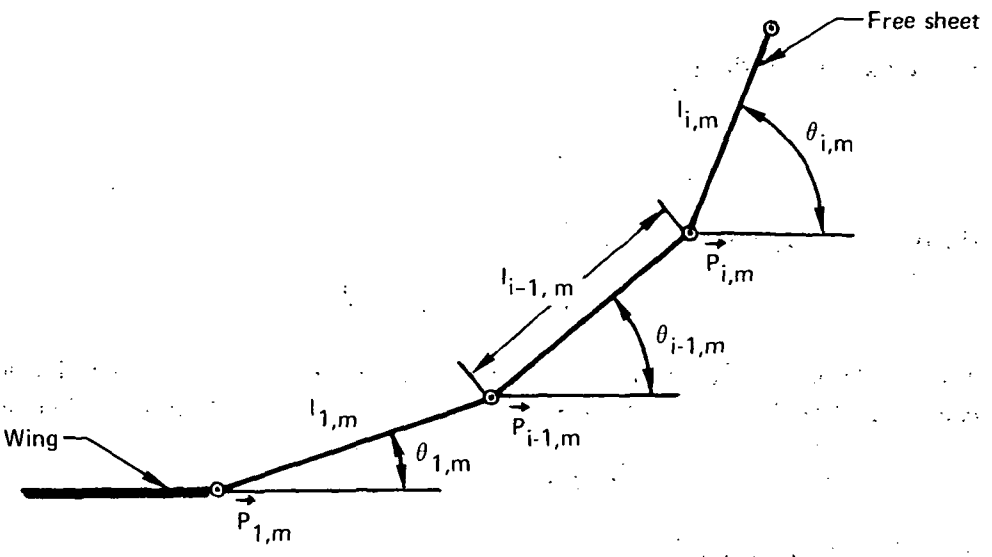

b. Single Panel

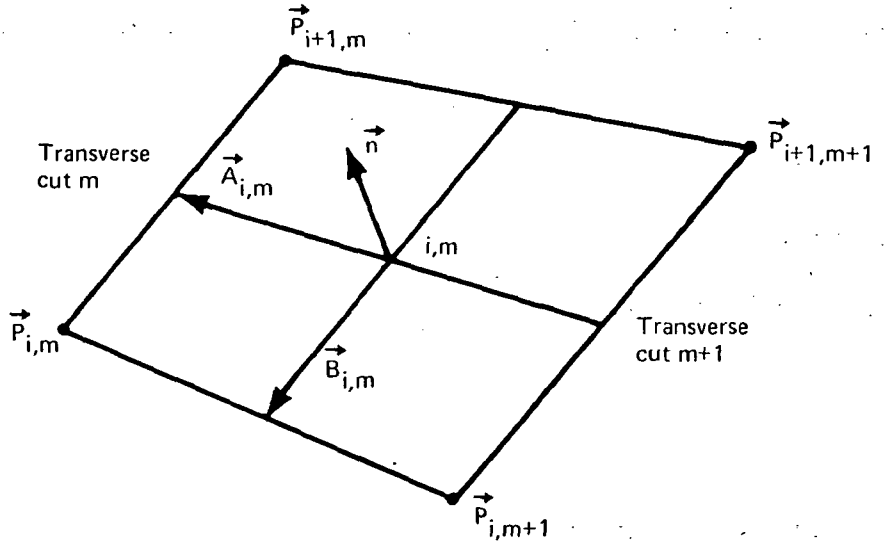

Figure 32.—Notation for Updating of Free-Sheet Geometry

$$\frac{\partial F_2}{\partial \theta} = \frac{2}{U_\infty{}^2} \vec{V}^S \cdot \frac{\partial}{\partial \theta} (\nabla \mu) \tag{C-5}$$

$\nabla \mu$ is a vector parallel to the free sheet; i.e.,

$$\nabla \mu \cdot \vec{n} = 0 \tag{C-6}$$

Differentiating equation (C-6) for θ gives

$$\frac{\partial}{\partial \theta} (\nabla \mu) \cdot \vec{n} = - \nabla \mu \cdot \frac{\partial \vec{n}}{\partial \theta} \tag{C-7}$$

Noting that $\partial/\partial\theta(\nabla\mu)\Delta\theta$ is a vector normal to the free-sheet surface for small rotations $\Delta\theta$, and recalling that $\vec{n}$ is the unit normal vector ($\vec{n} \cdot \vec{n} = 1$), equation (C-7) leads to

$$\frac{\partial}{\partial \theta} (\nabla \mu) = - \left(\nabla \mu \cdot \frac{\partial n}{\partial \theta} \right) \vec{n} \tag{C-8}$$

Equation (C-5) thus takes the form

$$\frac{\partial F_2}{\partial \theta} = - \frac{2}{U_\infty{}^2} \left(\vec{n} \cdot V^S \right) \left(\nabla \mu \cdot \frac{\partial \vec{n}}{\partial \theta} \right) \tag{C-9}$$

Expressions for $\partial\vec{n}/\partial\theta$ will be derived below.

Coefficient $\partial G/\partial\theta$

$G = \vec{n} \cdot \vec{V}^S$ is the normal velocity component at the center of a free-sheet panel. Hence,

$$\frac{\partial G}{\partial \theta} = \vec{V}^S \cdot \frac{\partial \vec{n}}{\partial \theta} \tag{C-10}$$

taking assumption a) into account.

Derivative $\partial\vec{n}/\partial\theta$

The panel normal vector is

$$\vec{n} = \frac{\vec{N}}{|\vec{N}|} \tag{C-11}$$

with

$$\vec{N} = \vec{A} \times \vec{B}$$

illustrated in figure 32b. Hence,

$$\frac{\partial \vec{n}}{\partial \theta} = \frac{1}{|\vec{N}|} \left[\frac{\partial \vec{N}}{\partial \theta} - \left(\vec{n} \cdot \frac{\partial \vec{N}}{\partial \theta} \right) \vec{n} \right] \tag{C-12}$$

$$\frac{\partial \vec{N}}{\partial \theta} = \frac{\partial \vec{A}}{\partial \theta} \times \vec{B} + \vec{A} \times \frac{\partial \vec{B}}{\partial \theta} \tag{C-13}$$

The vectors $\vec{A}$ and $\vec{B}$ are expressed in terms of vectors pointing in direction of the panel corner points from some common origin. They read for panel i,m

$$\vec{A}_{i,m} = \vec{P}_{i,m} + \vec{P}_{i+1,m} - \vec{P}_{i,m+1} - \vec{P}_{i+1,m+1} \tag{C-14}$$

$$\vec{B}_{i,m} = \vec{P}_{i,m} + \vec{P}_{i,m+1} - \vec{P}_{i+1,m} - \vec{P}_{i+1,m+1}$$

Assumptions c) and d) are used for the calculation of the changes in panel corner-point positions. Adopting the notation of figure 32a for the mth transverse cut through the free sheet, the partial derivatives $\partial\vec{P}/\partial\theta$ take the form

$$\frac{\partial \vec{P}_{i,m}}{\partial \theta_{j,n}} = \begin{Bmatrix} 0 \\ 0 \\ 0 \end{Bmatrix} \qquad (n \neq m \text{ or } j \geqslant i)$$

$$\frac{\partial \vec{P}_{i,m}}{\partial \theta_{j,n}} = \begin{Bmatrix} 0 \\ -l_{j,n} \sin\theta_{j,n} \\ l_{j,n} \cos\theta_{j,n} \end{Bmatrix} \qquad (n = m, j < i) \tag{C-15}$$

Consequently, the derivatives of $\vec{A}_{i,m}$, $\vec{B}_{i,m}$, $\vec{N}_{i,m}$ are zero for $n \neq m$, $m + 1$, or $j \geqslant i$. Hence,

$$\frac{\partial \vec{n}_{i,m}}{\partial \theta_{j,n}} = 0 \qquad (n \neq m, m + 1, \text{ or } j \geqslant i)$$

APPENDIX D
DOUBLET-STRENGTH UPDATE COEFFICIENTS

The following coefficients of the Jacobian, equation (48), are termed doublet-strength update coefficients.

$$\frac{\partial E}{\partial \mu_e} \; ; \; \frac{\partial E}{\partial \mu_r} \; ; \; \frac{\partial F}{\partial \mu_e} \; ; \; \frac{\partial F}{\partial \mu_r} \; ; \; \frac{\partial G}{\partial \mu_e} \; ; \; \frac{\partial G}{\partial \mu_r}$$

The boundary conditions $F = 0$ are divided into

$$F_1 = \vec{n} \cdot \vec{V}^S = 0 \qquad \text{(wing)} \qquad \text{(D-1)}$$

$$F_2 = \Delta c_P = \frac{2}{U_\infty{}^2} \vec{V}^S \cdot \nabla\mu = 0 \qquad \text{(free sheet/wake)} \qquad \text{(D-2)}$$

Coefficients $\partial E/\partial\mu$, $\partial F_1/\partial\mu$, $\partial G/\partial\mu$ ($\mu = \mu_e, \mu_r$)

The symbols E, F, and G represent normal velocities at control points

$$V_\zeta{}^S = \vec{n} \cdot \vec{V}^S \qquad \text{(D-3)}$$

which can be written in subscripted notation as

$$V_\zeta{}^S = A_{\zeta_j} \mu_j + U_\zeta \qquad \text{(D-4)}$$

The derivative of $V_\zeta{}^S$ with respect to a particular doublet parameter μ_n is

$$\frac{\partial V_\zeta{}^S}{\partial \mu_n} = A_{\zeta_n} \qquad \text{(D-5)}$$

Hence, the coefficients $\partial E/\partial\mu_e$, $\partial E/\partial\mu_r$, $\partial F_1/\partial\mu_e$, $\partial F_1/\partial\mu_r$, $\partial G/\partial\mu_e$, $\partial G/\partial\mu_r$ are aerodynamic influence coefficients.

Coefficients $\partial F_2/\partial\mu$ ($\mu = \mu_e, \mu_r$)

Differentiating F_2 with respect to a particular doublet parameter μ_n gives

$$\frac{\partial F_2}{\partial \mu_n} = \frac{2}{U_\infty{}^2}\left(\frac{\partial \vec{V}^S}{\partial \mu_n} \cdot \nabla\mu + \vec{V}^S \cdot \frac{\partial}{\partial \mu_n}(\nabla\mu)\right) \qquad \text{(D-6)}$$

Recalling equation (26)

$$\vec{V}^S = \left(A_{k_j} \mu_j + U_k\right) \vec{e}_k \quad (k = \xi, \eta, \zeta) \qquad \text{(D-7)}$$

one obtains

$$\frac{\partial \vec{V}^S}{\partial \mu_n} = A_{kn} \vec{e}_k \quad (k = \xi, \eta, \zeta) \qquad \text{D-8)}$$

Next, the gradient of $\mu = \mu(\xi,\eta)$ is to be expressed in terms of the doublet parameters μ_j before the indicated differentiation can be performed. Applying

$$\nabla = \frac{\partial}{\partial \xi}\vec{e}_\xi + \frac{\partial}{\partial \eta}\vec{e}_\eta + \frac{\partial}{\partial \zeta}\vec{e}_\zeta$$

to the quadratic distribution of doublet strength defined by equation (10) yields

$$\nabla\mu = (\mu_\xi + \mu_{\xi\xi}\xi + \mu_{\xi\eta}\eta)\,\vec{e}_\xi + (\mu_\eta + \mu_{\xi\eta}\xi + \mu_{\eta\eta}\eta)\,\vec{e}_\eta \qquad \text{(D-9)}$$

The six coefficients of the panel doublet distribution are linearly related to the doublet parameters μ_j by

$$\begin{Bmatrix} \mu_0 \\ \mu_\xi \\ \mu_\eta \\ \mu_{\xi\xi} \\ \mu_{\xi\eta} \\ \mu_{\eta\eta} \end{Bmatrix} = \begin{bmatrix} C_{00} \\ C_{0\xi} \\ C_{0\eta} \\ C_{0\xi\xi} \\ C_{0\xi\eta} \\ C_{0\eta\eta} \end{bmatrix} \begin{Bmatrix} \\ \mu_j \\ \\ \end{Bmatrix} \qquad \text{(D-10)}$$

This is equation (41) rewritten with C_{00}, $C_{0\xi}$, $C_{0\eta}$ etc., denoting the rows of the matrix $[C_0]$. Then $\nabla\mu$ takes the form

$$\nabla\mu = \left(C_{0\xi} + \xi C_{0\xi\xi} + \eta C_{0\xi\eta}\right)\{\mu_j\}\,\vec{e}_\xi + \left(C_{0\eta} + \xi C_{0\xi\eta} + \eta C_{0\eta\eta}\right)\{\mu_j\}\,\vec{e}_\eta \qquad \text{(D-11)}$$

Hence,

$$\frac{\partial}{\partial \mu_n}(\nabla\mu) = \left(C_{0\xi} + \xi C_{0\xi\xi} + \eta C_{0\xi\eta}\right)_n \vec{e}_\xi + \left(C_{0\eta} + \xi C_{0\xi\eta} + \eta C_{0\eta\eta}\right)_n \vec{e}_\eta \qquad \text{(D-12)}$$

Introducing the terms given by equations (D-7), (D-8), (D-11), and (D-12) to equation (D-6) results in

$$\frac{\partial F_2}{\partial \mu_n} = \frac{2}{U_\infty{}^2}\left\{\left[A_{\xi n}\left(C_{0\xi} + \xi C_{0\xi\xi} + \eta C_{0\xi\eta}\right) + A_{\eta n}\left(C_{0\eta} + \xi C_{0\xi\eta} + \eta C_{0\eta\eta}\right)\right]\{\mu_j\}\right. \qquad \text{(D-13)}$$

$$\left. + V_\xi{}^S\left(C_{0\xi} + \xi C_{0\xi\xi} + \eta C_{0\xi\eta}\right)_n + V_\eta{}^S\left(C_{0\eta} + \xi C_{0\xi\eta} + \eta C_{0\eta\eta}\right)_n\right\}$$

The subscript n of

$$A_{\xi n},\ A_{\eta n},\ \left(C_{0\xi} + \xi C_{0\xi\xi} + \eta C_{0\xi\eta}\right)_n,\ \left(C_{0\eta} + \xi C_{0\xi\eta} + \eta C_{0\eta\eta}\right)_n$$

indicates the nth term of the row of the coefficients.

APPENDIX E
PRESSURE EQUATIONS

For incompressible flow the pressure coefficient c_P reads

$$c_P = 1 - \frac{\vec{V} \cdot \vec{V}}{U_\infty{}^2} \tag{E-1}$$

where $\vec{V}$ is the velocity vector and U_∞ is the magnitude of the freestream velocity. The velocities of the two sides of a doublet sheet are different, say $\vec{V}_u$ on the upper side and $\vec{V}_l$ on the lower side. Introducing the average velocity $\vec{V}^S$ and the jump in velocity $\vec{V}^D$, i.e.,

$$\vec{V}^S = \frac{1}{2}\left(\vec{V}_u + \vec{V}_l\right) \tag{E-2}$$

$$\vec{V}^D = \vec{V}_u - \vec{V}_l \tag{E-3}$$

one obtains

$$\vec{V}_u = \vec{V}^S + \frac{1}{2}\vec{V}^D \tag{E-4}$$

$$\vec{V}_l = \vec{V}^S - \frac{1}{2}\vec{V}^D \tag{E-5}$$

Recalling that doublet strength μ is the jump in potential across the sheet,

$$\mu = \Phi_u - \Phi_l \tag{E-6}$$

the gradient of μ

$$\nabla\mu = \nabla\Phi_u - \nabla\Phi_l = \vec{V}_u - \vec{V}_l = \vec{V}^D \tag{E-7}$$

is seen to be equivalent to the jump in velocity across the sheet.

Hence, the pressure coefficients on upper and lower sides of the doublet sheet take the form

$$c_{P_u} = 1 - \frac{1}{U_\infty{}^2}\left(\vec{V}^S \cdot \vec{V}^S + \vec{V}^S \cdot \nabla\mu + \frac{1}{4}\nabla\mu \cdot \nabla\mu\right) \tag{E-8}$$

$$c_{P_l} = 1 - \frac{1}{U_\infty{}^2}\left(\vec{V}^S \cdot \vec{V}^S - \vec{V}^S \cdot \nabla\mu + \frac{1}{4}\nabla\mu \cdot \nabla\mu\right) \tag{E-9}$$

The pressure jump, defined by

$$\Delta c_P = c_{P_l} - c_{P_u} \tag{E-10}$$

becomes

$$\Delta c_P = \frac{2}{U_\infty{}^2} \vec{V}^S \cdot \nabla\mu \tag{E-11}$$

Page intentionally left blank

REFERENCES

1. Maskell, E. C.: *Some Recent Developments in the Study of Edge Vortices.* Proceedings of 3rd Congress of Int. Counc. Aero. Sci., 1962, pp 737-749, Spartan Books, Inc., Washington, 1964.

2. Fink, P. T.; and Taylor, J.: *Some Low Speed Experiments With 20 Degree Delta Wings.* ARC R&M 3489, September 1966.

3. Polhamus, E. C.: *A Concept of the Vortex Lift of Sharp-Edge Delta Wings Based on a Leading-Edge-Suction Analogy.* NASA TN D-3767, December 1966.

4. Polhamus, E. C.: *Application of the Leading-Edge-Suction Analogy of Vortex Lift to the Drag-Due-to-Lift of Sharp-Edge Delta Wings.* NASA TN D-4739, August 1968.

5. Polhamus, E. C.: "Predictions of Vortex-Lift Characteristics by a Leading-Edge-Suction Analogy." *J. of Aircraft,* vol. 8, p 193, 1971.

6. Smith, J. H. B.: *Improved Calculation of Leading-Edge Separation From Slender Delta Wings.* RAE technical report 66070, March 1966.

7. Mangler, K. W.; and Smith, J. H. B.: *A Theory of the Flow Past a Slender Delta Wing With Leading-Edge Separation.* Proc. Roy. Soc., May 1959.

8. Lamar, J. E.: *A Modified Multhopp Approach for Predicting Lifting Pressures and Camber Shape for Composite Planforms in Subsonic Flow.* NASA TN D-4427, July 1968.

9. Jones, R. T.: *Properties of Low-Aspect-Ratio Pointed Wings at Speeds Below and Above the Speed of Sound.* NACA report 835, 1946.

10. Rehbach, C.: "Etude numerique de l'influence de la forme de l'extrémite d'une aile sure l'enroulement de la nappe tourbillonaire." *Rech. Aerosp.* 1971-6, 1971, pp 367-8.

11. Mook, D. T.; and Maddox, S. A.: "Extension of a Vortex-Lattice Method to Include the Effects of Leading-Edge Separation." *Journal of Aircraft 11, 2,* 1974, pp 127-8.

12. Kandil, O. H.; Mook, D. T.; and Nayfeh, A. H.: *Nonlinear Prediction of the Aerodynamic Loads on Lifting Surfaces.* AIAA paper 74-503, June 1974.

13. Kandil, O. H.; Mook, D. T.; and Nayfeh, A. H.: *Effect of Compressibility on the Nonlinear Prediction of the Aerodynamic Loads on Lifting Surfaces.* AIAA paper 75-121, January 1975.

14. Johnson, F. T.; and Rubbert, P. E.: *Advanced Panel-Type Influence Coefficient Method Applied to Subsonic Flows.* AIAA paper 75-50, January 1975.

15. Weber, J. A.; Brune, G. W.; Johnson, F. T.; Lu, P.; and Rubbert, P. E.: *A Three-Dimensional Solution of Flows Over Wings With Leading Edge Vortex Separation.* AIAA paper 75-866, June 1975.

16. Broyden, C. G.: *Quasi-Newton, or Modification Methods.* Numerical Solution of Systems of Nonlinear Algebraic Equations, edited by G. D. Byrne, and C. A. Hall, Academic Press, 1973.

17. Peckham, D. H.: *Low-Speed Wind-Tunnel Tests on a Series of Uncambered Slender Pointed Wings With Sharp Edges.* RM3186, British Aeronautical Research Council, 1961.

18. Marsden, D. J. et al.: *An Investigation Into the Flow Over Delta Wings at Low Speeds With Leading-Edge Separation.* Rep. 114, ARC 20409, The College of Aeronautics, Cranfield, February 1958.

19. Batchelor, G. K.: *An Introduction to Fluid Dynamics,* Cambridge at the University Press, 1967.